

POLITECNICO DI TORINO

MASTER's Degree in Materials Engineering



MASTER's Degree Thesis

**DEVELOPMENT OF MATERIALS
BASED ON RECYCLED
POLYPROPYLENE FOR 3D
PRINTING - FDM**

Supervisors

Prof.ssa Rossella ARRIGO

Prof. Alberto FRACHE

Candidate

David N. RIBERO

OCTOBER - 2025

Summary

Al giorno d'oggi, un problema significativo in tutto il mondo riguarda la non adeguata gestione dei rifiuti in materiale plastico. Per cercare di porre rimedio alle problematiche legate all'accumulo di rifiuti in plastica nell'ambiente terrestre e marino, la ricerca accademica e quella industriale si stanno concentrando negli ultimi anni sullo sviluppo di prodotti formulati a base di polimeri derivanti dai processi di riciclo dei rifiuti. Contemporaneamente, sono stati sviluppati nuovi processi produttivi caratterizzati da maggiore sostenibilità rispetto alle tecnologie tradizionali, che consentono di ridurre l'apporto energetico necessario per la formulazione di un dato prodotto. In questo ambito, le tecnologie di Additive Manufacturing (AM) hanno avuto un notevole sviluppo negli ultimi anni, riuscendo in alcuni settori a sostituire alcune tecnologie tradizionali.

Il presente lavoro di tesi si pone come obiettivo quello di progettare e sviluppare un materiale polimerico a base di polipropilene derivante da processi di riciclo meccanico, che abbia le caratteristiche adeguate a poter essere lavorato per Fused Deposition Modeling (FDM), una tecnologia AM comunemente impiegata per la stampa 3D di termoplastici. Il primo stadio del lavoro ha riguardato uno studio dello stato dell'arte sui diversi processi di Additive Manufacturing, e soprattutto sulla tecnica FDM. Quest'ultima tecnologia presenta delle grandi opportunità ma anche delle limitazioni a livello economico e tecnologico, che ne impediscono il pieno sfruttamento a livello industriale per molti materiali polimerici. Una delle principali opportunità a livello tecnologico è la facilità di realizzare geometrie molto complesse, solitamente non ottenibili attraverso le tecnologie di trasformazione tradizionali.

Allo stesso tempo, una limitazione significativa di tale tecnica è la bassa qualità dell'oggetto prodotto e le peggiori proprietà finali (soprattutto meccaniche) rispetto a quelle tipicamente ottenibili con processi tradizionali. Nonostante ciò, è stato possibile fare un'ampia ricerca sui diversi argomenti per rendere questa tecnologia alla pari degli altri. Inoltre, lo studio dello stato dell'arte sull'impiego del polipropilene per processi FDM ha mostrato che tale deve essere opportunamente modificato attraverso l'introduzione di filler, cariche o additivi capaci di modificare le caratteristiche termiche e reologiche, affinché possa essere efficacemente

processato attraverso questa tecnologia.

La parte sperimentale ha, quindi, riguardato la progettazione e la formulazione di miscele di polipropilene riciclato (rPP) e polipropilene vergine caricato con particelle di talco (PPt), processabili per FDM. A tale scopo, è stato seguito un approccio di Design of Experiment basato sul metodo di Taguchi per ottenere una formulazione con quantità di rPP massimizzata e con una processabilità FDM ottimizzata. In particolare, si è deciso di dividere lo studio in quattro fasi. Durante le quattro diverse fasi, si è cercato di ottimizzare il comportamento reologico del blend attraverso lo utilizzo di modelli statistici e teorici. Per ciascun stadio sono state eseguite diverse prove reologiche, termiche e meccaniche, e dai risultati ottenuti è stato possibile confrontare gli effetti del processo produttivo sul comportamento del blend. Il primo stadio ha riguardato la caratterizzazione reologica e termica di miscele con diversi rapporti in peso fra PPt e rPP, ottenute per melt compounding in un mini-estrusore. Prima di valutare il comportamento reologico di ciascun blend, è stato necessario caratterizzare i materiali di partenza.

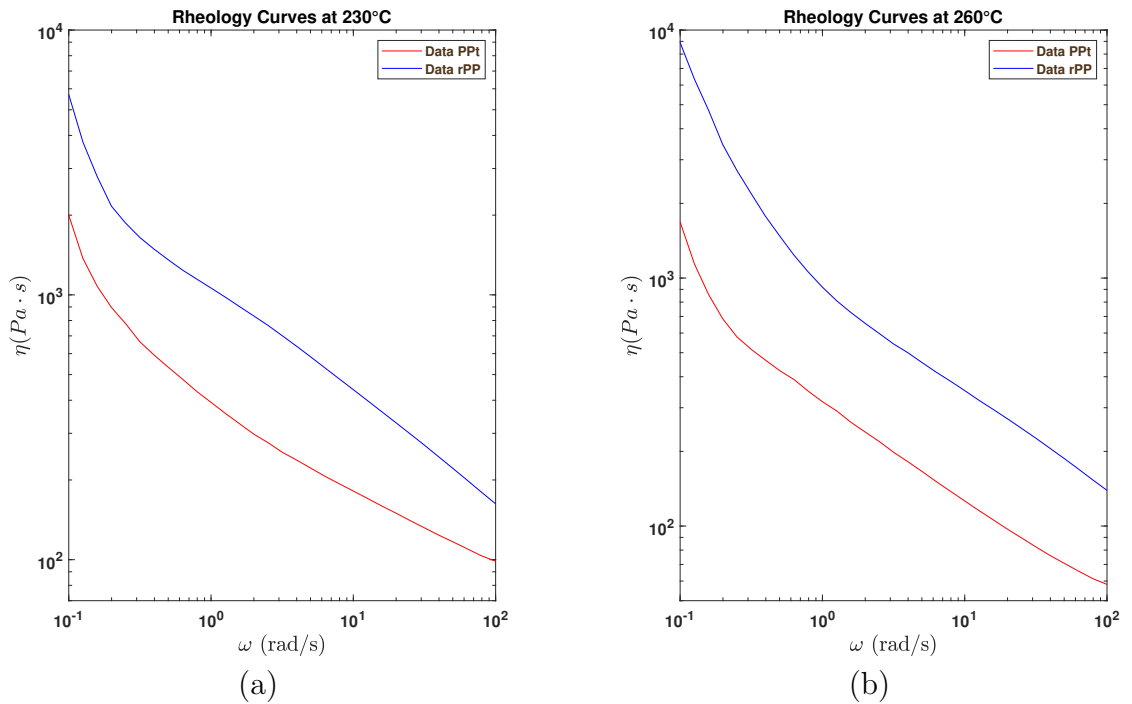


Figure 1: Comportamento reologico di rPP e PPt a diverse temperature. a) Comportamento reologico a 230°C. b) Comportamento reologico a 260°C.

La figura 1 mostra le curve di viscosità complessa in funzione della frequenza per i due materiali, rPP e PPt registrate a due valori di temperatura. Entrambi i materiali

mostrano un comportamento spiccatamente non-newtoniano, con comparsa di yield-stress nella regione a basse frequenze. Nel caso di PPt, tale comportamento può essere attribuito all'effetto delle particelle di talco che rallentano le dinamiche macromolecolari della matrice, impedendo il completo rilassamento delle catene di PP. Per il rPP, il comportamento reologico non-Newtoniano può essere spiegato considerando la presenza di piccole quantità di carica o di altri polimeri ad elevato punto di fusione (solitamente presenti nel caso di polimeri riciclati) che potrebbero esercitare un'azione simile a quella delle particelle di talco. In modo da avere un ampio spettro di formulazioni, sono state prodotte in mini-estrusore cinque miscele nelle quali la quantità di rPP è stata aumentata fino al 50 %wt, con una varianza di 10 %wt, come si può vedere nella tabella 1.

Run	rPP[%w]	PPt [%w]
50:50 rPP - PPt	50	50
40:60 rPP - PPt	40	60
30:70 rPP - PPt	30	70
20:80 rPP - PPt	20	80
10:90 rPP - PPt	10	90

Table 1: Rapporti utilizzati per i diversi blends.

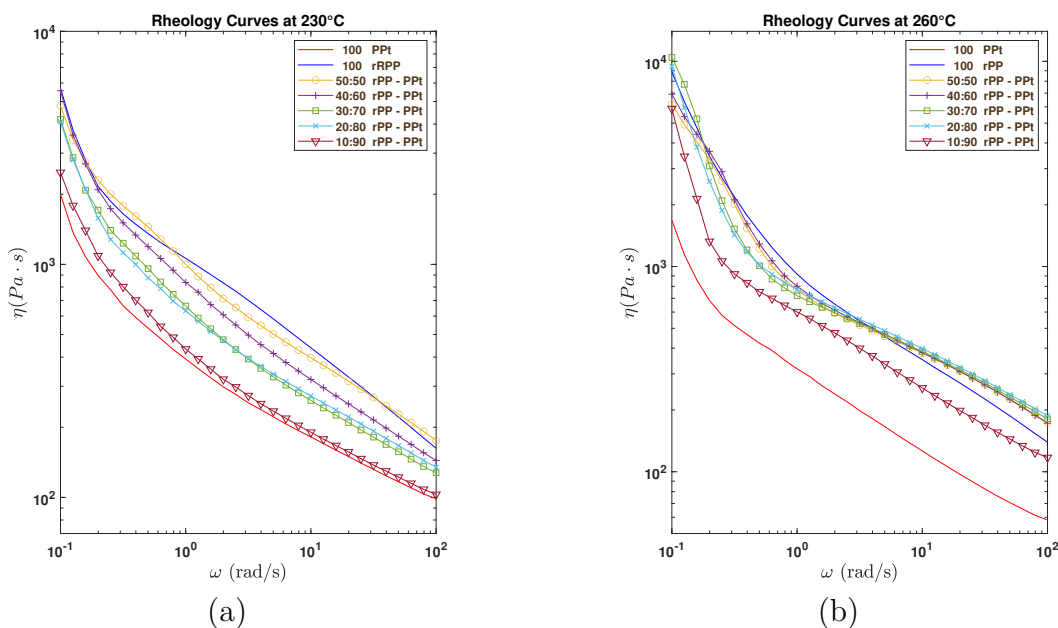


Figure 2: Confronto delle curve di viscosità per ciascuna blend prodotto con mini-estrusore. (a) Curve di viscosità a 230°C. (b) Curve di viscosità a 260°C.

In figura 2 sono riportate le curve di viscosità complessa per ciascun blend prodotto, misurate a due diversi valori di temperatura. Si può osservare come le miscele mostrino un comportamento non-Newtoniano simile a quello dei polimeri di base, con dei valori di viscosità che rispecchiano il rapporto in peso fra PPt e rPP presente.

È noto dalla letteratura come, affinché un materiale termoplastico sia stampabile FDM, è necessario che presenti un comportamento di yield stress accentuato. La presenza di tale comportamento, infatti, garantisce una buona stabilità del filamento in uscita dall'ugello di stampa e una buona stabilità dimensionale del materiale anche nello stadio di post-deposizione. Per scegliere fra le miscele prodotte i materiali con la migliore processabilità, i dati reologici raccolti sono stati modellati con diversi modelli teorici, tra i quali è stato scelto il modello di Khoshkava and Kamal, al fine di scegliere il materiale con yield-stress ottimizzato.

Le tabelle 2 e 3 riassumono i valori trovati per ciascun blend. Dunque, sono selezionati i due blends in cui lo Yield Stress è massimizzato, ovvero le formulazioni contenenti il 30%wt e 40%wt di rPP.

Campioni	Simbolo	Valore	Unita
50:50 rPP - PPt	$\sigma_{T=230\text{ }^{\circ}C}$	326,1	Pa
40:60 rPP - PPt	$\sigma_{T=230\text{ }^{\circ}C}$	368,2	Pa
30:70 rPP - PPt	$\sigma_{T=230\text{ }^{\circ}C}$	292,9	Pa
20:80 rPP - PPt	$\sigma_{T=230\text{ }^{\circ}C}$	269,4	Pa
10:90 rPP - PPt	$\sigma_{T=230\text{ }^{\circ}C}$	181,7	Pa

Table 2: Yield Valori di sollecitazione per tutte le miscele a 230°C.

Campione	Simbolo	Valore	Unita
50:50 rPP - PPt	$\sigma_{T=260\text{ }^{\circ}C}$	488,7	Pa
40:60 rPP - PPt	$\sigma_{T=260\text{ }^{\circ}C}$	536,9	Pa
30:70 rPP - PPt	$\sigma_{T=260\text{ }^{\circ}C}$	520,3	Pa
20:80 rPP - PPt	$\sigma_{T=260\text{ }^{\circ}C}$	445,6	Pa
10:90 rPP - PPt	$\sigma_{T=260\text{ }^{\circ}C}$	266,8	Pa

Table 3: Yield Valori di sollecitazione per tutte le miscele a 260°C.

È possibile notare come l'aumento della quantità di rPP provochi un aumento dei valori di Yield Stress. Dai dati riportati in Tabella 2, è possibile notare come le miscele prodotte possano essere suddivise in tre gruppi a seconda del valore di yield-stress: 10:90 rPP - PPt con yield stress inferiore a 200 Pa, miscele contenenti il 20 e il 30 %wt di rPP con valore compreso tra 200 e 300 Pa e miscele con un

quantitativo di rPP superiore al 30 %wt di rPP che mostrano un valore superiore a 300 Pa. Differentemente, dalla valutazione del comportamento reologico effettuata a 260°C, non è possibile notare un andamento di questo tipo in quanto, come osservabile dai valori riportati in Tabella 3, le miscele 40:60 rPP – PPt e 30:70 rPP – PPt mostrano valori superiori a 500 Pa.

Inoltre, le miscele prodotte sono state caratterizzate attraverso analisi termiche TGA e una DSC, dalle quali è possibile ricavare informazioni sulle temperature caratteristiche, la composizione chimica e la cristallinità del blend. Come fatto in precedenza, sono state condotte delle prove in primis sui materiali di base e dopo sui diversi blend.

La figura 3 mostra i risultati ottenuti per i materiali base. Da questi due grafici è possibile determinare la temperatura alla quale entrambi i materiali iniziano a degradare, che è circa pari a 350°C, nonostante rPP mostri dei valori leggermente più bassi di PPt. Dal residuo collezionato a fine prova è possibile determinare che la quantità di talco presente nel campione Pt sia pari al 16 %wt. Inoltre, il residuo di circa 10 %wt osservato per rPP dimostra la presenza di filler (ad esempio carbon black, solitamente presente in PP riciclato) già desunta dall'analisi del comportamento reologico.

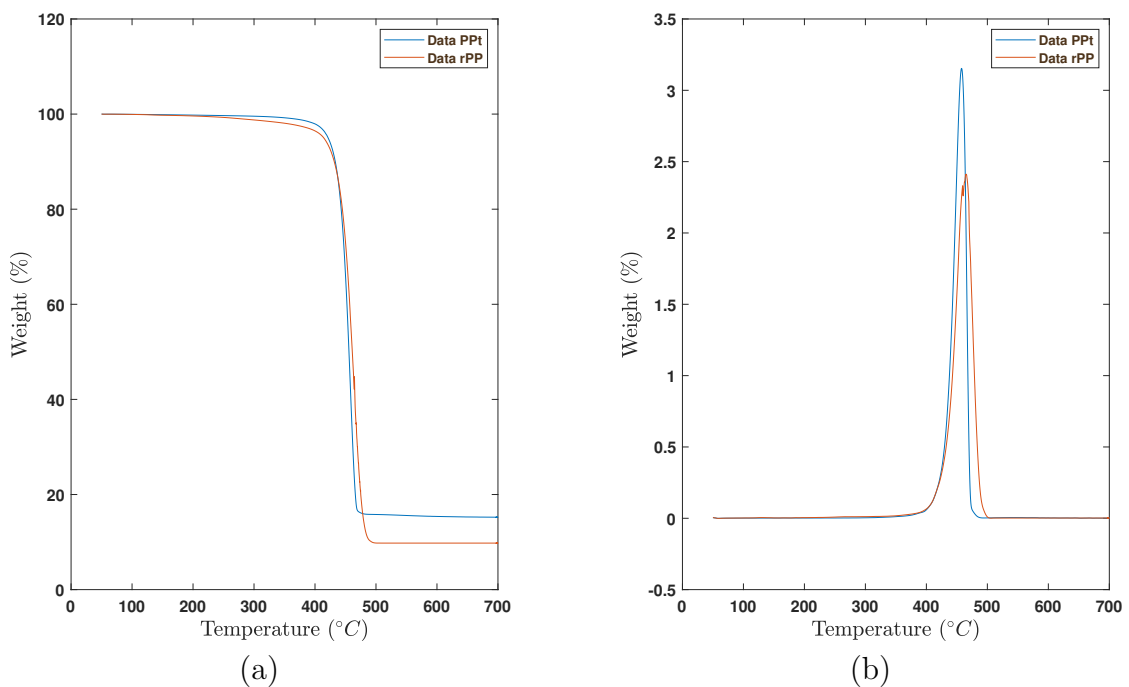


Figure 3: Risultati TGA per materiali di base, PPt e rPP. (a) Perdita di massa misurata (TG). (b) Derivata di massa (DTG).

La figura 4 mostra i risultati ottenuti per tutti i blends. Per tutti i campioni la

temperatura di degradazione massima è compresa tra 380°C e 393°C. In tabella ?? sono riportate le temperature di inizio degradazione la temperatura del picco della curva DTG e il residuo a 700°C.

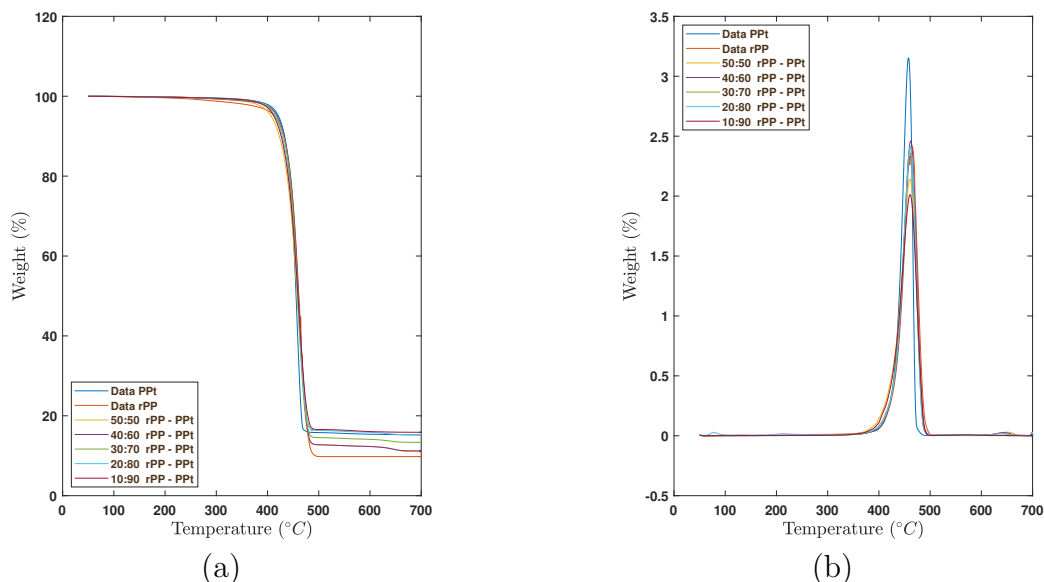


Figure 4: Risultati TGA per materiali di base e tutte blends. (a) Perdita di massa misurata (TG). (b) Derivato di massa (DTG).

Sample	Temperature (98 % wt)	Residue	Peak
50:50 rPP - PPt	379,9	11,5	460,4
40:60 rPP - PPt	391,8	11,5	462,1
30:70 rPP - PPt	393,1	13,5	461,3
20:80 rPP - PPt	391,3	15,4	461,3
10:90 rPP - PPt	388,0	15,90	460,8

Table 4: Valori dei risultati TGA per ciascuna blend.

Infine, i blends prodotti sono stati caratterizzati tramite test DSC, principalmente per ottenere informazioni sul grado di cristallinità dei materiali. Infatti, la conoscenza del contenuto di fase cristallina è fondamentale per avere informazioni per quello che riguarda il ritiro della parte stampata durante la fase di solidificazione, e sulla sua conseguente deformazione.

La figure 5 mostra i termogrammi ottenuti per il PPt e il rPP, mentre la figura 6 mostre i risultati ottenuti per le miscele.

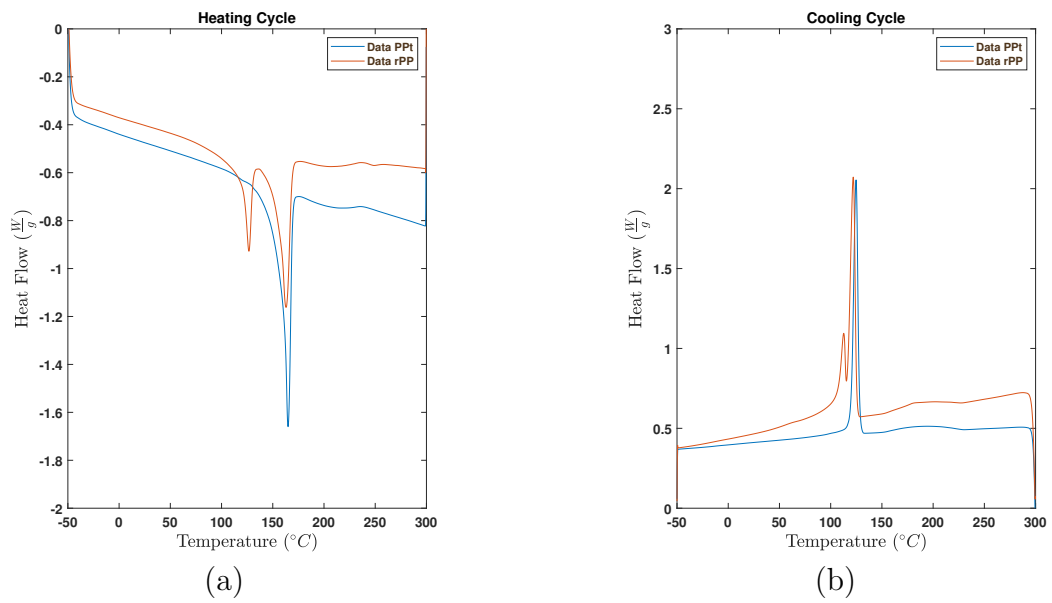


Figure 5: Risultati prova DSC. a) Ciclo di riscaldamento. b) Ciclo di raffreddamento.

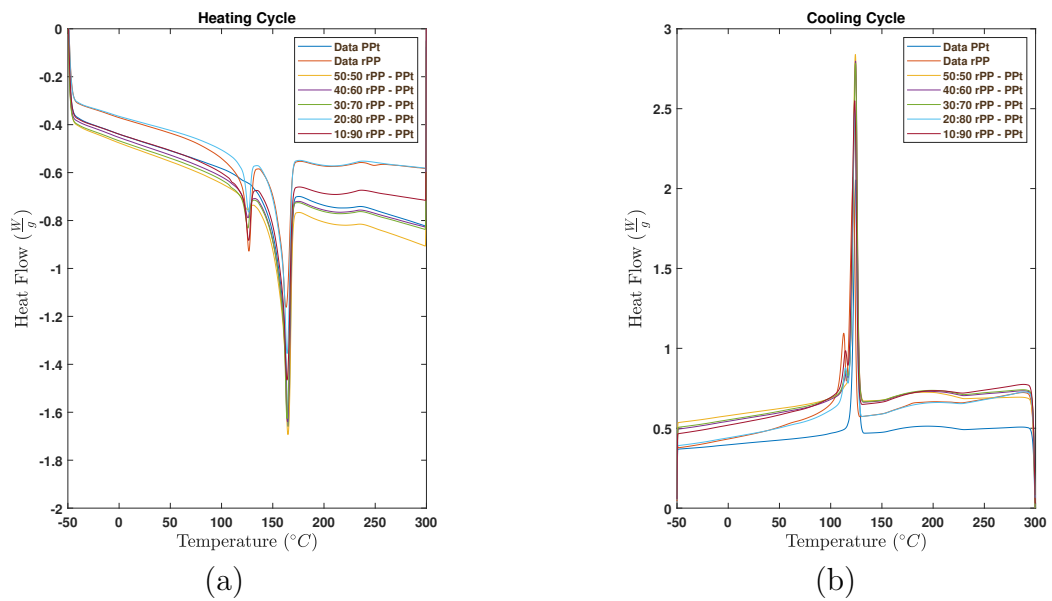


Figure 6: Risultati prova DSC. a) Ciclo di riscaldamento. b) Ciclo di raffreddamento.

I termogrammi di rPP mostrano, oltre al picco tipico del PP, la presenza di due ulteriori picchi, attribuibili alla presenza di polietilene (che mostra tipicamente

una temperatura di fusione inferiore rispetto al PP) e di altri polimeri altofondenti quali polimetilmetacrilato, polivinilcloruro o poliammidi. La tabella 5 riassume i valori delle temperature caratteristiche e dell'entalpia di fusione delle miscele, mentre in tabella 6 sono riportati i valori di cristallinità calcolati per i due picchi corrispondenti alla fusione della frazione in PE e della frazione in PP.

Material	$T_{melting}$ °C	$T_{crystallization}$ °C	ΔH_m (J/g)
50:50 rPP - PPt	126,3	120,8	9,7
	165,2	157,4	52,7
40:60 rPP - PPt	126,18	120,9	8,3
	165,08	157,7	50,5
30:70 rPP - PPt	126,31	120,4	4,3
	166,18	158,3	56,1
20:80 rPP - PPt	125,21	119,9	3,4
	165,31	158,5	57,8
10:90 rPP - PPt	125,55	119,0	1,5
	166,88	158,5	61,8

Table 5: Principle peak values of DSC test for all blends.

Run	Degree of Crystallinity of PE (%)	Degree of Crystallinity of PP (%)
50:50 rPP - PPt	11	36
40:60 rPP - PPt	9	35
30:70 rPP - PPt	5	39
20:80 rPP - PPt	4	40
10:90 rPP - PPt	2	43

Table 6: Degree of crystallinity for all blends.

A questo punto è stato possibile identificare le miscele che mostrano valori massimizzati di yield stress e, allo stesso tempo, valori inferiori di cristallinità. Sulla base di tali considerazioni il blend con 30 %wt rPP è stato selezionato per continuare il processo sperimentale, poiché questo rappresenta un punto intermedio tra tutti campioni valutati. Come è stato menzionato in precedenza, la seconda fase di questa ricerca consistite in un processo di ottimizzazione basato sul metodo Taguchi, in cui si è cercato di ottimizzare i parametri di processo in estrusione per massimizzare il parametro Yield Stress. Ciò è stato fatto tenendo in considerazione

4 fattori (portata, profilo vite, profilo di temperatura, velocità di rotazione delle viti) a due livelli (tabella 8), permettendo l'esecuzione di sedici test (tabella 7).

Factor	Level 1	Level 2
Feeding (rpm)	300	500
Screw Velocity (rpm)	150	400
Temperature (°C)	190	210
Extruder Screw	Standard	Transport

Table 7: Fattori e livelli.

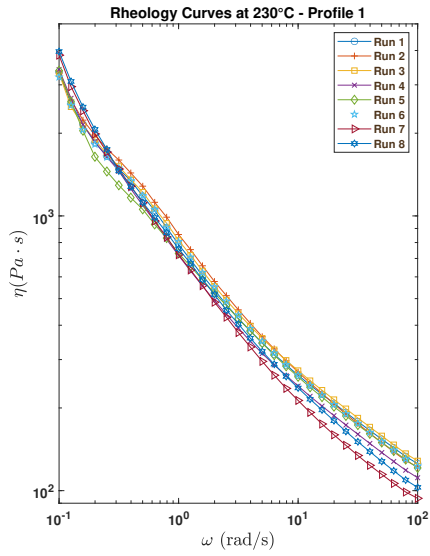
Run	Hopper Velocity	Screw Velocity	Temperature	Extruder Screw
Run 1	A1	B1	C1	E1
Run 2	A1	B1	C1	E2
Run 3	A1	B1	C2	E1
Run 4	A1	B1	C2	E2
Run 5	A1	B2	C1	E1
Run 6	A1	B2	C1	E2
Run 7	A1	B2	C2	E1
Run 8	A1	B2	C2	E2
Run 9	A2	B1	C1	E1
Run 10	A2	B1	C1	E2
Run 11	A2	B1	C2	E1
Run 12	A2	B1	C2	E2
Run 13	A2	B2	C1	E1
Run 14	A2	B2	C1	E2
Run 15	A2	B2	C2	E1
Run 16	A2	B2	C2	E2

Table 8: Taguchi Arrays L16.

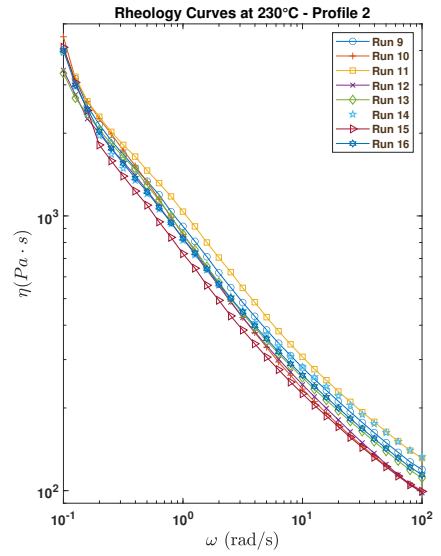
Sono quindi state condotte 16 estrusioni, variando i parametri operativi come mostrato in tabella 7, e i materiali ottenuti sono stati caratterizzati attraverso misure reologiche.

La figura 7 mostra le curve di viscosità per tutti test condotti a 230°C, mentre la figura 8 le curve di viscosità ottenute a 260°C.

La tabella 9 mostra i valori di yield stress derivati dalla modellazione delle curve di viscosità mostrate nelle figure precedenti. Come già osservato in precedenza, si ottengono valori di yield stress più elevati a 260°C. A questa temperatura la Run 14 ha mostrato il maggiore valore per questo fattore (844,9) Pa. Inoltre a 230°C, la

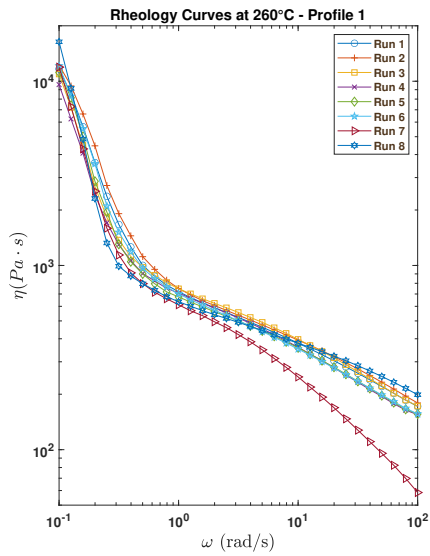


(a)

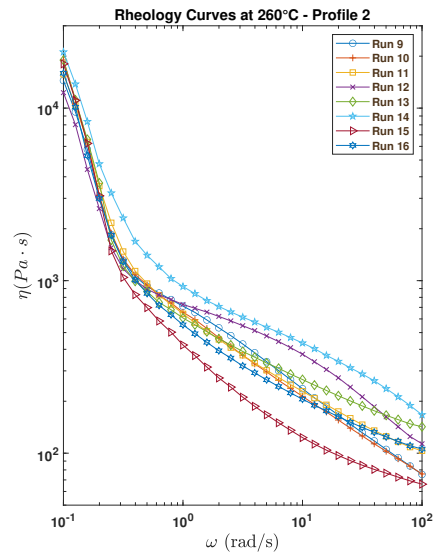


(b)

Figure 7: Confronto delle curve di viscosità per ciascuna serie prodotta con il profilo 1. (a) Curve di viscosità a 230 °C. (b) Curve di viscosità a 260 °C.



(a)



(b)

Figure 8: Confronto delle curve di viscosità per ciascuna serie prodotta con il profilo 1. (a) Curve di viscosità a 230 °C. (b) Curve di viscosità a 260 °C.

Run 7 ha rivelato il valore maggiore, 294,01 Pa. Infine, si ottiene un comportamento più marcatamente non newtoniano utilizzando durante l'estrusione dei materiali il

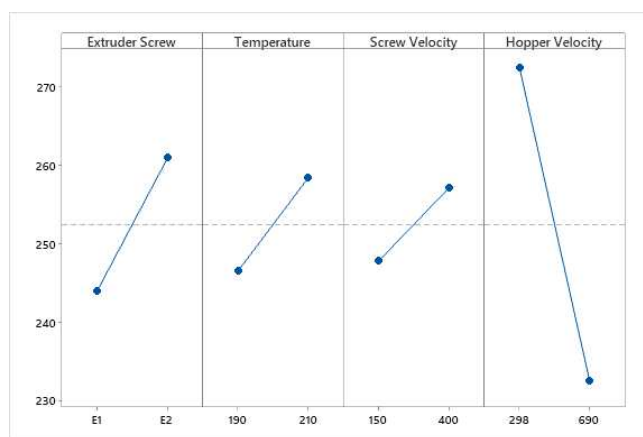
secondo profilo (vite estrusore di trasporto). Tuttavia, dato il complesso andamento delle curve di viscosità ottenuto a 260°C per questa configurazione, il fitting dei dati sperimentali non è ottimale e ciò potrebbe aver inficiato i dati ottenuti dalla modellazione.

Sample	Symbol	Value	Unit	Sample	Symbol	Value	Unit
Run 1	$\sigma_{T=230\text{ }^{\circ}C}$	236,73	Pa	Run 9	$\sigma_{T=230\text{ }^{\circ}C}$	260,88	Pa
	$\sigma_{T=260\text{ }^{\circ}C}$	710,12	Pa		$\sigma_{T=260\text{ }^{\circ}C}$	567,79	Pa
Run 2	$\sigma_{T=230\text{ }^{\circ}C}$	218,66	Pa	Run 10	$\sigma_{T=230\text{ }^{\circ}C}$	320,48	Pa
	$\sigma_{T=260\text{ }^{\circ}C}$	792,16	Pa		$\sigma_{T=260\text{ }^{\circ}C}$	621,70	Pa
Run 3	$\sigma_{T=230\text{ }^{\circ}C}$	222,86	Pa	Run 11	$\sigma_{T=230\text{ }^{\circ}C}$	233,80	Pa
	$\sigma_{T=260\text{ }^{\circ}C}$	629,70	Pa		$\sigma_{T=260\text{ }^{\circ}C}$	629,46	Pa
Run 4	$\sigma_{T=230\text{ }^{\circ}C}$	258,06	Pa	Run 12	$\sigma_{T=230\text{ }^{\circ}C}$	220,61	Pa
	$\sigma_{T=260\text{ }^{\circ}C}$	528,57	Pa		$\sigma_{T=260\text{ }^{\circ}C}$	438,91	Pa
Run 5	$\sigma_{T=230\text{ }^{\circ}C}$	216,04	Pa	Run 13	$\sigma_{T=230\text{ }^{\circ}C}$	228,40	Pa
	$\sigma_{T=260\text{ }^{\circ}C}$	627,98	Pa		$\sigma_{T=260\text{ }^{\circ}C}$	599,85	Pa
Run 6	$\sigma_{T=230\text{ }^{\circ}C}$	212,99	Pa	Run 14	$\sigma_{T=230\text{ }^{\circ}C}$	267,32	Pa
	$\sigma_{T=260\text{ }^{\circ}C}$	688,15	Pa		$\sigma_{T=260\text{ }^{\circ}C}$	844,90	Pa
Run 7	$\sigma_{T=230\text{ }^{\circ}C}$	294,01	Pa	Run 15	$\sigma_{T=230\text{ }^{\circ}C}$	286,67	Pa
	$\sigma_{T=260\text{ }^{\circ}C}$	469,63	Pa		$\sigma_{T=260\text{ }^{\circ}C}$	506,45	Pa
Run 8	$\sigma_{T=230\text{ }^{\circ}C}$	292,10	Pa	Run 16	$\sigma_{T=230\text{ }^{\circ}C}$	269,28	Pa
	$\sigma_{T=260\text{ }^{\circ}C}$	561,09	Pa		$\sigma_{T=260\text{ }^{\circ}C}$	563,09	Pa

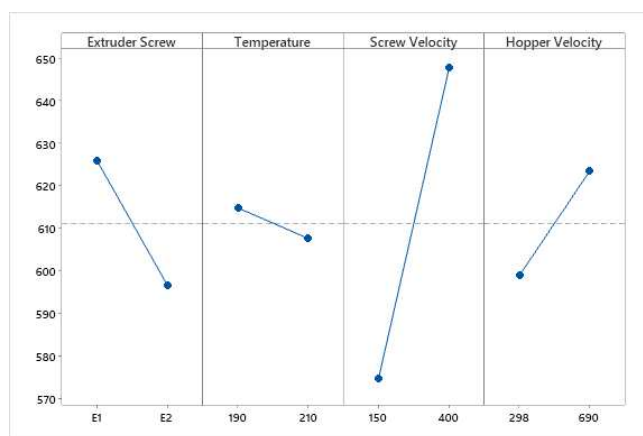
Table 9: Valori di Yield Stress per tutte le possibili configurazioni e temperature.

Per comprendere la rilevanza e l'impatto per ciascun fattore e livello, si è deciso di utilizzare un processo di ottimizzazione basato sul metodo Taguchi, in cui si è cercato di massimizzare la risposta. L'obiettivo non era solo comprendere l'importanza e gli effetti dei parametri di processo, ma anche trovare il massimo valore di Yield Stress. Come si vede nella tabella 8, l'array utilizzato in questa ricerca è L16 che dispone di sedici diverse combinazioni (Runs) di parametri e livelli.

I risultati di questo processo mostrano in tutto due figure che evidenziano la media caratteristica per ogni fattore e livello. Il valore della pendenza della linea in queste figure è una indicazione della rilevanza di ciascun fattore e livello. Se il valore della pendenza è zero, il fattore e livello hanno influenzato i risultati allo stesso modo. Invece, se la pendenza è maggiore di zero, i fattori e i livelli di influenza sono significativi. Di conseguenza, è possibile organizzare per rilevanza i fattori e determinare quale livello governa maggiormente i risultati.



(a)



(b)

Figure 9: Principali effetti per i parametri di estrusione. (a) Yield Stress a 230 °C. (b) Yield Stress a 260 °C.

La figura 9 mostra la risposta media per tutti i parametri e livelli in entrambi i casi. È stato possibile concludere che, a 230°C, il valore di Yield Stress più alto è stato ottenuto con il secondo livello per il profilo vite, il profilo di temperatura e la velocità di rotazione delle viti, e con il primo livello per la portata. D'altra parte, a 260°C, il valore massimo è stato ottenuto come combinazione di livelli e fattori. In questo caso, non è stato possibile scegliere una soluzione univoca. Inoltre, la temperatura potrebbe essere trascurata a causa della piccola differenza tra i livelli di risposta. In conclusione, non c'è una univoca configurazione che consente di massimizzare il valore di yield stress. Inoltre, la risposta ottenuta in termini di yield stress è fortemente influenzata dalla temperatura e cui si conduce la misura reologica. Per i motivi sopra menzionati, i parametri possono essere organizzati in

ordine di importanza come segue: velocità di rotazione delle viti, portata, profilo vite e profilo di temperatura. A bassa temperatura (230°C), il parametro principale risulta essere la portata, mentre ad alte temperature (260°C), è la velocità di rotazione delle viti. In base ai risultati e alle conclusioni sopra menzionati (reologia e risultati di Taguchi), è stato deciso di ripetere il processo sperimentale per le prove 10, 11, 14 e 15. Lo scopo è stato simulare un processo continuo (produzione in linea), che ha confermato i risultati precedentemente ottenuti.

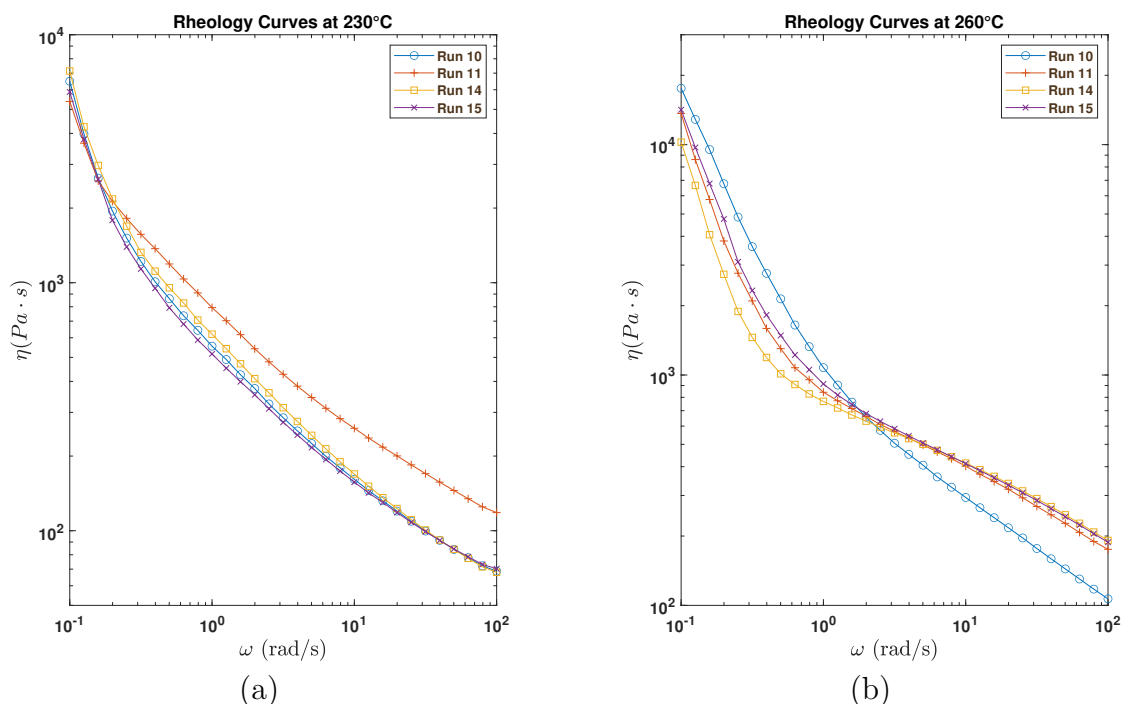


Figure 10: Curva di viscosità per tutte le prove selezionate a) Curva di viscosità a 230°C . b) Curva di viscosità a 260°C .

La figura 10 mostra le curve di viscosità per le prove selezionate sopra. Come visto nelle figure precedenti, le curve mostrano un marcato comportamento non newtoniano.

Analizzando l'andamento delle curve a bassa frequenza, la Run 14 ha esposto un comportamento non newtoniano più marcato. Tuttavia, la differenza tra tutte le Runs è minima.

In base ai risultati di cui sopra (tabella 10), è stato possibile scegliere la Run 10 come configurazione migliore. Questa Run non solo mostra il valore di Yield Stress più elevato, ma include anche i risultati di Taguchi. La configurazione per questa Run corrisponde al livello uno per i parametri della macchina di estrusione, mentre è il secondo livello per la velocità della tramoggia. A questo punto è possibile

Sample	Symbol	Value	Unit
Run 10	$\sigma_{T=230\text{ }^{\circ}C}$	381,47	Pa
	$\sigma_{T=260\text{ }^{\circ}C}$	1135,35	Pa
Run 11	$\sigma_{T=230\text{ }^{\circ}C}$	369,66	Pa
	$\sigma_{T=260\text{ }^{\circ}C}$	663,73	Pa
Run 14	$\sigma_{T=230\text{ }^{\circ}C}$	422,86	Pa
	$\sigma_{T=260\text{ }^{\circ}C}$	466,37	Pa
Run 15	$\sigma_{T=230\text{ }^{\circ}C}$	354,15	Pa
	$\sigma_{T=260\text{ }^{\circ}C}$	767,21	Pa

Table 10: Valori di Yield Stress per la selezione di tutte le Runs.

utilizzare la configurazione della Run 10 e produrre due blends, uno a 30 %wt rPP sia anche a 40 %wt rPP, e continuare con il processo per produrre il filamento per la stampante.

Sulla base di studi precedenti, sono stati condotti diversi test per trovare la o le combinazioni dei parametri operativi durante lo stadio di produzione del filamento che consentano di ottenere un filamento che soddisfi determinati requisiti dimensionali (diametro costante) e di qualità superficiale (bassa rugosità). La tabella 11 riassume i diversi tentativi fatti per trovare la configurazione in cui i requisiti prima menzionati siano massimizzati. I parametri valutati sono stati la temperatura, la velocità di rotazione della vite e il Fan Speed. A bassa velocità della vite (test 1-3) il diametro del filamento non soddisfaceva il target. Inoltre, a parità di condizione di temperatura, è stato evidenziato che aumentando questo parametro si riduce il diametro.

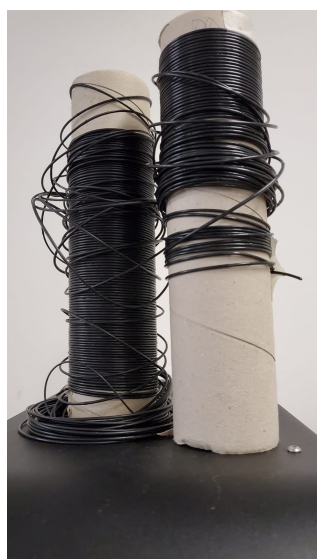
Attempent	Temperature ($^{\circ}C$)	Screw Velocity (RPM)	Fan Speed (%)
1	200 - 200 - 195 - 195	2,3	10
2	200 - 200 - 195 - 195	2,7	10
3	200 - 200 - 195 - 195	2,7	10
4	200 - 200 - 195 - 195	3,7	30
5	220 - 215 - 215 - 210	3,7	30
6	220 - 215 - 215 - 210	4,5	30

Table 11: Parametri utilizzati per produrre il filamento per entrambe blends (30%wt e 40%wt rPP).

A velocità costante della vite (test 3 e test 4), il filamento mostrava un intervallo di diametri adeguato per il successivo processo FDM. Tuttavia, il test 3 ha mostrato un problema durante la raccolta del filamento, dovuto all'eccessiva fragilità del filamento. Quindi si è deciso di aumentare il fan speed (test 4). In questo caso i range di valori del diametro erano accettabili (1,7 - 2,0 mm) ed era possibile il ritiro della bobina.

Inoltre, è stato necessario diminuire gli intervalli di variazione del diametro per evitare la produzione di filamenti con diametro maggiore di 1.8mm, non stampabili. Così, si è deciso di aumentare la temperatura e valutare la risposta ottenuta (test 5). Per questa prova, il range di valori trovati per i diametri è effettivamente ridotto, con una variazione tra 1,5 - 1,9 mm, in più è stato possibile produrre un filamento continuo.

Infine, durante la prova 6 si è deciso di continuare ad aumentare la temperatura nuovamente, nel tentativo di proseguire la riduzione dei diametri del filamento prodotti. Il cambiamento del diametro non è stato significativo per cui i risultati sono simili a quelli del test 5. A seguito delle diverse prove effettuate è stata scelta la configurazione della prova 5, poiché sono stati ottenuti i migliori risultati. In più fu possibile garantire una produzione continua sia per il 30%wt rPP sia per il 40%wt rPP.



(a)



(b)

Figure 11: Filamenti prodotti per entrambe le proporzioni con la migliore configurazione. (a) 30%wt rPP. (b) 40 %wt rPP.

La figura 11 mostra i due filamenti prodotti. Per entrambi i filamenti è stata osservata, attraverso un'ispezione visiva, la presenza di zone sul filamento in cui la

rugosità aumenta in modo significativo. Tali zone potrebbero essere correlate alla presenza del materiali riciclato e alla sua intrinseca eterogeneità, le quali risultano impossibile da eliminare completamente. In queste aree l'aumento di diametro è un parametro significativo nel generare problemi per la stampante.

Per validare i risultati ottenuti è stata analizzata la morfologia della superficie dei filamenti attraverso osservazioni SEM, che hanno permesso anche la valutazione del diametro degli stessi. Le figure 12 e 13 mostrano i risultati per le miscele contenenti il 30 e il 40 %wt, rispettivamente, di rPP. Entrambe le figure mostrano due tipi di misurazione per validare i valori di diametro ottenuti.

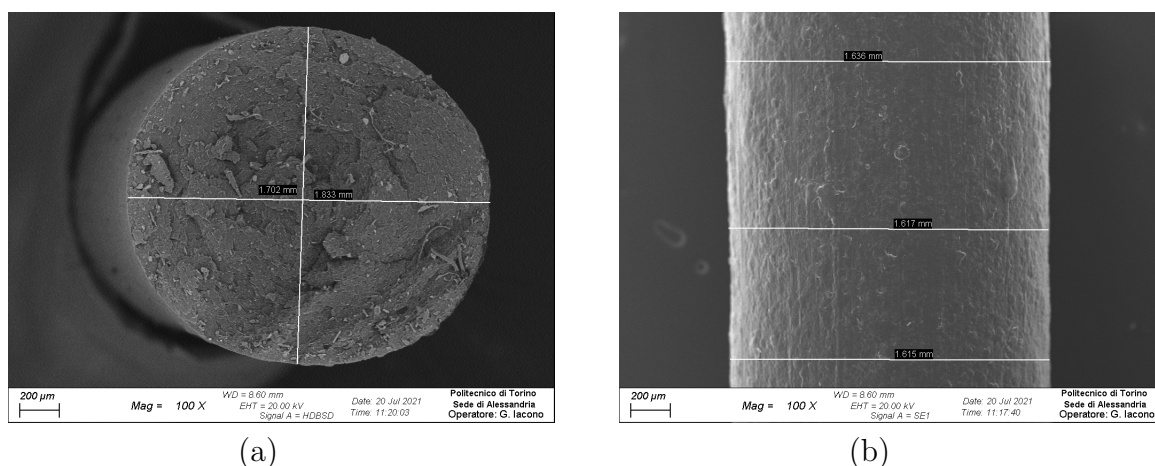


Figure 12: Risultati del test SEM a 30 %wt rPP. (a) Vista superiore (b) Vista laterale.

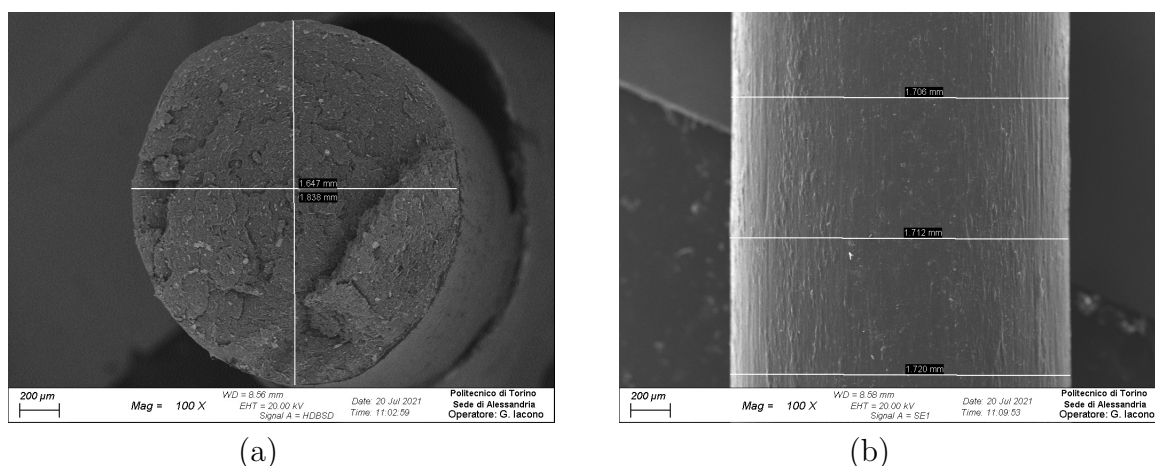


Figure 13: Risultati del test SEM a 40 %wt rPP. (a) Vista superiore (b) Vista laterale.

La differenza tra i due raggi (1.702 mm e 1.833 mm) è molto piccola, con un 7% di errore relativo. Tuttavia, come si vede nella figura 12 (a), il filamento non è perfettamente circolare. Come accennato in precedenza, la superficie del filamento non è liscia. La differenza tra il valore massimo e minimo è inferiore a 0,02 mm, ciò rappresenta una variazione minima.

Nel caso del 40%wt di rPP, figura 13 (a), la differenza tra i due raggi (1.647 mm e 1.838 mm) è leggermente maggiore. Tuttavia, l'errore relativo è solo del 10%, il quale è accettabile come tolleranza. Come nel caso precedente, il filamento presenta una matrice continua senza zone vuote.

In entrambi i casi, il filamento ha soddisfatto tutti i requisiti per essere utilizzato nella stampa 3D. Come nei casi precedenti, è stato effettuato un test reologico per evidenziare il comportamento del materiale dopo un nuovo processo termico.

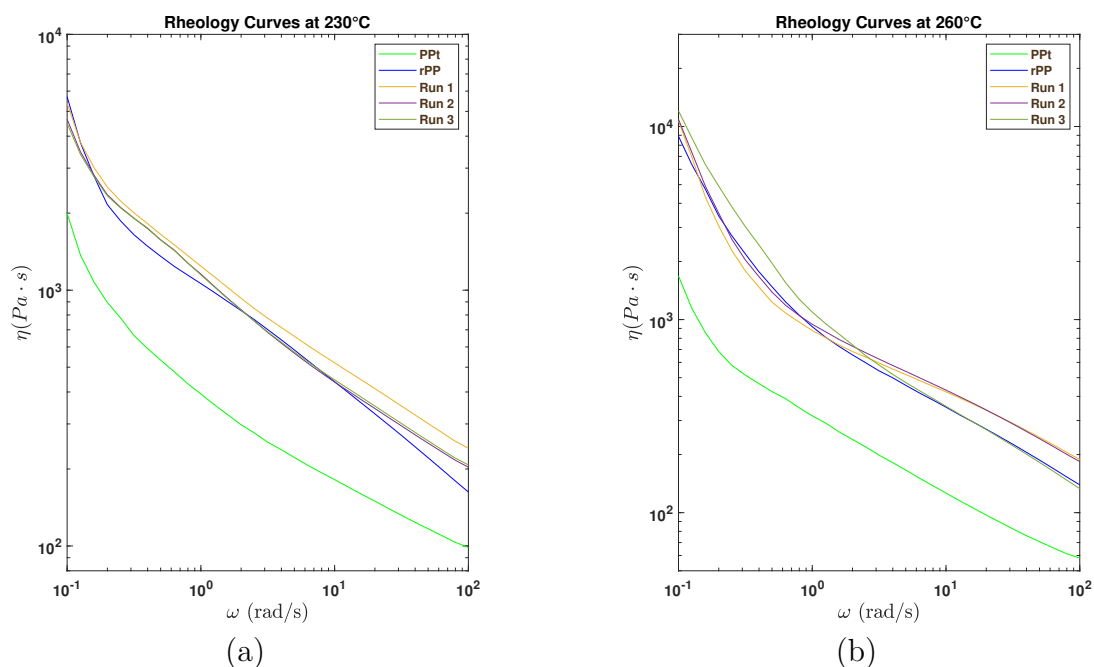


Figure 14: Confronto tra i risultati della prima e della terza fase (30%wt rPP). (a) Curva di viscosità a 230 °C. (b) Curva di viscosità a 260 °C.

La figura 14 mostra i risultati per il filamento con 30%wt rPP, confrontandoli con i risultati ottenuti nella prima fase. In questo stadio, sono stati valutati tre diversi campioni. Tutti i campioni mostrano un comportamento marcatamente non newtoniano, con una tendenza simile al rPP. Inoltre, la tabella 12 mostra i risultati ottenuti per tutti i campioni ad entrambe le temperature. L'intervallo dello Yield Stress fu tra 297 - 331 Pa a 230°C mentre 575 - 916 Pa a 260°C.

A bassa temperatura, i campioni mostrano un andamento analogo. Tuttavia,

alle alte temperature, la variazione tra i loro valori è rilevante. La media per entrambe le temperature è rispettivamente di $312,3 \pm 17,2$ Pa e $712,5 \pm 179,5$ Pa. Rispetto ai risultati delle fasi precedenti, i risultati mostrano una maggiore omogeneità tra di loro, il che permette di ottenere una ridotta dispersione tra i valori raccolti.

Sample	Symbol	Value	Unit
Run 1	$\sigma_{T=230\text{ }^\circ\text{C}}$	331,23	Pa
	$\sigma_{T=260\text{ }^\circ\text{C}}$	575,27	Pa
Run 2	$\sigma_{T=230\text{ }^\circ\text{C}}$	307,86	Pa
	$\sigma_{T=260\text{ }^\circ\text{C}}$	646,67	Pa
Run 3	$\sigma_{T=230\text{ }^\circ\text{C}}$	297,74	Pa
	$\sigma_{T=260\text{ }^\circ\text{C}}$	915,73	Pa

Table 12: Risultati trovati per lo Yield Stress per il filamento a 30 %wt rPP.

La figura 15 mostra i risultati per il filamento con 40%wt rPP. A 230°C, tutti i campioni mostrano un aumento significativo dei valori di viscosità.

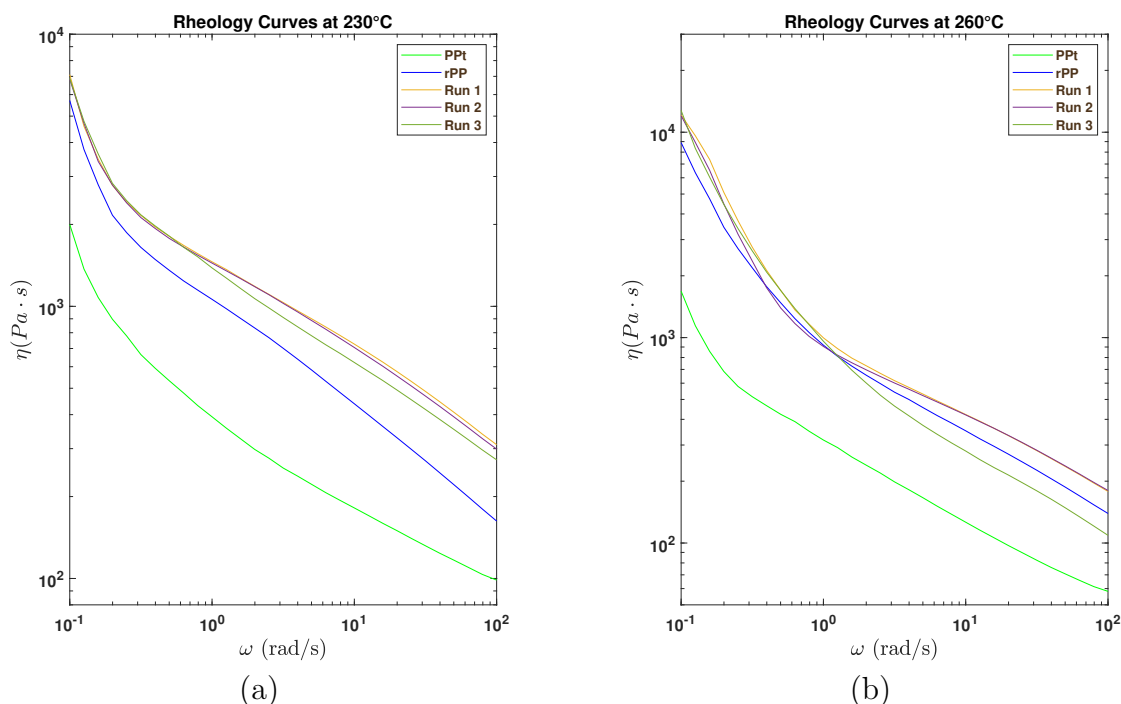


Figure 15: Confronto tra i risultati della prima e della terza fase (40%wt rPP). (a) Curva di viscosità a 230 °C. (b) Curva di viscosità a 260 °C..

Questo effetto potrebbe generare problemi per la stampa 3D poichè a valori di viscosità più elevati l'energia necessaria per estrarre il materiale aumenta. Tuttavia, la relazione (differenza) tra viscosità alle alte e basse frequenze non è cambiata in modo significativo (diminuisce). A bassa frequenza, la curva di viscosità mostra una forte pendenza che indica un marcato comportamento non newtoniano, in più gli andamenti in tutti i casi sono stati maggiore della curva rPP. In generale, i campioni mostrano un andamento analogo, il quale dimostra una omogeneità nei risultati.

Sample	Symbol	Value	Unit
Run 1	$\sigma_{T=230\text{ }^{\circ}C}$	418,26	Pa
	$\sigma_{T=260\text{ }^{\circ}C}$	855,47	Pa
Run 2	$\sigma_{T=230\text{ }^{\circ}C}$	410,94	Pa
	$\sigma_{T=260\text{ }^{\circ}C}$	743,10	Pa
Run 3	$\sigma_{T=230\text{ }^{\circ}C}$	441,86	Pa
	$\sigma_{T=260\text{ }^{\circ}C}$	847,31	Pa

Table 13: Risultati trovati per lo Yield Stress per il filamento a 40 %wt rPP.

Infine, la tabella 13 mostra i valori di Yield Stress per entrambe le temperature. La prima cosa da evidenziare è stata la mancata variazione nel comportamento non newtoniano dovuto al processo di produzione del filamento. Addirittura, è stato possibile aumentare nuovamente questo comportamento.

A 230°C, si trova un intervallo ristretto di valori di Yield Stress con media di $423,7 \pm 16,1$ Pa, mentre a 260°C, viene visualizzato un intervallo ampio con media di $815,2 \pm 62,5$ Pa.

Infine, è stato ottimizzato ed eseguito il processo di stampa. Durante questo ultimo stadio, sono stati condotti diversi test per ottimizzare i parametri di processo in modo da ottenere bassa rugosità e basso ritiro della parte stampata. Tuttavia, il processo sperimentale ha fatto in modo di definire e comprendere l'effetto dei parametri più rilevanti coinvolti nel processo di stampa come extruder temperature, bed temperature, infill e adesione tra i layers (tabella 14).

Factor	Range	Case 1	Case 2	Case 3
Extruder Temperature (°C)	200 - 280	280	280	280
Bed Temperature (°C)	23 - 70	30	50	70
Infill (%)	100 - 200	100	100	100

Table 14: Valori dei parametri utilizzato per il processo di stampa.

Come accennato nella terza fase, entrambi i filamenti (30%wt e 40%wt rPP)

hanno mostrato una rugosità significativa. In alcune sezioni, questa variazione causa un aumento del diametro al di fuori del valore di diametro di riferimento (1,5 - 1,8 mm). I risultati sperimentali hanno mostrato che a bassa temperatura (230°C), la variazione di diametro ostacola l'estrusione. Di altra parte, con il blend a 40%wt rPP è stato impossibile realizzare un processo a questa temperatura.

Aumentando la temperatura (>260°C) si riduce l'effetto prima menzionato, aumenta la fluidità, in più aumenta l'adesione tra gli strati. Si è dunque trovato un compromesso tra temperatura e adesione. E' stato individuato un altro parametro coinvolto nella adesione tra i layers cioè la temperatura del letto. Aumentando questo parametro si ottiene una migliore adesione tra gli strati poiché si riduce il flusso di calore tra l'ambiente circostante e il prodotto stampato. Per entrambi i filamenti, le alte temperature del letto aumentano l'adesione sufficiente a generare il problema menzionato prima.

Successivamente, sono stati determinati gli effetti della velocità e della percentuale di riempimento. È stato riscontrato che l'alta velocità genera una scarsa adesione e zone vuote. Inoltre, il perimetro esterno perde dimensione e forma. Una possibile ragione per i problemi menzionati potrebbe essere trovata nell'eccessiva variazione di diametro e alla rugosità di entrambi filamenti.

Insomma, la combinazione di tutti parametri prima menzionati dipenderà dalla percentuale di rPP. Ad esempio, La migliore combinazione di entrambe le temperature si aveva nel caso 2 (280°C e 50°C) a 40%wt rPP, mentre al 30%wt rPP i migliori parametri di combinazione si sono riscontrati nel caso 1 (280°C e 50°C). In ogni caso, con i parametri sopra citati, fu stato possibile eseguire la stampa continua.

Le figure 16 e 17 mostrano due viste isometriche sullo stampato. La prima figura mostra i risultati trovati per il 30%wt rPP mentre la seconda mostra quelli di 40%wt rPP

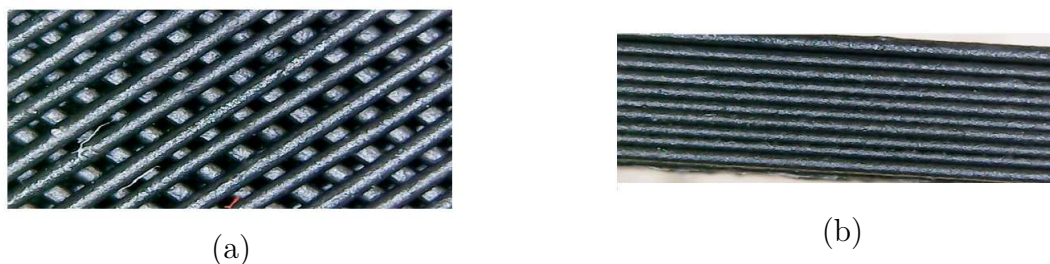


Figure 16: Risultato della microscopia ottica per la miscela a 30%wt rPP a 260 °C. (a) Fill pattern. (b) Vista frontale della stampa.

Per valutare le proprietà meccaniche delle parti stampate, i provini sono stati sottoposti a test di trazione. La figura 18 mostra i risultati ottenuti per i due blend. Sono stati valutati 4 campioni per ogni blend e sono stati ricavati il modulo

elastico, Resistenza alla trazione, allungamento massimo e la resistenza prima di frattura.

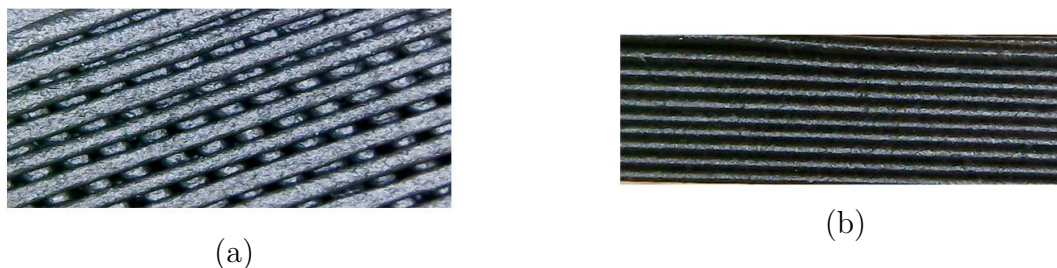


Figure 17: Risultato della microscopia ottica per la miscela a 40%wt rPP a 260 °C. (a) Fill pattern. (b) Vista frontale della stampa.

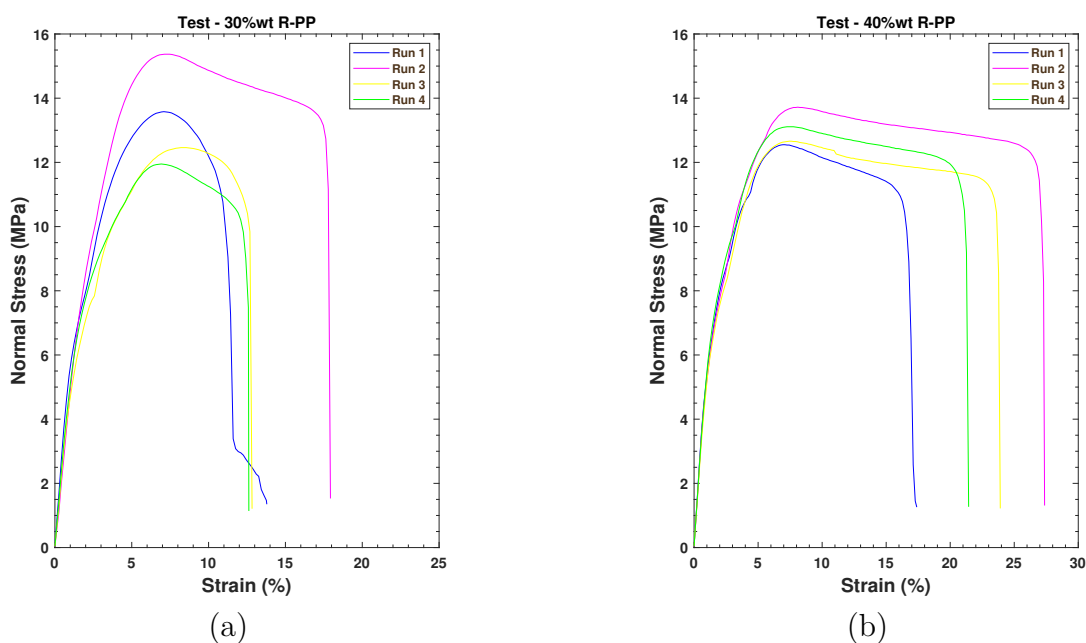


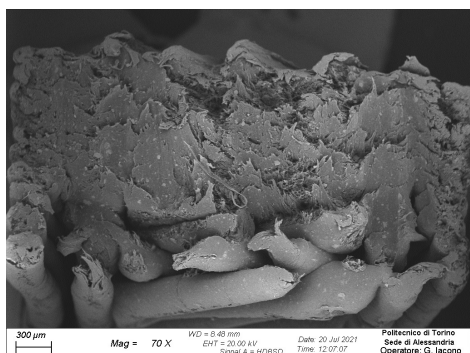
Figure 18: Prova meccanica, curva σ vs ϵ . (a) Prova meccanica per 30%wt rPP. (b) Prova meccanica per 40% peso di rPP.

Per il caso di 30%wt rPP, sono ricavati in media i seguenti valori 654 ± 100 MPa, $13,4 \pm 1,4$ MPa, $13,4 \pm 2,9$ % e $8,7 \pm 3,9$ MPa. Mentre per il 40%wt rPP sono 604 ± 22 MPa, $13 \pm 0,5$ MPa, $22,2 \pm 4,5$ % e $9,4 \pm 0,7$ MPa.

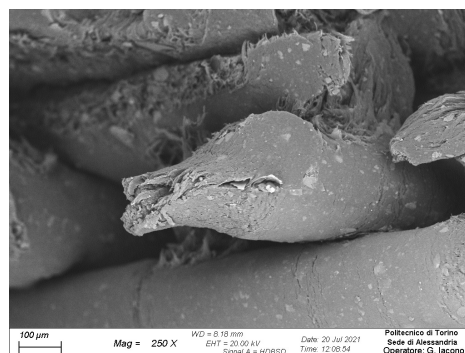
La prima differenza trovata riguarda la duttilità. In particolare, i provini a base della miscela con il 30%wt di rPP mostrano un allungamento a rottura medio del 13%, mentre i provini contenenti il 40%wt di rPP mostrano un valore del 24%. Ciò

potrebbe essere imputato al minore contenuto di PP caricato con talco nel secondo provino.

Per avere una visione del processo di stampa, si è deciso anche di eseguire dei test SEM prima e dopo il test meccanico.



(a)

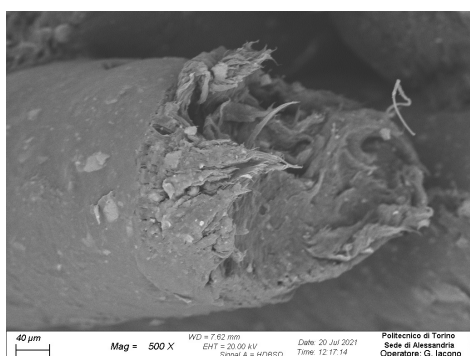


(b)

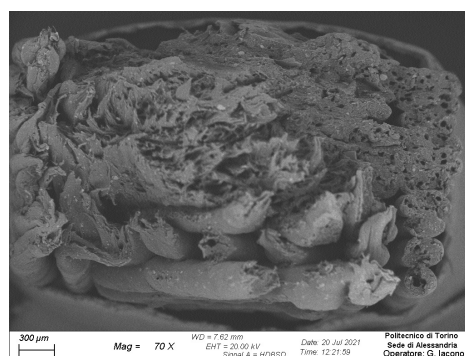
Figure 19: SEM risultati per il blend a 30 %wt rPP.

La figura 19 mostra i risultati ricavati al 30%wt rPP. La figura (a) fornisce non solo informazioni riguardo la deformazione plastica, ma fornisce anche informazioni sull'adesione dei layers. Come si nota in basso in questa figura, gli angoli di riempimento ($\pm 45^\circ$) generano un riempimento del 100%.

Inoltre, la figura (b) mostra la deformazione plastica di un singolo filamento del prodotto stampato. L'evoluzione di questo parametro nella sezione trasversale prima della rottura permette di dedurre che il materiale presenta un notevole allungamento. Tuttavia, come è visto nella prova di trazione, l'allungamento varia tra i campioni.



(a)



(b)

Figure 20: SEM risultati per il blend a 40 %wt rPP.

Infine, la figura 20 mostra i risultati al 40%wt rPP. E' stato possibile notare

due diversi tipi di deformazione, plastica e fragile. Queste due deformazioni si ritrovano a sinistra in basso per la zona plastica mentre a destra in alto per la zona fragile. La differenza tra i due modi di rottura riguarda la reazione del materiale alla trazione.

La figura (a) mostra una singola rottura del filamento. La riduzione dell'area della sezione trasversale ha un comportamento analogo al caso del 30%wt rPP.

Summary

This thesis is related to developing new materials for Additive Manufacturing. A common problem around the world is plastic waste and its issues to reuse it. For that reason it was decided to research the possible use of it in the new manufacturing process (FDM).

The most common plastic waste is derived that Polypropylene (PP). For that reason, this research was focused on it.

The experimental process was divided into four different stages, in which it was looked for understanding and evaluating the rheological behavior that allows the blend to use in 3D Printing. The objective was to maximize the non-Newtonian behavior of the blend at low frequencies, which avoids the different phenomena that limited the use of recycled material on 3D Printing. It was confirmed the potential of using recycled material in 3D Printing. Through experimental and optimization processes, it was been able to print two blends at different ratios of rPP (recycled Polypropylene). Both blends exhibited enough non-Newtonian behavior and mechanical performance.

Acknowledgements

First of all, I would like to express my sincere gratitude to Politecnico di Torino for letting me be part of this incredible University and fulfill this dream. Further, I would like to thank my supervisors Ph.D. Rossella Arrigo and Ph.D. Alberto Frache for their thoughtful support, comments, recommendations, and guidance during research.

Moreover, I would like to say a special thank you to MSc. Fulvia Cravero and MSc. Giulia Bernagozzi for their support, patience, advice, and guidance during the experimental process. It has been a great experience working alongside you.

It is impossible to extend enough thanks to my family, especially my parents and brothers, who gave me encouragement, advice, and support throughout this process. I could not have completed this work without the unwavering support.

A debt of gratitude also to Ph.D. Cesar Diaz and Ph.D. Student Gustavo Ramirez, who gave me their support and patience to finish this document.

To my friends, this would have been a more difficult feat without you. Thank you all for your unwavering, support, advice, and for reminding me of the significant things.

Finally, I would like to thank God, for letting me through all the difficulties, and dedicate this new academic achievement to my grandmother Virginia Cadena, I hope that, wherever you are, you feel proud. It has been a challenging process, there was mourning, suffering, crying, but it has been learned a lot.

*“Our greatest weakness lies in giving up. The most certain way to succeed is
always to try just one more time”
Thomas A. Edison*

Table of Contents

List of Tables	XXVIII
List of Figures	XXX
1 Introduction	1
2 State of the Art	3
2.1 Additive Manufacturing - 3D Printing	3
2.1.1 Materials of AM	6
2.1.2 Commodities of AM	7
2.2 Fused Deposition Modeling - FDM	9
2.2.1 Polypropylene - PP	12
2.2.2 Reinforcement Materials	14
2.2.3 Recycled Polypropylene	15
2.2.4 Challenges of FDM	15
3 Experimental Designs	17
3.1 Design of Experiments DoE	17
3.1.1 The six steps of experimental design	17
3.2 Experimental Methods	18
3.2.1 Mixture Method	19
3.2.2 Taguchi Method	19
3.2.3 Factorial Method	20
3.2.4 Fractional Factorial Method	20
3.3 Matlab	20
3.3.1 Function - <i>fmincon</i>	21
3.3.2 Fitting	22
4 Experimental Process	25
4.1 Materials	26
4.2 Compound Preparation	28

4.2.1	Mini-Extruder and Hydraulic Press	28
4.3	Extrusion	29
4.3.1	Level and Factors	30
4.3.2	Taguchi's Arrays	30
4.3.3	Thermo Fisher Extruder	31
4.4	Filament	33
4.4.1	Fillament Extruder - 3Devo	33
4.5	3D Printing	34
4.5.1	3D Printing - Roboze One & software Simplify 3D	34
4.6	Characterization Analysis	37
4.6.1	Rheological Test	37
4.6.2	Differential Scanning Calorimetry - DSC	39
4.6.3	Thermal Gravimetric Analysis - TGA	40
4.6.4	Mechanical Test	41
4.6.5	Optical Microscope Test	42
4.6.6	Scanning Electron Microscope - SEM	42
5	Experimental Results	44
5.1	First stage	44
5.1.1	Rheology Test Results	47
5.1.2	Thermal Gravimetric Analysis - TGA Results	51
5.1.3	Differential Scanning Calorimetry - DSC Results	54
5.2	Second stage	58
5.2.1	Rheology Test Results	58
5.2.2	Taguchi Test Results	61
5.2.3	Final selection	64
5.3	Third stage	66
5.3.1	SEM results - Filament	68
5.3.2	Rheology results	74
5.4	Fourth stage	78
5.4.1	Rheology Results	79
5.4.2	Optical Microscopy Results - Printed	81
5.4.3	SEM Results - Printed	84
5.4.4	Mechanical Test Results	86
6	Conclusion	88
	Bibliography	90

List of Tables

1	Rapporti utilizzati per i diversi blends.	iii
2	Yield Valori di sollecitazione per tutte le miscele a 230°C.	iv
3	Yield Valori di sollecitazione per tutte le miscele a 260°C.	iv
4	Valori dei risultati TGA per ciascuna blend.	vi
5	Principle peak values of DSC test for all blends.	viii
6	Degree of crystallinity for all blends.	viii
7	Fattori e livelli.	ix
8	Taguchi Arrays L16.	ix
9	Valori di Yield Stress per tutte le possibili configurazioni e temperature.	xi
10	Valori di Yield Stress per la selezione di tutte le Runs.	xiv
11	Parametri utilizzati per produrre il filamento per entrambe blends (30%wt e 40%wt rPP).	xiv
12	Risultati trovati per lo Yield Stress per il filamento a 30 %wt rPP.	xviii
13	Risultati trovati per lo Yield Stress per il filamento a 40 %wt rPP.	xix
14	Valori dei parametri utilizzato per il processo di stampa.	xix
2.1	AM opportunities and limitations from a technological perspective. Taken from:« <i>Economic implications of 3D printing: Market structure models in light of additive manufacturing revisited</i> »[4].	5
2.2	AM opportunities and limitations from a economic perspective. Taken from:« <i>Economic implications of 3D printing: Market structure models in light of additive manufacturing revisited</i> » [4].	5
2.3	Comparison of different 3D Printing technologies. Taken from:« <i>A Review of 3D Printing Technologies for Soft Polymer Materials</i> »[5].	5
2.4	Filling patter. Taken from: « <i>An overview of fused deposition modelling (FDM): research, development and process optimisation</i> »[3][18].	11
3.1	Documentation of function <i>fmincon</i> [39].	21
3.2	Documentation of parameters and models for constrained optimization [38].	22
3.3	Documentation of parameters and model for constrained optimization [40].	23

4.1	Technical sheet PP ISPLEN® PB 170 G2M. « <i>Taken from: Repsol Technical data Sheet</i> » [43].	26
4.2	Technical sheet Talc IMI FABI HTP1. « <i>Taken from: IMI Fabi SpA</i> » [45].	27
4.3	Technical sheet of Bretene PP by Breplast SpA. « <i>Taken from: Material data center</i> » [46].	27
4.4	Parameters process Mini-Extrude.	28
4.5	Parameters process Hydraulic Press.	29
4.6	Factors and Levels values.	30
4.7	Taguchi's Arrays L16.	31
4.8	Data Sheet Thermo Fisher Extrusion « <i>Taken from: Thermo Fisher Scientific</i> » [50].	33
4.9	Parameters and range of Filament process.	34
4.10	Values for someone parameters used to printing.	35
4.11	Data Sheet of Roboze One.	36
4.12	Parameters value used to 3D printing.	36
4.13	Parameters of Rheological Test.	38
5.1	The ratio of the mixture	44
5.2	Viscosity values at low frequency ($\omega = 0,1$)	45
5.3	Yield Stress for each base materials.	46
5.4	Viscosity values for each blend at low-frequency ($\omega = 0,1$).	48
5.5	Yield Stress values for all blends at 230°C.	49
5.6	Yield Stress values for all blends at 260°C.	50
5.7	TGA results values for each blend.	52
5.8	DSC results for PPt and rPP	55
5.9	Degree of crystallinity for PPt and rPP	56
5.10	Principle peak values of DSC test for all blends.	57
5.11	Degree of crystallinity for all blends.	57
5.12	Yield Stress values for all possible configuration and temperatures.	61
5.13	Yield Stress values for all runs selection.	65
5.14	Parameters used to produce filament for both blends (30%wt and 40%wt rPP).	67
5.15	Weight fractions (%wt) of the elements at points 1 and 2.	73
5.16	Yield Stress values for filament at 30 %wt rPP.	75
5.17	Yield Stress values for filament at 40 %wt R-PP.	77
5.18	Yield Stress values for filament at 30 %wt rPP and 40 %wt rPP.	80
5.19	Mechanical results for 30%wt rPP at 260 °C.	87
5.20	Mechanical results for 40%wt rPP at 260 °C.	87

List of Figures

1	Comportamento reologico di rPP e PPt a diverse temperature. a) Comportamento reologico a 230°C. b) Comportamento reologico a 260°C.	ii
2	Confronto delle curve di viscosità per ciascuna blend prodotto con mini-estrusore. (a) Curve di viscosità a 230°C. (b) Curve di viscosità a 260°C.	iii
3	Risultati TGA per materiali di base, PPt e rPP. (a) Perdita di massa misurata (TG). (b) Derivata di massa (DTG).	v
4	Risultati TGA per materiali di base e tutte blends. (a) Perdita di massa misurata (TG). (b) Derivato di massa (DTG).	vi
5	Risultati prova DSC. a) Ciclo di riscaldamento. b) Ciclo di raffreddamento.	vii
6	Risultati prova DSC. a) Ciclo di riscaldamento. b) Ciclo di raffreddamento.	vii
7	Confronto delle curve di viscosità per ciascuna serie prodotta con il profilo 1. (a) Curve di viscosità a 230 °C. (b) Curve di viscosità a 260 °C.	x
8	Confronto delle curve di viscosità per ciascuna serie prodotta con il profilo 1. (a) Curve di viscosità a 230 °C. (b) Curve di viscosità a 260 °C.	x
9	Principali effetti per i parametri di estrusione. (a) Yield Stress a 230 °C. (b) Yield Stress a 260 °C.	xii
10	Curva di viscosità per tutte le prove selezionate a) Curva di viscosità a 230 °C. b) Curva di viscosità a 260 °C.	xiii
11	Filamenti prodotti per entrambe le proporzioni con la migliore configurazione. (a) 30%wt rPP. (b) 40 %wt rPP.	xv
12	Risultati del test SEM a 30 %wt rPP. (a) Vista superiore (b) Vista laterale.	xvi
13	Risultati del test SEM a 40 %wt rPP. (a) Vista superiore (b) Vista laterale.	xvi

14	Confronto tra i risultati della prima e della terza fase (30%wt rPP). (a) Curva di viscosità a 230 °C. (b) Curva di viscosità a 260 °C.	xviii
15	Confronto tra i risultati della prima e della terza fase (40%wt rPP). (a) Curva di viscosità a 230 °C. (b) Curva di viscosità a 260 °C.. . . .	xviii
16	Risultato della microscopia ottica per la miscela a 30%wt rPP a 260 °C. (a) Fill pattern. (b) Vista frontale della stampa.	xx
17	Risultato della microscopia ottica per la miscela a 40%wt rPP a 260 °C. (a) Fill pattern. (b) Vista frontale della stampa.	xxi
18	Prova meccanica, curva σ vs ϵ . (a) Prova meccanica per 30%wt rPP. (b) Prova meccanica per 40% peso di rPP.	xxi
19	SEM risultati per il blend a 30 %wt rPP.	xxii
20	SEM risultati per il blend a 40 %wt rPP.	xxii
2.1	Additive manufacturing process. Taken from: <i>«An overview of fused deposition modelling (FDM): research, development and process optimisation»</i> [3].	4
2.2	(a) Categories of thermoplastics (b) Kiviat diagram for polymer properties. Taken from: <i>«Polymer-based filament feedstock for additive manufacturing»</i> [8].	7
2.3	State of the industry 2020. Taken from: <i>«2020 Report. Analysis Trends Forecast. Feel the pulse of the 3D printing industry»</i> [16].	9
2.4	Schematic diagrams of FDM. Taken from: <i>«Additive manufacturing (3D printing): A review of materials, methods, applications and challenges»</i> [1][17].	10
2.5	Schematic parameters and path of FDM. Taken from: <i>«Fused deposition modeling with polypropylene»</i> [19].	12
2.6	Molecular structure from propylene monomer. Taken from: <i>«Creative mechanisms Blog. All about Polypropylene (PP) plastic»</i> [21].	12
2.7	Tacticity of PP. Taken from: <i>«British plastic federation. Polypropy- lene (PP)»</i> [22].	13
4.1	Steps of experimental process.	25
4.2	Mini-Extruder Xplore MC 15. <i>«Taken from: Brochure of Xplore MC 15 micro compounder»</i> [48].	28
4.3	Hydraulic Press Collin P200T [49].	29
4.4	Process 11 Thermo Fisher Scientific. <i>«Taken from: Thermo Fisher Scientific»</i> [50].	31
4.5	Blueprint of assembly by Process 11 Thermo Fisher Scientific. <i>«Taken from: Thermo Fisher Scientific»</i> [50].	31
4.6	Screw Profile - Blueprint <i>«Taken from: Thermo Fisher Scientific»</i> [50].	32

4.7	3Devo Filament Machine. (1) Control Panel (2) Hopper (3) Extruder (4) Cooling (5) Diameter sensor (6) Positioner (7) Winder. « <i>Taken from: 3Devo Filament makers</i> » [51].	34
4.8	Roboze One. « <i>Taken from: Roboze Print Strong Like Metal</i> » [52].	35
4.9	Rheometer Ares TA Instruments.	37
4.10	DSC machine [54].	40
4.11	TGA TA Instruments.	40
4.12	Instron series 5966. « <i>Taken from: Instron 5960 Series Dual Column table frames System</i> » [55].	41
4.13	Optical Microscope. « <i>Taken from: Techmate enabling science</i> » [56].	42
4.14	Scanning Electron Microscope - SEM [41].	43
5.1	Rheological behavior of PPt and rPP at different temperatures. a) Rheological behavior at 230°C. b) Rheological behavior at 260°C . .	45
5.2	Rheological curves at different temperatures and fitting. a) Rheological curves at 230°C and fitting model. b) Rheological curves at 260°C and fitting model.	46
5.3	Comparison of rheological curves for each blend produced with mini-extruder. (a) Rheological curves at 230°C. (b) Rheological curves at 260°C.	47
5.4	Comparison between the rheological curves at 230°C, between base materials an mixtures produced with mini-extruder. (a) 50 %wt rPP. (b) 40 %wt rPP. (c) 30 %wt rPP. (d) 20 %wt rPP. (e) 10 %wt rPP.	49
5.5	Comparison between the rheological curves at 260°C, between base materials an mixtures produced with mini-extruder. (a) 50 %wt rPP. (b) 40 %wt rPP. (c) 30 %wt rPP. (d) 20 %wt rPP. (e) 10 %wt rPP.	50
5.6	TGA results for base materials, PPt and rPP. (a) Loss of mass measured (TG). (b) Derivative of mass (DTG).	51
5.7	TGA results for base materials and all blends. (a) Loss of mass measured (TG). (b) Derivative of mass (DTG).	52
5.8	Thermogravimetric analysis results of each mixtures. (a) 50 %wt rPP. (b) 40 %wt rPP. (c) 30 %wt rPP. (d) 20 %wt rPP. (e) 10 %wt rPP.	53
5.9	Derivative thermogravimetric analysis results of each mixtures. (a) 50 %wt rPP. (b) 40 %wt rPP. (c) 30 %wt rPP. (d) 20 %wt rPP. (e) 10 %wt rPP.	54
5.10	a) Heating Cycle b) Cooling Cycle	55
5.11	a) Heating Cycle. b) Cooling Cycle	56
5.12	Comparison of rheological curves for each run produced with profile 1. (a) Rheological curves at 230 °C. (b) Rheological curves at 260 °C.	59
5.13	Comparison of rheological curves for each run produced with profile 2. (a) Rheological curves at 230 °C. (b) Rheological curves at 260 °C.	60

5.14	Main effects for Extrusion parameters. (a) Average of Yield Stress at 230 °C. (b) Average Yield Stress at 230 °C.	62
5.15	Main effects for SN ratios of Extrusion parameters. (a) SN of Yield Stress at 260 °C. (b) SN of Yield Stress at 260 °C.	63
5.16	Viscosity curve for all runs selected a) Viscosity curve at 230. b) Viscosity curve at 260.	64
5.17	Comparison between First stage and Second stage results a) Complex viscosity curve at 230 °C. b) Complex viscosity curve at 260 °C. . .	66
5.18	Filaments produced for both proportion with the best configuration. (a) 30%wt rPP. (b) 40 %wt rPP.	68
5.19	Top view of filament at 30 %wt rPP.	69
5.20	Side view of filament at 30 %wt rPP.	70
5.21	Side view of filament at 40 %wt rPP.	71
5.22	Side view of filament at 40 %wt rPP.	72
5.23	AA.	73
5.24	Comparison between First stage and third stage results (30%wt rPP). (a) Complex viscosity curve at 230 °C. (b) Complex viscosity curve at 260 °C.	74
5.25	Comparison between First stage and third stage results (30%wt R-PP). (a) Complex viscosity curve at 230 °C. (b) Complex viscosity curve at 260 °C.	75
5.26	Comparison between First stage and third stage results (40%wt rPP). (a) Complex viscosity curve at 230 °C. (b) Complex viscosity curve at 260 °C.	76
5.27	Comparison between First stage and third stage results. (a) Complex viscosity curve at 230 °C. (b) Complex viscosity curve at 260 °C. . .	77
5.28	Comparison of rheological curves between First Stage and Four Stage . (a) Rheological curves at 260 °C for 30%wt rPP. (b) Rheological curves at 260 °C for 40%wt.	79
5.29	Rheological curves for 30%wt R-PP. (a) Run 1 . (b) Run 2.	80
5.30	Rheological curves for 40%wt rPP. (a) Run 1. (b) Run 2.	81
5.31	Optical Microscopy result for blend at 30%wt rPP at 260 °C. (a) Top view of printing. (b) Fill pattern. (c) Front view of printing. . .	82
5.32	Optical Microscopy result for blend at 40%wt rPP at 260 °C. (a) Top view of printing. (b) Fill pattern. (c) Front view of printing. . .	83
5.33	SEM results for blend at 30 %wt rPP.	84
5.34	SEM results for blend at 40 %wt rPP.	85
5.35	Mechanical Test, σ vs ϵ curve. (a) Mechanical Test for 30%wt rPP. (b) Mechanical Test for 40%wt rPP.	86

Chapter 1

Introduction

Nowadays, a significant issue around the world is plastic waste. Academic research and industries are focusing on developing products based on recycling and virgin material. Although, there are critical topics right now that the traditional techniques cannot give a correct approach. For that reason, a new process, like Additive Manufacturing, has taken a relevant development in the last years. Additive manufacturing (AM) is overgrowing, and it is forecasted to expand even more in the following years. In the first moment, it was developed as rapid prototyping. Nowadays, this process is being used to replace traditional methods and produce final products. It is here an enormous possibility to work and research on it.

The scope of research was obtaining a proportion between recycling plastic and virgin material, which must be able to be used in FDM. The object was to use a broad amount of recycled material without cutting down the mechanical, physical, and chemical properties. For that reason, it was decided to divide this study into four steps, such as compounding, extrusion, filament, and 3D Printing.

The first step was studying the rheological and thermal behavior for different ratios of recycled material (R-PP). It was possible to determine the characteristic temperatures and the parameter that governance the non-Newtonian behavior. As a result, it was chosen the blends which exhibit the maximum Yield Stress.

Then, the second step was related to the extrusion process. Throughout an optimization was found condition process in which the non-Newtonian behavior is maximized. This stage was divided into two parts. The former was evaluated the rheological behavior at diverse condition processes through Taguchi's method. The latter produced a continuous process for the condition in which non-Newtonian behavior is maximized.

The third step was to produce a filament for blends chosen in the previous processes. Several experimental was carried out where understand the effect of the parameters process. As a result, it obtained a continuous filament, with a diameter range between 1,5 to 1,9 mm.

Finally, it was carried out the printing process. In this step was analyzed the possibility to employ in FDM the filaments produced. Then, it was found the parameter in which adhesion was maximized and shrinkage was minimized. As a result, it was obtained a printed for two blends. Furthermore, this pieces was mechanical characterized.

Chapter 2

State of the Art

This chapter is showed a state the art of Additive Manufacturing (AM) and is subdivided into two sections, such as Additive manufacturing and Fused deposition Modeling. The former included a brief resume of AM and showed the different types of materials and products. The latter focused on one specific methodology and one type of material (PP).

2.1 Additive Manufacturing - 3D Printing

Additive manufacturing (AM), also known as 3D Printing, is a technique for produce structures with complex geometries and high resolutions. The process consists of printing the object with successive layers of material [1].

AM has been used to produce aesthetic and functional prototypes due to their low cost and time production. However, in the last 30 years, this technology has been fully applied in various industries to produce end-user products. The growing and adapting of AM systems over traditional techniques are attributed to producing complex geometry with high precision, flexibility in design, and product customization [2].

This type of manufacturing process can be categorized into three different groups. These groups, based on state of raw material, are powder, liquid and solid. Figure 2.4 shows a brief organizational chart that presented whole techniques and highlights the technique that was used in this project.

However, this is not the only way to classify AM methods. According to the American Society for Testing and Materials (ASTM), there are five families, which are: (1) Stereolithography (SLA), (2) Selective Laser Melting (SLM), (3) Fused Deposition Modeling (FDM), (4) Material Jetting (MJ), and (5) Sheet lamination.

The processes mentioned have specific features and materials to build a product[3].

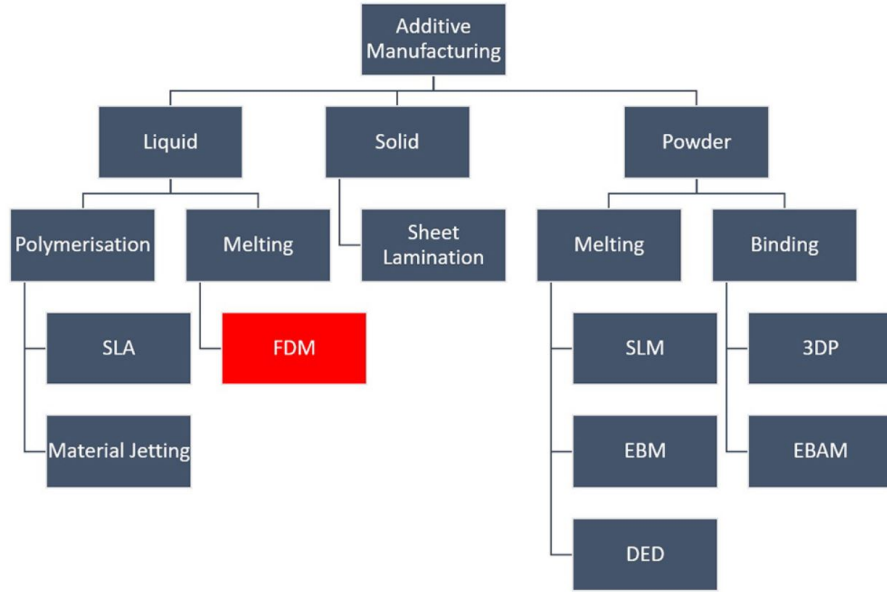


Figure 2.1: Additive manufacturing process. Taken from: *«An overview of fused deposition modelling (FDM): research, development and process optimisation»*[3].

As a mention above, one of the main advantages of the additive method is the rapid prototyping and enhancing mechanical properties of products. A study by Weller et al. evaluated the impact of AM technology at the industry level. According to the authors, the advantages of AM in the market are customization, flexibility, design, acceleration and simplification of innovation, local production, and cost. Moreover, it is a method that is cataloged like a green process by the capacity to reduce waste and optimize the process of the build. Although, there are several number of limitations, such as marginal production cost, skilled labor, speed, materials, quality standards, technological feasibility, intellectual property, build speed, etc.

Tables 2.1 and 2.2 summarizes the opportunities and limitations from a technological and economic perspective [4].

In the case of polymers, it is relevant to highlight that not all of the techniques mentioned above are available. However, a study by Zhou et al. shows a brief comparison between families mention above in which polymers could be used. From the table 2.3, we can show that polymers showed a great range of parameters that could attract different markets, like the resolution or materials[5].

Moreover, thermoplastic polymers are the most common material in AM process. While the limits of polymers are not only related to the mentioned previously, but also with the mechanical properties, materials, and dimensional accuracy.

Technological Perspective	
Opportunities	Limitations
Direct digital manufacturing of 3D product designs without the need for tools or molds	Solution space limited to "printable" materials and by size of build space
Change of product designs without cost penalty in manufacturing	Quality issues of produced parts: limited reproducibility of parts, missing resistance to environmental influences
Increase of design complexity	Significant efforts are still needed for surface finishing
High manufacturing flexibility: objects can be produced in any random order without cost penalty	Lacking design tools and guidelines to fully exploit possibilities of AM
Production of functionally integrated designs in one-step	Low production throughput speed
Less scrap and fewer raw materials required	Skilled labor and strong experience needed

Table 2.1: AM opportunities and limitations from a technological perspective. Taken from: *«Economic implications of 3D printing: Market structure models in light of additive manufacturing revisited»* [4].

Economic Perspective	
Opportunities	Limitation
Acceleration and simplification of product innovation	High marginal cost of production (raw material costs and energy intensity)
Price premiums can be achieved through customization or functional improvement of products	No economies of scale
Customer co-design of products without incurring cost penalty in manufacturing	Missing quality standards
Resolving "scale-scope dilemma": no cost penalties in manufacturing for higher product variety	Product offering limited to technological feasibility (solution space, reproducible, quality, speed)
Reduction of assembly work with one-step production of functional products	Intellectual property rights and warranty related limitations
Lowering barriers to market entry	Training efforts required
Local production enabled	Skilled labor and strong experience needed
Cost advantages of low-wage countries might diminish in the long run	

Table 2.2: AM opportunities and limitations from an economic perspective. Taken from: *«Economic implications of 3D printing: Market structure models in light of additive manufacturing revisited»* [4].

Categories	Methods	Approximate build speed	Approximate maximum resolution	Suitable materials	Multimaterial ability
Power bed fusion	SLS	Good	> 100 μm	Thermoplastic polymers	Poor
	SLA	Fair	> 5 μm		Fair
	DPL	Fair	> 5 μm		Fair
Vat photopolymerization	CLIP	Good	> 100 μm	Photopolymers with low viscosity	Poor
	CAL	Good	$\approx 300 \mu m$		Poor
	TPP	Poor	> 100 nm		Poor
Material jettin	Inkjet Printing	Fair	> 10 μm	Low viscosity polymer fluids	Good
	E-jet	Fair	100 nm-10 μm		Fair
	FDM	Poor	> 100 μm		Fair
Material extrusion	DIW	Poor	1-100 μm	Curable pseudoplastic polymer fluids	Good
	EHDP	Poor	100 nm - 50 μm	Thermoplastic or soluble polymers	Fair

Table 2.3: Comparison of different 3D Printing technologies. Taken from: *«A Review of 3D Printing Technologies for Soft Polymer Materials»* [5].

Nowadays, researchers are working to solve some limits which keep this process only as a rapid prototype. The first limit is related to anisotropic behavior due to orientation of printing, the second one is to improve the range of materials that could be applied to AM methods. Finally, the last limit is the dimension of parts, if we compared to traditional processes, the size of the piece produced by AM method is modest [1].

2.1.1 Materials of AM

A systematic review, based on current researches, has shown that it is possible to use different types of materials on AM, like metal, ceramic and polymer. Each one have a distinctive characteristic and markets.

In general, metal has been used for research, prototyping, or advanced applications. It has shown an excellent perspective of growth and provides freedom for manufacturing complex geometries. Furthermore, metal on AM has been developed to provide multi-functional, protective, and insulation components. The 3D printing process of metals consists of melting metallic powder using energy sources such as a laser or an electron beam. The most common techniques for printing metals are powder bed fusion (PBF) and direct energy deposition (DED). Material like tool steels, aluminum alloys, titanium, and nickel-based alloys can be manufactured using AM process [1].

In the medical area, AM has become an essential method for manufacturing ceramics for biomaterials, like bones and teeth. The main advantage is the product customization. However, the challenge is to increase the type of materials and the accuracy of printing. The main methods of printing ceramics are inkjet, powder bed fusion, paste extrusion, and stereolithography. The difference between the printing of other materials and ceramic is that the former will require a post-processing step. This additional step consists of sintering ceramic parts to obtain the desired shape, therefore AM has a higher cost and cycle time[1].

Finally, polymers are the most common material that used on AM. The advantage of polymer is the thermoplastic behavior, which allows changing of physical state, as mentioned above. The benefit of print polymers is the ability to customize the geometry. Furthermore, the process has been more cost-effective than the traditional method.

This study emphasized in one type of AM techniques which is Fused Deposition Modeling (FDM). In this technique, the most common materials are ABS, PLA, HIPS, PC, and PA [1][6][7].

- ABS (Acrylonitrile Butadiene Styrene) is the most common thermoplastic used in 3D Printing. The main advantage is adherence whereby high-speed printing is possible.

- PLA (Polylactic Acid) is thermoplastic derived from renewable resources, which is biodegradable and compostable. The same as ABS, printing speeds are possible. The main advantages are its low viscosity and hardness. However, PLA is susceptible to heat and moisture, so it is not ideal for long-term outdoor use or high-temperature environments.
- HIPS (High Impact PolyStyrene) is a low-warp thermoplastic. It is available in a wide range of colors, and it is often used to make prototypes. The main advantage is the great dimensional stability. From the point of view of processing properties, it is very similar to ABS.
- PC (Polycarbonate) is an engineering polymer. It is used to make a part to support high loads and impacts. The main problem of it is the hygroscopic behavior.
- PA (Polyamide) or Nylon is a semi-crystalline thermoplastic which prints are flexible and wear-resistant. Unlike ABS and PLA, PA is less brittle and therefore stronger. However, it tends to warp more than ABS and PLA, and bed adhesion is problematic.

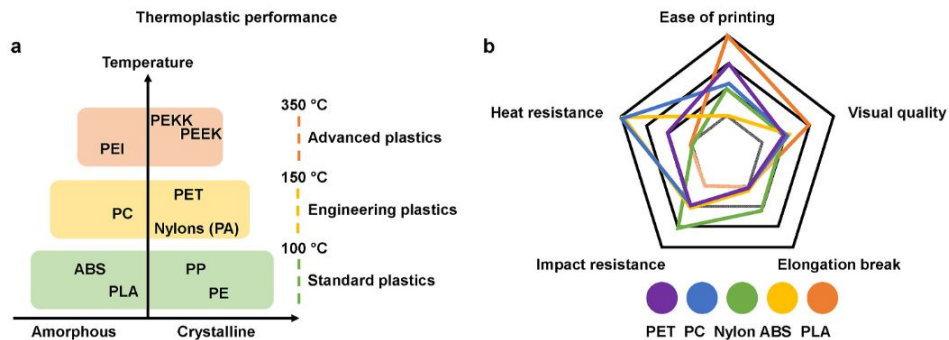


Figure 2.2: (a) Categories of thermoplastics (b) Kiviati diagram for polymer properties. Taken from: *« Polymer-based filament feedstock for additive manufacturing »* [8].

2.1.2 Commodities of AM

As mentioned above, the range of materials of 3D printing is not only limited by polymers but also can be used metals and ceramics. The idea that 3D printing is

still a developing technology and has some barriers is accepted. So the applications are limited to some products and prototypes. Various studies were conducted to analyze and estimate the potential of the process in the circular economy.

For example, the study by Hernandez et al. shows the potential of AM on industry 4.0 and highlighted the advantages of process and capabilities for reused materials [9]. Another viewpoint is presented in the study by Shekhar et al. in which the perspectives in e-commerce channels for additive manufacturing. According to the author, there are four factors (cost and revenue, environmental, sustainability, and social) for which AM processes are attractive.

According to Attrana, it is possible group the different industries which benefits from additive manufacturing as follow[10]:

1. **Aerospace**
2. **Automotive**
3. **Machine Tool Production**
4. **Healthcare and Medical**
5. **Dentistry and Dental Technology**
6. **Architectural and Construction**
7. **Retail/Apparel**
8. **Food**

In the aerospace industry, AM processes are used to prototyping and manufacture some pieces like satellite components. The goals in this area are to produce very complex geometries at low cost, supply on-demand manufacturing for astronauts, eliminate excess parts that cause drag and add weight, which reduces cost. Materials like PEEK and semi-crystalline thermoplastic polymers are used to replace light alloys (aluminum-based). Moreover, in the automotive industry, this technology began to use as prototyping to increase the speed up time to market and reduce the cost involved in product development. Nowadays, it is used to manufacture tools and print parts. An example of the former is BMW in which is printing handheld tools [11], while the latter is General Motors in which is printing parts of cars like grille [12].

Another important industry is Dentistry and Dental Technology which AM processes are used to produce prototyping and dental parts. The advantages are associated with the potential of using new material, reducing time production, and customization of end-user. In addition, there are some advantages in the medical industry, which are the possibility of printing implants and prosthetics. The goal of AM was the possibility to customize the components, which reduces the cost and the risk of post-operative complications. Now, AM is not only allowed to produce prosthetics but also the parts human body as heart or skin [11] [13] [14].

Furthermore, AM also can use in the building sector. The benefits of using AM are: reducing the cost and time to make scale models with realism and detail. On the other hand, the new developments are related to machines that could print large dimension parts. For example, a research group of Dutch scientists built a print with 6 meters of size, which can print part of 2.2 x 2.2 x 3.5 m [11].

Finally, the retail/apparel areas show an attractive and innovative market in which increasing the durability of plastic and metal accessories, reducing the supply chain, and creating a new business for small quantities in real-time is possible thanks to printing [15].

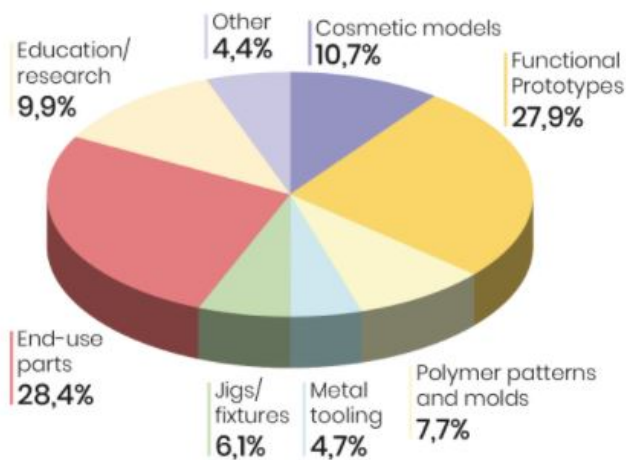


Figure 2.3: State of the industry 2020. Taken from: *«2020 Report. Analysis Trends Forecast. Feel the pulse of the 3D printing industry»* [16].

Figure 2.3 shows a pie graph in which subdivides the market. It is relevant to highlight that more than 50% of the market is related to end-used parts and functional prototypes which means the important of this technology. In addition, there is a huge percentage of market (10%) dedicated to education and research.

2.2 Fused Deposition Modeling - FDM

Fused Deposition Modeling (FDM) is an Additive Manufacturing technique whose process is based on extrusion. It was developed by Scott Crump in 1989 and has been grown up throughout the last 30 years [17]. The process starts when polymer filament is heating at the nozzle to reach a semi-liquid state and then extruded [1]. The advantage of this process is the rapid solidification of fuse filament, which

allows to grow up the structure layer by layer. Figure 2.4 shows two schematic diagram of FDM device.

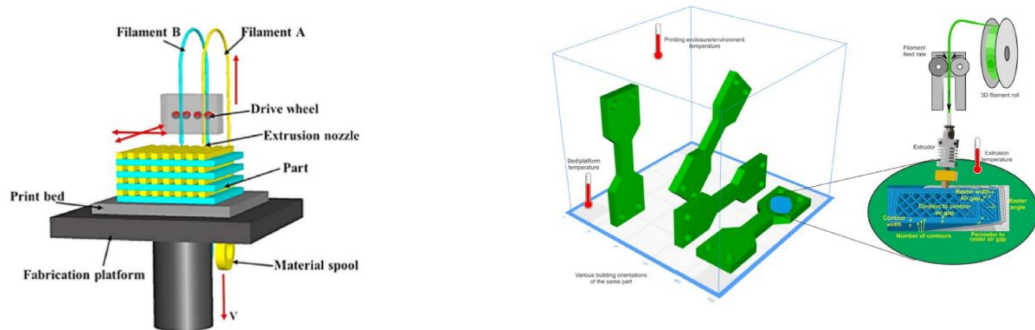


Figure 2.4: Schematic diagrams of FDM. Taken from: *«Additive manufacturing (3D printing): A review of materials, methods, applications and challenges»* [1][17].

According to different authors, it is possible to organize the main parameters of the FDM process into three groups, as follows: slicing, building orientation, and temperature conditions. The first group it's related to layer thickness/height, nozzle diameter, flow rate, deposition speed, raster orientation/angle, air gaps, and top and bottom thickness. The second one has been dependent on geometry, usually testing specimens are oriented horizontal, vertically, or laterally. Finally, the last group is linked to environmental, bed and extrusion temperature [17]. Nevertheless, these groups could be divide into eight parameters, as follows:

1. **Filling pattern**
2. **Nozzle temperature**
3. **Nozzle diameter**
4. **Bed temperature**
5. **Build orientation**
6. **Air gap**
7. **The thickness of the gap between the nozzle and bed**
8. **Raster width and raster angles**

The first parameter has been related to the mechanical properties and stiffness of the sample. A variation on the percentage of infill allows generating solid or hollow structures. Table 2.4 shows different types of shapes and geometries that could printing. The authors subdivide the patter in eight categories, such as lineal, rectilinear, cubic, star, honeycomb, curve, chords, and spiral [18].

Fill Patterns	First Mode	Second Mode	Third Mode	Fill Patterns	First Mode	Second Mode	Third Mode
Line				Concentric			
Rectilinear				Honeycomb			
Grid				3D Honeycomb			
Triangle				Hilbert Curve			
Star				Arehimedeian Chords			
Cubic				Octagram Spiral			

Table 2.4: Filling patter. Taken from: *«An overview of fused deposition modelling (FDM): research, development and process optimisation»*[3][18].

The second and third parameter concern the nozzle. In the first case, the temperature is related to the adhesion capacity as increasing the temperature carries out a good adhesion between layers. However, improving adhesion will create dis-join (dis-attack) problems. On the other hand, the size of the nozzle affects the surface quality, mechanical properties, and cycle time, usually the size of it is from 0.2 mm to 0.8 mm.

Bed temperature is a vital parameter because it prevents heat transfer and helps to bond the next layer. The range of this temperature is from 0°C to 80°C depending on the material thermal properties.

The following two parameters, build orientation and air gap, contribute to mechanical behavior. The latter is related to the chance to produce the part at diverse angles in all directions, while the former is linked to the space between layers, and it causes a fluctuation in tension strength.

Finally, the last two parameters have been related to geometrical restrictions and the velocity of the process. Modify the distance between the nozzle and bed, generate a decrease of the piece surface roughness. On the other hand, a variation in raster width and raster angles causes deformation and shrinkage of the layer.

Figure 2.5 shows a schematic view of these parameters.

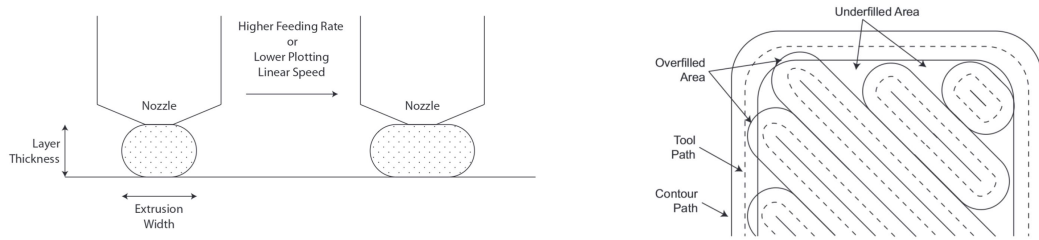


Figure 2.5: Schematic parameters and path of FDM. Taken from: *«Fused deposition modeling with polypropylene»* [19].

The main advantages of this process are the low cost, high speed, and simplicity. However, some drawbacks limit this technique, such as weak mechanical properties, poor surface quality, and a limited number of materials [1][20].

In relation to materials, the most common in FDM are PLA and ABS. However, this techniques allows to work with different types of semi-crystalline thermoplastic polymers, hence the purpose to study polypropylene and its composites.

2.2.1 Polypropylene - PP

According to different handbooks and journals, polypropylene was first polymerized in 1951 by a pair of Phillips petroleum scientists and then by Italian and German scientists Giulio Natta and Karl Rehn in 1954. It is used in different applications such as packaging for consumer products, plastic parts for various industries as automotive, textiles, aerospace, and others. The current global demand for this material generates an annual market of about 45 million tons, and it will increase to approximately 62 million tons. PP (Polypropylene) is a thermoplastic polymer made from propylene monomers. Figure 2.6 shows the chemical formula and the structure of it [21][22].

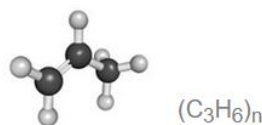


Figure 2.6: Molecular structure from propylene monomer. Taken from: *«Creative mechanisms Blog. All about Polypropylene (PP) plastic»* [21].

There are different types of PP, divided by the tacticity or orientation of the polymer chain, such as isotactic polypropylene (IPP), syndiotactic polypropylene

(sPP), and atactic polypropylene (aPP). This variation is representing a change in crystallinity, mechanical and chemical properties. Figure 2.7 shows the molecular structures of the different types of PP tactics.

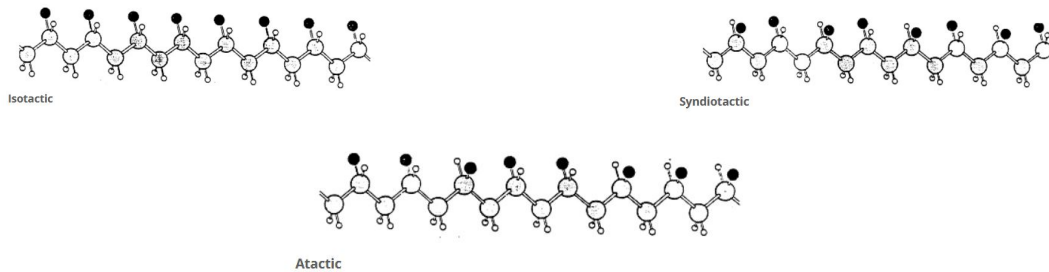


Figure 2.7: Tacticity of PP. Taken from: *«British plastic federation. Polypropylene (PP)»* [22].

Polypropylene is made from the polymerization of propylene gas in the presence of a catalyst system (Ziegler-Natta or Metallocene). The parameter for polymerization like temperature, pressure, and reactant are set according to the polymer grade to be produced [23].

Some of the most significant properties are, as follows [21][22]:

Chemical Resistance: Diluted bases and acids do not react readily with polypropylene, which makes it a good choice for containers of such liquids.

Elasticity and Toughness: Like all plastic material, PP shows an elasticity over a certain range of load, but also shows an early plastic deformation. Hence it is considering as "tough" material.

Fatigue Resistance: Polypropylene retains its shape after a lot of torsions, bending, and flexing.

Insulation polypropylene has a very high resistance to electricity and is very useful for electronic components.

Transmissivity: Polypropylene can be used for applications where some transfer of light is important or where it is of aesthetic value.

On the other hand, the disadvantages of polypropylene are [21][22]:

High thermal expansion coefficient

Susceptible to UV degradation

Poor resistance to chlorinated solvents and aromatics

Highly flammable

Susceptible to oxidation

As mention above, PP is an important commodity thermoplastic in the market attributed to its versatility. However, a review of several studies shows that ABS and PLA are the most popular materials used in 3D printing [24]. According to Bertolino et al., there are two reasons why PP is difficult to process with FDM, which are volumetric shrinkage (dimensional stability) and rheology (viscosity). As well know, PP has a high crystallinity grade, due to the isotactic macromolecular structure. However, it could be minimized by making a blended or copolymerized with other polymers [25].

Printing of semicrystalline materials is a challenge, especially when compared with regular amorphous materials such as PLA. Numerous studies have been conducted to improve the stability (chemical and physical) and widening its applications field.

2.2.2 Reinforcement Materials

As mention in the previous chapters, the main problem with AM is the material types used on it, hence it is used reinforcement material, which helps to increase the behavior and expand the material types. The most common material that is used as reinforcement are carbon and glass fiber, that increases the tensile strength and Young modulus.

Depending on the purpose of the final product there are different types of fillers including carbon nanomaterials, biomaterials, metals, and ceramics [8]. A study by Tekinako et al. highlighted the challenges associated with 3D printing fiber-reinforced composites and evaluated the potential of composite parts made from carbon fiber and ABS resin feedstock. The samples fabricated through FDM and compression molding resulted in a significant increase in strength and stiffness.

A study by Mazzanti et al. displayed the challenges of biodegradable thermoplastic and the potential to enter the market of filaments for FDM. The results showed that bio-fillers are not beneficial for some polymers (ABS and PLA), while others (polyolefins) had have positive effects. According to this research, it is possible to stand out that the reinforcement material is linked with the nature of the based material [26].

Besides, the ceramic fillers show high mechanical strength and hardness, good chemical and thermal stability, and favorable optical and electrical performances. The main reason for using them as a filler has been looking for new ways to produce them. For that reason, 3D printing has been an alternative with the fastest growing.

In the case of PP, the main problems highlight above, are related to crystallinity and rheology. Commercial PP filament produces shrinkage and warpage and has poor mechanical properties. Amumnate et al. put forward a possible solution for this, which is the fabrication of a PP filament with graphene-polylactic acid microcapsules reducing its crystallinity. This filament exhibit higher mechanical

performance than commercial PP [27].

Another example to solve the issues mention previously is the addition of fiber, which can enhance the mechanical properties of the polymer. A study by Gholamhossein et al. highlighted the challenges associated with manufacturing a composite filament and evaluated the potential of the mechanical performance [24].

Han et al. evaluated multiscale thermoplastic compounds, which were based on polypropylene reinforces with thermotropic liquid crystalline polymer and carbon nanotubes. Significant enhancement of properties was observed at different weight percentages of each one. Even more, these composites showed an advanced interfacial adhesion which resulted in an increment of tensile strength [28].

However, only a few studies had evaluated the effect to use recycled material and filler.

2.2.3 Recycled Polypropylene

Nowadays, plastic consumption is continuing to grow despite environmental issues. The main problem is the gap between this growth and the reprocessing techniques. Furthermore, the drawback of recycle polymer is that products could have more than one type of polymer [29]. For example, the packaging contains more than one type of plastic as PET for bodies and PP for caps. For that reason, the first possible solution is to make a blend of plastic waste. However, the problems of polymer blends are incompatibility, poor morphology, and mechanical properties. PP is considered incompatible with the most common plastic found on packaging and bottles (PS and PET). For that reason, many researchers focus on evaluating the effect of different compatibilizers to improve the stability of the blend [30].

In FDM, the use of filament made from recycled plastic has been done, but it is still very limited [29]. Herianto et al. evaluated different parameters to obtain a filament based on recycled polypropylene (rPP) which could be used in 3D Printing. Unfortunately, the results concluded that the filament has rough and easily curved.

2.2.4 Challenges of FDM

FDM offers new opportunities to the industry when developing applications for the high-tech industrial and consumer market. However, some challenges limited its diffusion in the industry. A study by Stansbury et al. shows the recent growth of 3D printing and evaluated the ability of these technologies to replace traditional processes. They also highlight that the transition between traditional techniques and 3D printing will depend on founding new materials and adapting them to increase the design accuracy and, physical and mechanical properties [31].

Another possible view has been proposed by Professor P. Krawczak. She stabilised that the challenges of 3D printing are [32]:

1. Extend the range of materials that can be used. In the case of polymers, extended the range of suitable amorphous and semicrystalline polymers and filled compounds.
2. Reduce the cost of fixtures and materials to be more attractive in the process.
3. Improved the accuracy and stability of printing over time.
4. Improved the surface finish.
5. Increase build-up rates.
6. Increase process control and monitoring.

So, we can assume that the challenges of Fused Deposition Modeling are divided in three macro-topics. The first one is related to types of materials that can be used. Second one is associated with the parameters and accuracy of the printing process. Finally, the last one is the mechanical properties and performances of products.

Chapter 3

Experimental Designs

3.1 Design of Experiments DoE

Experimental design was used firstly in hard science. Subsequently, it has spread through different engineering fields, including mechanical, chemical, thermal, and physical analysis. There are many reasons for this rapid growth, mainly the possibility of developing decision-making techniques that helped to optimized processes to formulate a product.

According to Berger P. et al., an experiment is an analysis in which an investigator chooses one or more inputs (independent) and observes the output (dependent). So, an experimental design is a process that should get answers to three questions: (1) Which factor should you study? (2) How should the levels of these factors vary, and (3) What way should these levels be combined? In other words, the design of experiments (DoE) is a technique to describe and explain the variation of results under conditions that are hypothesized. This process allows to know with more accuracy the relationship of behavior and their factors [33] [34].

3.1.1 The six steps of experimental design

According to Experimental design book, there are six steps to follow [33]:

Plan the experiment: The first step of experimental design is a crucial collaboration between knowledge, experience, and requirements. It is at this stage that there is an evaluation of the critical process factors (qualitative or quantitative). In short, it is a brainstorming in which all team members participate and choose the inputs and outputs of the experiment. It is possible to used lists, diagrams, and other techniques to generate a general view of factors. The planning stage consists of five levels: (i) Identify the dependent (output) variables, (ii)

Translate output variables to measurable quantities, (iii) Determine the independent factors (input) that potentially affect the results, (iv) Determine the number of levels or values for each factor and what those levels are, (v) Identify potential synergy between different factors. After this step, the number factors of them must be simplified.

Design the experiment: The second step of DoE may determine how many factors are appropriated, and their possible combinations should be considered. According to the authors, before selecting the number of factors and their levels, it is necessary to evaluate two critical issues, such as replication and blocking. The first one is related to the measurements that are carried out; however, it is important to note that replication is not analogous to repetition. Instead, it relates to guaranteeing that measures can be replicated. Finally, the second one explains which factor may be of interest to evaluate and its possible relationship between each of them.

Perform of the experiment: This step is related to the number of runs that should be followed in the experiment. The main characteristic of the runs is randomization. Randomization prevents unexpected effects or bias in the process.

Analyze the data form the experiment: The conclusion and results from an experiment must be analyzed to distinguish between human error, tolerance and discrepancy. This distinction is called hypothesis testing, achieved by a statistical analysis evaluation. The role of statistical analysis is to evaluate if each factors are independent. The most common statistical method is the analysis of variance (ANOVA), developed by Sir Ronald Fisher [35].

Confirm the result of experiment: This process consists of evaluating the results through statistical practice to obtain the same validation. For example, if we determine which factor affects the result, we assume that a variation on it produces different results.

Evaluate the conclusion: The last step is to identify whether our conclusions correspond to an error or a result.

3.2 Experimental Methods

Nowadays, the standardization process allows to replicate and obtain the same result around the world. Industries and Academic sectors are always looking to develop a unified standard for their methods and optimization that will reduce costs and increase the performance of products and services. There are different ways to standardize and optimize a process, but the most common is based on statistical

analysis. For that reason, this section presents four experimental methods which are evaluated in the experimental process.

3.2.1 Mixture Method

According to Cornell, the first definition of a mixture problem is an experiment in which the response only will depend on the proportion of the components present in the mixture [36]. However, a new definition was established where the response of the mixture problem will depend on the ratio of components and also the total amount of them.

Mixture Method or Mixture Design is one type of response surface experiment, in which is analyzed and predicted, with mathematical equation, the response of a mixture or blend. There are two purposes for its use:

- (1) Predicted the response of any mixture.
- (2) Identify the influences on response of each component as singly and their possible combination that can be obtained.

This experimental method is divided into three types: simplex centroid, simplex lattice, and extreme vertices designs. The difference between each one is the number of components of the mixture and their relationship. However, the most common is the simplex lattice in which a polynomial equation represents the response by an array of points called a lattice. Each lattice has an specific polynomial equation, which is supported by a model degree m and q components $\{m, q\}$.

According to Cornell and Piepel, this type of experiment needed to follow six steps:

- (1) Define the target of the experiment
- (2) Select the mixture components and any other factors that could be modified the mixture.
- (3) Identify the limits on the mixture and factors.
- (4) Identify the variables (response) to be measured.
- (5) Propose a model for modeling the response data as functions of parameters and components.
- (6) Select an experimental design with test the model.

3.2.2 Taguchi Method

Nowadays, engineers are using diverse types of methods to plan experiments. One of the most common is the Taguchi method. This approach was created by engineer Genichi Taguchi to optimize the process of the experiments, and it is based on orthogonal arrays and statistical analysis. Orthogonal arrays (OAs) is an $n \times x$

m matrix that can be viewed like a series of multi-factor experiments where the columns correspond to the factors and the rows the number of tests. The goal of OAs is to do a fraction of total experiments to evaluate the relationship between factors and their different levels. This goal is the main reason to use this approach [33][34].

However, there are experiments in which the factors and levels are not linearly associated. This new type of orthogonal array is called a mixed element. The mixed element, denoted by OAN(sm x tn), is a matrix where the columns m and s have a different number of levels s and t.

3.2.3 Factorial Method

The Factorial Method is the most complete experimental method because it evaluates the individual effects of each factors and the possible relation between them, so a huge number of tests is needed. One of its advantages is its availability to study quantitative and qualitative factors. Factorial method needs that all tests (runs), at least, have two levels for each factor.

3.2.4 Fractional Factorial Method

The disadvantage of the Factorial Method is that increasing the number of factors to evaluate, also increases the number of experiments that will be made. Nowadays, it is impossible to make a extensive number of experiments due to the time and cost. For that reason, it was created the Fractional Factorial Method which evaluates a fraction of parameters. These parameters are chosen based on their relevance and the number of interactions.

When this method is used, two situations are expected. First, there is a possibility of losing information due to segregation between all parameters. Second, it is that parameters that will be evaluated have the same effects that those not taken into account.

3.3 Matlab

Choosing a model and determining its associated parameters for fitting is a decisive step to reproduce the experimental data. Nowadays, there are different resources that could be used for that such as MATLAB.

MATLAB is a programming and numeric computing platform used by millions of engineers and scientists to analyze data, develop algorithms, and create models [37]. One common function used is Optimization Toolbox, which finds parameters that minimize or maximize objectives. This tool has linear programming (LP), mixed-integer linear programming (MILP), quadratic programming (QP), second-order

cone programming (SOCP), nonlinear programming (NPL), constrained linear least squares, nonlinear least squares, and nonlinear equations.

The models mentioned above have been applied in diverse computational studies. For example, a study by Gallagher et al. evaluated rheological models (Carreau, Cross, Yasuda) and generated data sets through simulations on Matlab [38].

Another important point to highlight in this study was the function used in order to make a fitting. As mentioned formerly, Matlab has different optimization functions which are depending on the number of parameters to be evaluated or the grade of a polynomial function. In this study, the authors proposed to use an optimization function: `fmincon`, which is based on reducing the variance between experimental data and models.

3.3.1 Function -*fmincon*

`Fmincon` is a nonlinear function on Matlab, which has five optimization algorithm options: interior-point, trust-region reflective, `sqp`, `sqp-legacy`, and active set. Moreover, this function allows defining the convergence criteria, maximum interactions, and gradients. The sequence of steps to use it is:

- (1) Define the optimization variables
- (2) Define the function to minimize and restriction.
- (3) Define the algorithm to used according to the target

Table 3.1 shows a brief documentation of this function, while equations 3.1 and 3.2 shows two different style to codify the function `fmicon`. The latter equation represents the form used by Gallagher et al. [38].

Type	Name	Symbol
Independent Variable	Solution	$y=f(x)$
	Lower bounds	lb
	Upper bounds	ub
Output Variable	Parameter of model	$x=(a,b,c,\dots)$
	Function to minimize	fun
Parameters	Objective function value at a solution	fval
	Matrix of second partial derivatives	hessian
	Function or Model	CrFit

Table 3.1: Documentation of function *fmincon* [39].

$$x = fmincon(fun, x_0, a, b) \quad (3.1)$$

$$[x, fval] = fmincon(fun, init, lb, up, options) \quad (3.2)$$

3.3.2 Fitting

Performing a maximum likelihood fit of rheological curves yields difficulties with parameters identification and the choice of model. Constrained optimization has been presented as a possible solution to identify the parameters throughout a boundary problem. Gallagher et al. shows an optimization model which uses this type of methodology, and compare three diverse rheological models (Carreau, Cross, and BCCY) with rheometry data [38].

Type	Name	Symbol	Units
Independent Variable	Shear rate	$\dot{\gamma}$	s^{-1}
	Viscosity	η	$Pa \cdot s$
Output Variable	Elastic Modulus	G'	Pa
	Viscous Modulus	G''	Pa
	Transition Time	λ	s
Parameters	Viscosity Exponent	n	-
	Zero - shear Viscosity	μ_0	$Pa \cdot s$

Table 3.2: Documentation of parameters and models for constrained optimization [38].

The authors begin defining a functional form $\mu(\dot{\gamma}, \theta)$ for the viscosity μ at shear rate $\dot{\gamma}$ with parameters $\theta = (\mu_0, n, \dots)$. The former is considered the rheological model, while the latter can see like initial values.

$$\mu = f(\dot{\gamma}, \theta) \quad (3.3)$$

$$\theta = (\mu_0, n, \lambda, \dots) \quad (3.4)$$

Therefore, they are considered the maximum likelihood estimation as a normally distributed error, and it is estimated as least squares between $\mu(\dot{\gamma}, \theta)$ and rheometry data (μ_m).

$$\theta^* = \underset{\theta}{\operatorname{argmin}} \sum_{m=1}^M (\mu(\dot{\gamma}, \theta) - \mu_m)^2 \quad (3.5)$$

In order to follow the same nomenclature of rheological literature, rheological behavior is expressed on a log-log scale, thereby the error can be expressed in log-log scale as shown in equation 3.6.

$$\theta^* = \underset{\theta}{\operatorname{argmin}} \sum_{m=1}^M (\log(\mu(\dot{\gamma}, \theta)) - \log(\mu_m))^2 \quad (3.6)$$

Finally, it is defining the boundary problem as a limit value in which the parameters have been interpolated to minimize the least-squares error. For doing that, it is necessary to use computational resources, such as Matlab.

On the other hand, it was decided to follow Gallagher's approach due to being able to control the optimization process and evaluate different models. However, it is necessary to look for new models allowing achieving better fitting (seen in chapter 4). Moreover, the constrained optimization process was changed, reducing the number of steps/optimization and increasing the number of parameters.

Type	Name	Symbol	Units
Independent Variable	Frequency Sweep	ω	$\frac{rad}{s}$
	Output Variable	Viscosity	η
Output Variable	Elastic Modulus	G'	Pa
	Viscous Modulus	G''	Pa
	Transition Time	λ	s
Parameters	Viscosity Exponent	n	-
	Zero - shear Viscosity	μ_0	Pa·s
	Yield Stress	σ	Pa

Table 3.3: Documentation of parameters and model for constrained optimization [40].

Table 3.3 shows the documentation for the new optimization model, while equations 3.7, 3.8 and 3.9 presented the different function used.

$$\mu = f(\omega, \theta) \quad (3.7)$$

$$\theta = (\mu_0, n, \lambda, \sigma) \quad (3.8)$$

$$\theta^* = \underset{\theta}{\operatorname{argmin}} \sum_{m=1}^M (\log(\mu(\omega, \theta)) - \log(\mu_m))^2 \quad (3.9)$$

Chapter 4

Experimental Process

According to the previous chapter, the experimental process was divided into four steps as shown in the figure 4.1, each one was a specific experimental method, but also was based on the result of previous works [41][42].

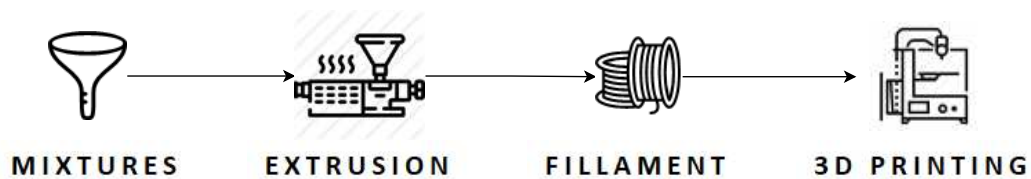


Figure 4.1: Steps of experimental process.

The first step was to mix PP and R-PP at different ratios and choose the rheological model, and the parameter to optimize. The goal was looking for a proportion that presented, the higher value of Yield Stress (σ_y), which guarantee the non Newtonian behavior.

The second step is more complex than the previous one because it involves an optimization based on Taguchi Method. The scope was to obtain optimal extrusion parameters maximizing the Yield Stress.

The third step was making a filament, which shows a higher values of Yield Stress. Based on the previous studies and reviews, the parameters to consider were temperature, screw velocity (rpm), and the filament radius. The target was to obtain a continuous filament that had constant radius and soft roughness.

Finally, the last step was related to 3D printing. It was printed at different parameters and evaluated their compromise such as: mechanical properties, dimensional accuracy, bonding of layer, among others.

4.1 Materials

As mentioned before, the scope of this investigation is to produce a filament for 3D-printing based on two materials, such as PP and recycled plastic (rPP). As established in their researches, Bertolino and Bernagozzi proposed a Polypropylene ISPLEN PB 170 G2M as a good material for printing. According to the authors, the features that allow printing this PP are the low levels of stretch and low shrinkage [41][42].

Table 4.1 shows the main characteristic (general, mechanical, thermal) of this type of polypropylene [43].

Properties	Value	Unit
Melt Flow Rate	12	g/10 min
Density	905	kg/m ³
Flexural modulus	1200	MPa
Impact Strength Notched	8	kJ/m ²
Heat Deflection Temperature	85	°C

Table 4.1: Technical sheet PP ISPLEN® PB 170 G2M. *«Taken from: Repsol Technical data Sheet»* [43].

Furthermore, Bernagozzi, in her investigation, identified three possible inorganic additives or fillers suitable for 3D printing in order to increase the mechanical properties of PP. One of them is the talc, which increased the sterness as compared to unfilled PP [41].

Talc or talcum is composed of hydrated magnesium silicate ($Mg_3Si_4O_{10}(OH)_2$), and the main characteristic are [41][44]:

- It is hydrophobic and organophilic.
- It is inert.
- It is a good electric and thermal insulator.
- It is resist well to acids.

The characteristics mentioned above allow using this material in different types of industries as plastic, food, cosmetics, and others. In general, the roles of this material are as a filler, lubricant, or coat [45]. The talc powder used in Bernagozzi’s work was HTP1 produced by IMI FABI [41] with a 2 μ m diameter average.

Table 4.2 shows the principal properties for it.

Type	Properties	Value	Unit
Physical	Density	2,8	g/cm ³
	Bulk Density	0,26	g/cm ³
	Tapped density	0,35	g/cm ³
	Specific Surface (B.E.T.)	10	m ² /g
	Hardness	1	1
	Oil absorption	54	g/100g
	Moisture content at 105°C	0,2	%
Chemical	<i>SiO₂</i>	61	%
	MgO	32	%
	CaO	0,2	%
	<i>Fe₂O₃</i>	0,4	%
	<i>Al₂O₃</i>	0,4	%
	Loss on ignition at 1050°C	6	%

Table 4.2: Technical sheet Talc IMI FABI HTP1. *«Taken from: IMI Fabi SpA»* [45].

The blend of both materials at ratio 7:3, which means at 70%wt of PP ISPLEN PB 170 G2M and 30%wt of IMI FABI HTP1, is used as based material on this research, henceforward named PPt.

On the other hand, the recycled material (hereinafter coded as rPP) was bought from Breplast S.p.A, from now on named rPP.

Type	Properties	Value	Units
Physical	Melt flow index	4,5 - 9,5	g/ 10 min
	Density	0,9	g/cm ³
	Temperature	230	°C
Mechanical	Strain at break	26	%
	Flexural Modulus	950	MPa
Thermal	Vicat Softening	130	°C

Table 4.3: Technical sheet of Bretene PP by Breplast SpA. *«Taken from: Material data center»* [46].

According to the supplier, the origin of this material is the urban waste and it is made up 80% of PP [47][46]. Table 4.3 shows the principal properties for it.

4.2 Compound Preparation

4.2.1 Mini-Extruder and Hydraulic Press

As mentioned above, the first step was to mix PPt and rPP at different ratios and evaluate the rheological behavior of the resulting materials. The former was made by using a mini-extruder Xplore MC 15, shown in figure 4.2. The main advantages of this machine is that allows using small quantities of materials, hence reducing the experimental waste.



Figure 4.2: Mini-Extruder Xplore MC 15. «Taken from: Brochure of Xplore MC 15 micro compounder» [48].

Table 4.4 shows the selected processing parameters. The values of each one were related with the properties of materials.

Parameter	Value
Temperature	190 °C
Screw Velocity	50 - 100 rpm
Time	5 - 7 min

Table 4.4: Parameters process Mini-Extrude.

On the other hand, the specimens for rheological characterization were obtained

through compression molding by using a hydraulic press Collin P200T, as seen in figure 4.3. It is a heated parallel plate press, where through compression force and heat, the materials take the desired shape. The mold used consists of four holes with 25 mm of diameter and 1 mm of thickness. These samples have the dimension for carrying out the rheological tests.



Figure 4.3: Hydraulic Press Collin P200T [49].

Table 4.5 shows the parameters and their values used to make the samples for rheological tests. It is important to highlight that values were chosen based on previous works and post processing process as extrusion and printing.

Parameter	Value
Temperature	190 °C
Pression	50 - 100 bar
Time	2- 5 min

Table 4.5: Parameters process Hydraulic Press.

4.3 Extrusion

The second step was divided into two parts. The former was determining the factor sand levels to use the Taguchi method. In addition, the orthogonal array then used was chosen. The latter was to produce the filament using the orthogonal array and evaluated the rheological behavior again.

4.3.1 Level and Factors

Following the steps mentioned in chapter two and the previous works, it was possible to identify the parameters that influence the behavior of the mix, such as feeding, velocity, temperature, and extruder screw. The next step was to determine the levels or range to be evaluated. In order to appraise all possible cases, we decided to use the extreme cases, which means highest and lowest values. Table 4.6 shows the values for each parameter:

Factor	Level 1	Level 2
Feeding (rpm)	300	500
Screw Velocity (rpm)	150	400
Temperature (°C)	190	210
Extruder Screw	Standard	Transport

Table 4.6: Factors and Levels values.

4.3.2 Taguchi's Arrays

The Taguchi method has different models of orthogonal arrays (OAs), which depend on factors and number of levels. In this case, there are three possible orthogonal arrays as L8, L16, and L32. The difference between each one is the number of tests and the number of levels for each factor. It was decided to work with L16 because it was allowed to evaluate the entire effects of each factor.

Table 4.7 shows the combination of parameter that was evaluated.

Run	Hopper Velocity	Screw Velocity	Temperature	Extruder Screw
Run 1	A1	B1	C1	E1
Run 2	A1	B1	C1	E2
Run 3	A1	B1	C2	E1
Run 4	A1	B1	C2	E2
Run 5	A1	B2	C1	E1
Run 6	A1	B2	C1	E2
Run 7	A1	B2	C2	E1
Run 8	A1	B2	C2	E2
Run 9	A2	B1	C1	E1
Run 10	A2	B1	C1	E2
Run 11	A2	B1	C2	E1
Run 12	A2	B1	C2	E2
Run 13	A2	B2	C1	E1

Run 14	A2	B2	C1	E2
Run 15	A2	B2	C2	E1
Run 16	A2	B2	C2	E2

Table 4.7: Taguchi's Arrays L16.

4.3.3 Thermo Fisher Extruder

Thermo Fisher is an extrusion machine used to generate polymer compounding (figure 4.4). The instrument is equipped with a twin-screw, eight heating zones, and pressure control on the die.



Figure 4.4: Process 11 Thermo Fisher Scientific. «Taken from: Thermo Fisher Scientific» [50].

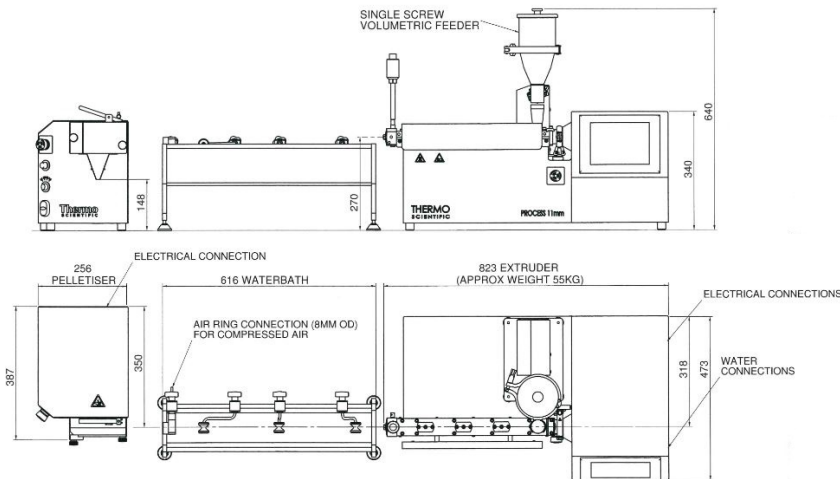


Figure 4.5: Blueprint of assembly by Process 11 Thermo Fisher Scientific. «Taken from: Thermo Fisher Scientific» [50].

The advantage of this equipment is the possibility to modify the elements of the screw (transport, mixed, and chewing). The process begins with constant feeding, which is regulated through gravimetric feeders. Afterward, the material is heated and mixed while flowing around twin-screw. Finally, the compounding is extruded and put to a rapid cooling in a reservoir of water followed by automatically cutting to form small pellets (2-3 mm), as schematically depicted in figure 4.5.

The main parameter of the process are:

Extruder Screw: There are different types of categorization of extruder screw as rotation (co-rotating and counter-rotating), contact between screw (inter meshing and non inter meshing), and screw design (one piece or modular barrels). Each one allows to obtain different types of materials and behaviors. For this study, it was used a co-rotating extruder which is available to change the segments of screw.

Twin-Screw Velocity: it is a fundamental parameter because allows determining the time in which materials are subjected into a processing transformation.

Temperature: It is the request energy to change the state of materials, and allows to make the mix.

Pressure: It is the force requested to move and pushed the material in order to obtain a filament. Also, it is a security parameter that allows to understand how many materials are being modify.

For the parameters mentioned above, it is relevant to highlight the extruder screw. It not only represents an advantage of this machine but also allows to make a modification of the compound. Figure 4.6 shows a blueprint of a single screw and its elements (feeding, transport, mixed, and chewing).

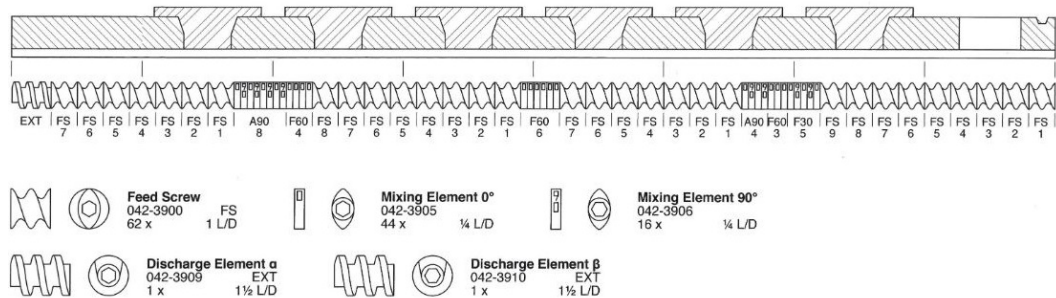


Figure 4.6: Screw Profile - Blueprint «Taken from: Thermo Fisher Scientific» [50].

Each screw element has a specific function and characteristic, as seen below:

Feeding (PS): Elements where material arrives.

Transport (FS): Transport elements.

Kneading block Elements (F30, F60, A90): These elements are classified by the angle (30°, 60°, 90°) which indicates the shift between each one.

Discharge (EXT): Discharge elements.

Table 4.8 resume the main values for each parameter mention above. Moreover, the values of each parameter used in this study were show in the previous section (table 4.6).

Factor	Range
Screw Profile	Feed Screw - Mixing Element - Discharge Element
Screw (rpm)	10 -1000
Temperature (°C)	20° - 450°
Cooling water	10° - 20°

Table 4.8: Data Sheet Thermo Fisher Extrusion \llcorner Taken from: *Thermo Fisher Scientific* \gg [50].

4.4 Filament

4.4.1 Fillament Extruder - 3Devo

The Next 1.0 (produced by 3DEVO) is a machine used to produce 3D printing filament, as seen in figure 4.7 [51].

This machine works similarly to a single screw extruder in which the material is heated and extruded. The Afterward, the filament is cooled and pulled by a winder. The process can be divided into four sub-systems as follows:

Heating: It is composed of a screw and four thermocouples. The main parameters are the temperature of thermocouples and the RPM of the screw. A good combination of both allows obtaining good filament.

Cooling: Consists of two fan systems that can be adjusted for optimal airflow and fan speeds.

Measuring: Made-up by optical sensor (laser) and pulled system. A combination of both allows obtaining the desired diameter.

Table 4.9 shows the range of each sub-system and the possible the final values for each parameter that was used to produce the filament.

System	Range	Parameters	Final Parameters
Heating	20 - 450 °C	190 - 220 °C	220-215-215-210 °C
Cooling	0 - 100 %	10 - 30 %	30 %
Measuring	0,5-3,0 mm	1,5 - 1,8 mm	1,5 - 1,85 mm

Table 4.9: Parameters and range of Filament process.

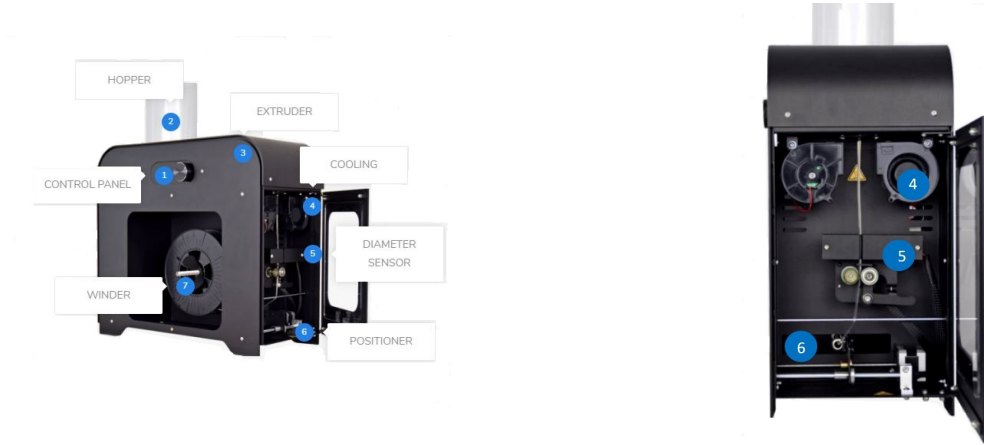


Figure 4.7: 3Devo Filament Machine. (1) Control Panel (2) Hopper (3) Extruder (4) Cooling (5) Diameter sensor (6) Positioner (7) Winder. «Taken from: *3Devo Filament makers*» [51].

4.5 3D Printing

4.5.1 3D Printing - Roboze One & software Simplify 3D

Finally, the last process is printing the filament. This process should be sub-divided into different steps. The first step is generating the CAD in STL format with the desired geometry. It is relevant to know the dimension of the work area and the dimensional restriction, like volume. In this case, the work area is 280 x 220 mm, and the geometry is a standard sample of tensile prove based on ISO 527A-5A.

The next step is using the software Simplify 3D in which is carried out the slicing process and setting the printer features. The former is a procedure where geometry is divided into n parallel planes. This one will be defining the time of the process, the roughness, and the percentages of filling. Also, it allows identifying the position in which geometry will be printed (horizontal or vertical) and optimizing the quantity of material used.

The latter is related to a set of guidelines that modify the behavior of the printed object and process, as follows:

Extruder: Referring to extrusion parameters.

Layer and Infill: Defines the thickness and percentage of filling of layers printed.

Support: For the case in which geometry needs support, it is possible to define the type of support used.

Temperatures: Defining the main temperatures of process, as plate work (bed) and nozzle.

Cooling: Defining the intensity of fans

Speed: It is related to the speed of printing.

Advanced: Referring to a set of values to take into account in the case of printing more than one geometry or different types of parameter in the same cycle.

Based on the previous works, the modified parameters were temperatures (bed and extruder) and filling. The reason was the relevance/impact of the final object. Table 4.10 shows the range of values that were tested.

Factor	Range	Case 1	Case 2	Case 3
Extruder Temperature (°C)	200 - 280	280	280	280
Bed Temperature (°C)	23 - 70	30	50	70
Infill (%)	100 - 200	100	100	100

Table 4.10: Values for someone parameters used to printing.

The last step was printing. The printer used is the Roboze One, as seems in figure 4.8.



Figure 4.8: Roboze One. «Taken from: *Roboze Print Strong Like Metal*» [52].

The main characteristics of this machine are the work area (280x220x200), high precision ($\pm 25\mu m$), nozzle diameter (0.4 mm or 0.6 mm), and different types of surface to print. Moreover, it has a touch control panel, in which it is possible setting some parameters such as the temperature of the bed, position of the extruder and the bed, speed of the cooling system, and lights. Through this panel, it is possible to level the work area, which allows symmetry during printing. For this work was used the code and script of previous studies, such as Bernagozzi's master thesis [41], and Bertolino's master thesis [42]. Table 4.11 resume some relevant parameter and a ranges of possible values for this machine.

Factor	Range
Dimension	280 x 220 x 200 mm
Resolution	0.18 - 0.24
Software	Simplify3D
Printed velocity	60 - 150 mm/s
Precision (Accuracy)	25 μm
Bed Temperature	20 °C - 100 °C
Extrusion Temperature	100°C - 300°C

Table 4.11: Data Sheet of Roboze One.

Another important condition to take into account during this process is the filament. It will have 1.85 mm diameter and smooth roughness. However, as it will highlighted in the next chapter, it was impossible to produce a filament with a constant diameter and smooth roughness. The main reason is the dispersion generated when working with recycled material. So, it was decided not to implement the optimization process and based only on the previous results and experiences.

Factor	Value
Extruder Temperature (°C)	260
Bed Temperature (°C)	30 - 50
Infill (%)	100

Table 4.12: Parameters value used to 3D printing.

Table 4.12 resume the parameter values used to 3D - Printing. To reduce the adhesion effect between raft-layer and raft-bed, it was decided to use two different bed temperatures. These values were related to the R-PP percentage.

4.6 Characterization Analysis

Nowadays, there is an enormous world of tests to characterize the materials, which are dependent not only on the purpose of objectives but also on the type of material. To obtain a footprint of materials is possible to conduct some tests such as mechanical, chemical, thermal and physical.

This study sought to characterize a polymer blend based on recycled plastic; hence there were chosen various tests, such as Thermal Gravimetric Analysis, Differential Scanning Calorimetry, Tensile test, and rheological measurements, to obtain a footprint of it.

4.6.1 Rheological Test

For this test, it was used the Rheometer Ares from TA instruments. As mentioned above, this machine consists of two parallel plates arranged inside an oven, which is heated by flowing air at a specific temperature. This temperature is related to the parameters of processing as *extruder* or *printer*.

The advantage of this machine is the different test modes as strain sweep or frequency sweep; the differences between both are the fixed parameters and the relationship between response and mechanical/physical characteristics. The former is a test with fixed temperature and frequency, whereby obtaining the linear viscoelastic zone. The latter sets the strain and temperature at variable frequencies, whence achieve the viscosity and the dynamic modulus as a function of the frequency.

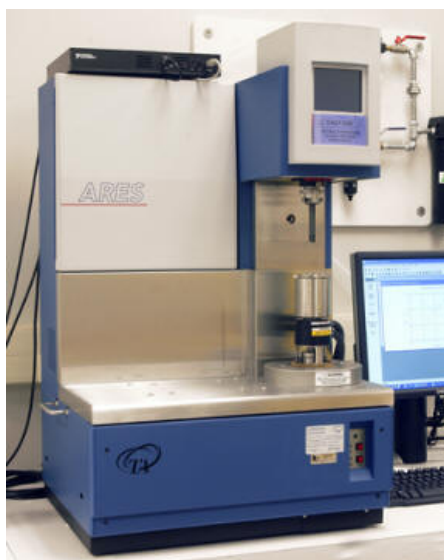


Figure 4.9: Rheometer Ares TA Instruments.

Table 4.13 resume the parameters and values that were used in the Rheological test. On the other hand, the dimension of sample was mention in mixture section.

Parameter	Range
Temperature (°C)	230 - 260
Strain (%)	5
Frequency Range (rad/s)	0.1 - 100
Gap (mm)	1 mm

Table 4.13: Parameters of Rheological Test.

Rheological models

Choosing a rheological model and determining its associated parameters for fitting is a crucial step for different types of studies. Actually, some models depend on the material type or the number of variables to evaluate. On the other hand, there are diverse types of computational resources to calculate and optimize the fitting. The joint of both is allows predicting the rheological behavior of the material.

Models of shear-thinning complex fluids, such Cross, Cross-Carreau, and Yasuda, are the most used in computational studies. The models mentioned above are focused on nonlinear algebraic equations [38][40], as follows:

$$\eta = \frac{\mu_0}{1 + \lambda\omega^n} \quad (\text{Cross - Model}) \quad (4.1)$$

$$\eta = \frac{\mu_0}{[1 + (\lambda\omega)^2]^{\left(\frac{n-1}{2}\right)}} \quad (\text{Carreau - Model}) \quad (4.2)$$

$$\eta = \frac{\mu_0}{[1 + (\lambda\omega)^a]^{\left(\frac{n-1}{a}\right)}} \quad (\text{Yasuda - Model}) \quad (4.3)$$

Where:

μ_0 : Zero shear viscosity.

λ : Average relaxation time

ω : Frequency.

η : Viscosity

n: Power law exponent.

a: Correction parameter introduced by Yasuda.

However, there is a limitation on all of them. This limitation is related to the accuracy of fitting at low frequency or low shear rate. For that reason, different

authors have proposed a variation for those models, either new ones, like Khoshkava and Kamal, Lerwimolnum and Vergnes, and Lui Cui et al [40].

$$\eta = \frac{\sigma_y}{\omega} + \frac{\mu_0}{1 + \lambda\omega^n} \quad (\text{Khoshkava and Kamal - Model}) \quad (4.4)$$

$$\eta = \frac{\sigma_y}{\omega} + \frac{\mu_0}{[1 + (\lambda\omega)^a]^{\left(\frac{1-n}{a}\right)}} \quad (\text{Lerwimolnum and Vergnes - Model}) \quad (4.5)$$

$$\eta = \frac{\sigma_y}{\omega} + \frac{k_1 n (\lambda\omega)^n}{\omega [(\lambda\omega)^n + 1]^2} \quad (\text{Lui Cui et al. - Model}) \quad (4.6)$$

Where:

σ_y : Yield stress

k_1 : Shear stress at infinite shear rate

As seen in equations 4.4, 4.5, and 4.6, the new models are composed of two terms or factors. The first factor, as a "corrective factor", allows fitting the viscosity curve at low frequency and fitting the non-Newtonian behavior, while the second term has allowed fitting the viscosity at a high frequency based on "classic" models (equation 4.1, 4.2, 4.3).

For this study, all the models mentioned above were evaluated and it was selected the model with the lesser cost function value, which is the sum of relative errors between the model and the experimental data. For that purpose, Matlab (section 3.3) was used as computational resources.

4.6.2 Differential Scanning Calorimetry - DSC

Differential Scanning Calorimetry (DSC) is a thermodynamical technique for direct assessment of heat energy uptake, which occurs in a sample within a regulated increase or decrease in temperature. The primary utilization is to monitor the changes of phase transitions [53].

In this case, the sample, which weighs 6 - 8 mg, is placed inside an aluminum crucible while the reference consists of an empty crucible. Then the temperature is increased with a rate of 10 °C/min until reaching 220 °C. The measure obtained is the heat flow rate as a function of temperature. After that, it begins the controlled cooling in which can be evaluated the crystallization enthalpy. Finally, heat flows again to determine the intrinsic characteristic temperatures of the material.



Figure 4.10: DSC machine [54].

4.6.3 Thermal Gravimetric Analysis - TGA

The instrument used was TGA Discovery, by TA Instruments, as seen in figure 4.11. The test was carried out by subjecting the materials to a temperature ramp from 50 °C to 800 °C, at 10 °C/min, under controlled atmosphere. The sample used weighs around 10 mg.



Figure 4.11: TGA TA Instruments.

4.6.4 Mechanical Test

Mechanical characterization or mechanical test is an in-situ process that determines the conditions for irreversible damage, where the most common is tensile testing. The tensile test was used to look for the mechanical properties such as yield strength, ultimate tensile strength, ductility, strain hardening characteristics, Young's modulus, and Poisson's ratio.

The test is conducted at a constant strain rate and measures the amount of force (F) and the elongation (ΔL) of the sample. The results are shown in a graphic in which plots Stress vs. Strain. This study used a procedure of previous works in which defines two strain rates. The former was 1 mm/min in which determines the elastic region, while the latter is 10 mm/min to the rest of the test to reduce the time.

Another important characteristic was the dimension of the sample. In this case, it is decided to use a sample based on ISO standard, as mentioned in section 4.5. For this test, it was used an Instron series 5966, as seen in figure 4.12.

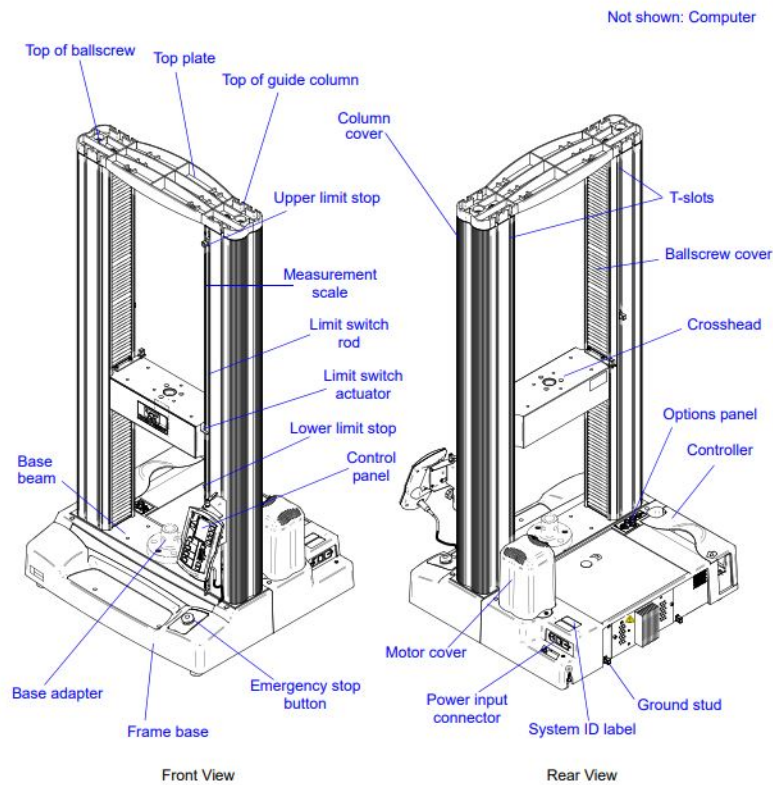


Figure 4.12: Instron series 5966. «Taken from: *Instron 5960 Series Dual Column table frames System* » [55].

4.6.5 Optical Microscope Test

For this study, there are two instances in which the metrological tests are used. The first one was on step 3 in which measured filament diameter. However, this process was conducted by the 3devo machine by laser control. The second one was on step 4, which evaluated the bonded of each layer and the shrinkage of the perimeter. These measures were made by an optical microscope, as seen in figure 4.13.



Figure 4.13: Optical Microscope. *«Taken from: Techmate enabling science» [56].*

4.6.6 Scanning Electron Microscope - SEM

A scanning electron microscope (SEM) is a type of electron microscope, used to study the morphology of the surface of solid objects (figure 4.14). The process begins by scanning the surface through a beam of focused electrons of relatively low energy, developed by the thermionic effect between the anode and cathode.

Different information can be picked up or analyzed through the detector as a result of the exchange between the electron beam gun and the surface. Secondary electron, an inelastic collision, provided information related to the topography of surfaces, while retro-scattered electrons, elastic collision, give information about the chemical composition.

The methodology to make the sample for the test is the same as the previous studies, in which the filaments, after immersion in liquid nitrogen, were brought to

brittle rupture. The scope for doing that is to guarantee the real surface and avoid plastic deformation. Another relevant point is to prevent the electrostatic charges which disturb the signals. This is achieved through a metalized with a gold layer. Therefore, the test is conducted in high vacuum conditions to guarantee the mean free path and avoid collision with impurities of the environment.



Figure 4.14: Scanning Electron Microscope - SEM [41].

Finally, the samples are positioned in two directions (vertical and horizontal) to study morphology, dimensions, and roughness of filaments.

Chapter 5

Experimental Results

5.1 First stage

The first step was to produce PPt - rPP blends at five different ratios of mixtures, the composition of the formulated blends are reported in table 5.1. The difference between each one was the quantity of recycled material (rPP). The purpose was to evaluate the effect of different amounts of rPP on the blend's rheological behavior.

Run	rPP[%w]	PPt [%w]
50:50 rPP - PPt	50	50
40:60 rPP - PPt	40	60
30:70 rPP - PPt	30	70
20:80 rPP - PPt	20	80
10:90 rPP - PPt	10	90

Table 5.1: The ratio of the mixture

Firstly, it was necessary to evaluate the rheological behavior of PPt and rPP. These curves will be considered a starting point or theoretical curves of materials. Figure 5.1 shows the complex viscosity as a function of frequency. The temperatures used for this test were 230°C and 260°C, corresponding to the values used in the printing step.

For this study, the materials should exhibit a low viscosity at high-frequency, while high viscosity at low frequency. Furthermore, as mentioned before, the rheological behavior of the material should be non-Newtonian, with yield stress at low frequencies. Figure 5.1 shows the complex viscosity of both materials; the red curves represent the PPt, while the blue curves are referred to the rPP.

The first thing to highlight is that both viscosity curves satisfy the requirements

mentioned above since both materials show a notable non-Newtonian behavior.

On the other hand, it is possible to observe that curves presented a similar behavior, either changing the temperature. The differences between the curves could correspond to the elements present of rPP, which shifts the curve.

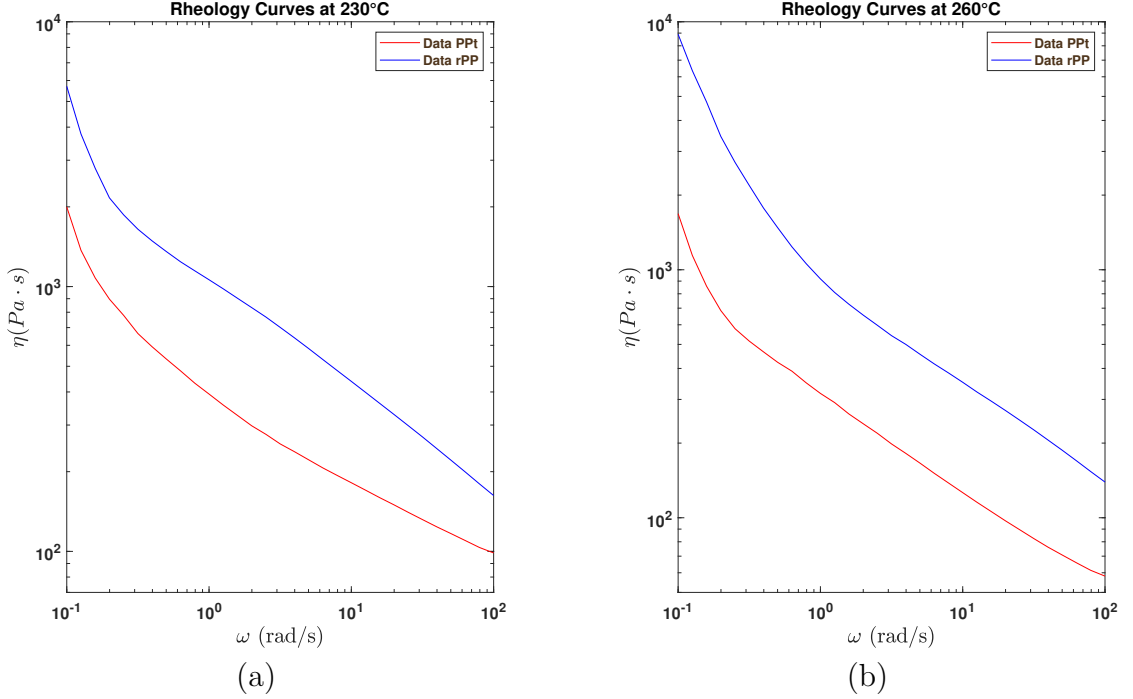


Figure 5.1: Rheological behavior of PPt and rPP at different temperatures. a) Rheological behavior at 230°C. b) Rheological behavior at 260°C

Material	Variable	Symbol	Value	Unit
Polypropylene (PPt)	Viscosity	$\eta_{T=230\text{ }C^\circ}$	1999	$Pa \cdot s$
		$\eta_{T=260\text{ }C^\circ}$	1683	$Pa \cdot s$
Recycled Polypropylene (rPP)	Viscosity	$\eta_{T=230\text{ }C^\circ}$	5705	$Pa \cdot s$
		$\eta_{T=260\text{ }C^\circ}$	8910	$Pa \cdot s$

Table 5.2: Viscosity values at low frequency ($\omega = 0,1$)

Table 5.2 resume the viscosity values at low-frequency. These values are important because are related to the material stability during the printing process.

As mentioned in previous chapters, it was necessary to identify a theoretical

model which replicated or fit the curves. This process will allow knowing which parameter governs the non-Newtonian behavior. It was decided to use the Khoshkava and Kamal model which replicates experimental data better. And for this case, the parameter to optimize is the Yield Stress.

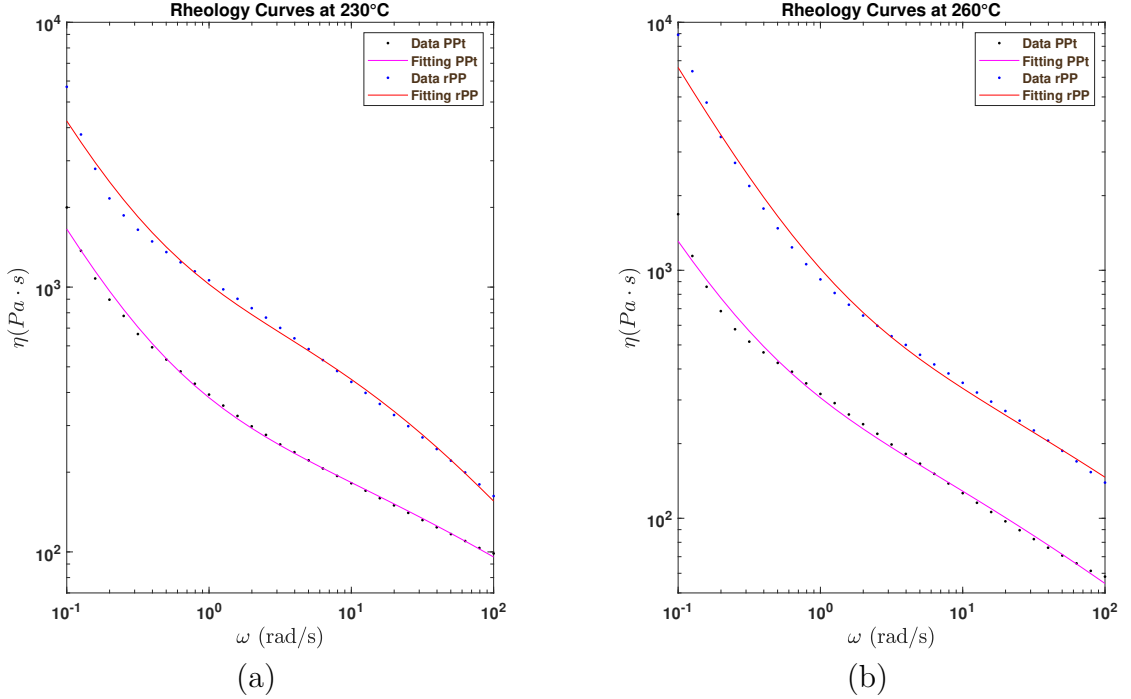


Figure 5.2: Rheological curves at different temperatures and fitting. a) Rheological curves at 230°C and fitting model. b) Rheological curves at 260°C and fitting model.

Material	Variable	Symbol	Value	Unit
PPT	Yield Stress	$\sigma_{T=230\text{ }^\circ\text{C}}$	135,54	Pa
		$\sigma_{T=260\text{ }^\circ\text{C}}$	104,36	Pa
rPP	Yield Stress	$\sigma_{T=230\text{ }^\circ\text{C}}$	344,09	Pa
		$\sigma_{T=260\text{ }^\circ\text{C}}$	608,41	Pa

Table 5.3: Yield Stress for each base materials.

Figure 5.2 shows the fit in both cases, while table 5.3 reports the values of Yield Stress.

As a result of changing the temperature, the value of Yield Stress changes likewise. However, this effect is not the same on PPT and rPP. In the former, the

Yield Stress decreases, while in the latter it increases.

5.1.1 Rheology Test Results

Figure 5.3 shows the rheological curves for all formulated blends, while table 5.4 shows the values for viscosity at low-frequency.

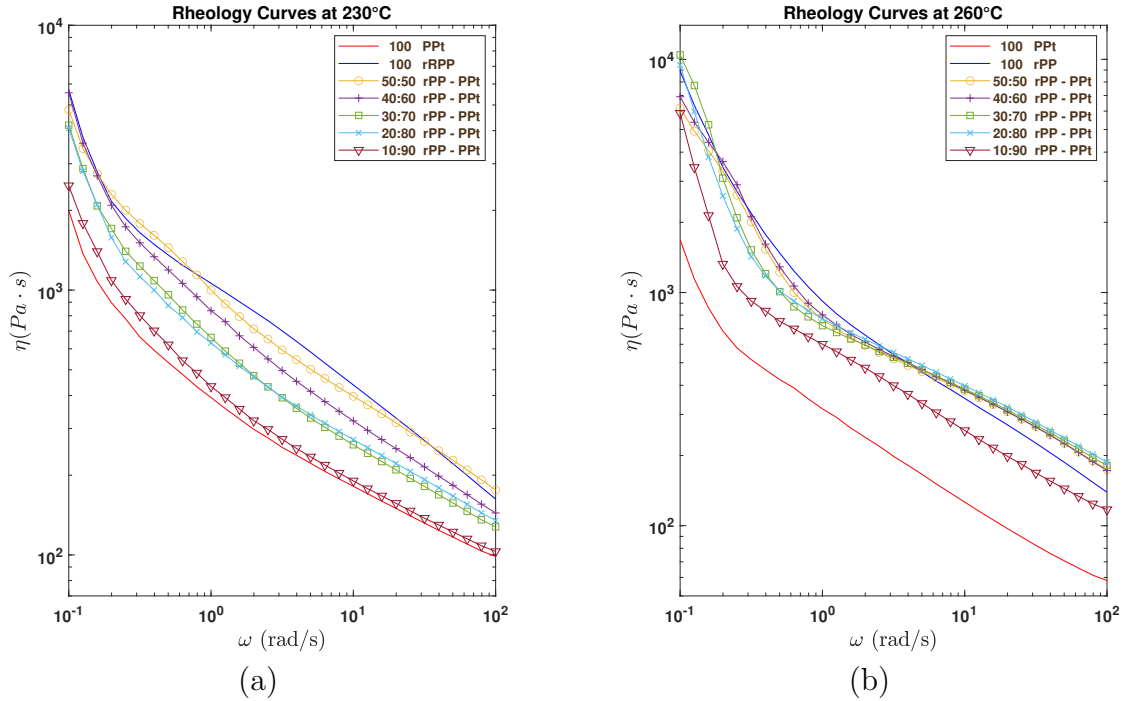


Figure 5.3: Comparison of rheological curves for each blend produced with mini-extruder. (a) Rheological curves at 230°C. (b) Rheological curves at 260°C.

According to figure (a), at 230°C, it was possible to notice that, based on their rheological behavior, the blends could be divided into three groups. The first group (10%wt of rPP and 90%wt of PPt) presented a similar behavior to PPt, so the effect of adding rPP at this proportion did not show an increase in non-Newtonian behavior. The second group (20-30 %wt of rPP and 80-70 %wt of PPt) exhibit a complex viscosity curve between PPt and rPP. Finally, the last group (60-50 %wt of rPP and 40-50 %wt of PPt) kept the same curve to rPP.

On the other hand, figure (b) shows that, at 260 °C, all the blends show a rheological behavior similar to that of the rPP curve, except the last sample (10%wt of rPP). Furthermore, non-Newtonian behavior is more pronounced at 260°C, in which samples 40%wt, 30%wt, and 20%wt of rPP have prominent Yield stress at low-frequency.

In the same way, the samples mentioned above show a viscosity increase at high frequencies, which could represent an issue in the extrusion and printing process. Nonetheless, all of them at low-frequency show drastic exponential growth that justifies their possible use in printing.

Sample	Symbol	Value	Unit
50:50 rPP - PPt	$\eta_{T=230\text{ }^{\circ}C}$	2062,4	$Pa \cdot s$
	$\eta_{T=260\text{ }^{\circ}C}$	5879,4	$Pa \cdot s$
40:60 rPP - PPt	$\eta_{T=230\text{ }^{\circ}C}$	4086,8	$Pa \cdot s$
	$\eta_{T=260\text{ }^{\circ}C}$	9447,3	$Pa \cdot s$
30:70 rPP - PPt	$\eta_{T=230\text{ }^{\circ}C}$	4196,6	$Pa \cdot s$
	$\eta_{T=260\text{ }^{\circ}C}$	10450	$Pa \cdot s$
20:80 rPP - PPt	$\eta_{T=230\text{ }^{\circ}C}$	5559,2	$Pa \cdot s$
	$\eta_{T=260\text{ }^{\circ}C}$	6916,8	$Pa \cdot s$
10:90 rPP - PPt	$\eta_{T=230\text{ }^{\circ}C}$	4790,5	$Pa \cdot s$
	$\eta_{T=260\text{ }^{\circ}C}$	6179,9	$Pa \cdot s$

Table 5.4: Viscosity values for each blend at low-frequency ($\omega = 0,1$).

Same as before, it is necessary to carry out the fit process and determine the Yield Stress parameter. Figures 5.4 and 5.5 show the fit curves while tables 5.5 and 5.6 resume the parameter values. Green and blue curves correspond to PPt and rPP, respectively. Besides, red curves and black points are related to fit and experimental data.

Through Matlab, it was viable to optimize the setting at both low and high frequencies. In fact, the difference between the experimental curves and model is minuscule and admissible for the study.

At first sight, Khoshkava and Kamal's model fits correctly with experimental results. As mentioned above, the lowest Yield Stress values are linked to last sample, while the highest values are in the second sample (20 %wt rPP). Third and Fourth sample have comparable values, which could be considered as a single behavior. Regarding reference value (PPt), it is possible to affirm that non-Newtonian behavior increases when adding rPP, which means an advantage for the printing process.

Nonetheless, figure 5.5 indicates an opposite situation. The fitting model presented differences at low frequency. These dissimilarities are taken as a limitation of the model and not as an error. As a previous case, the lower Yield Stress values correspond to last sample, but the highest values are in second and third. First and Fourth sample present similar values.

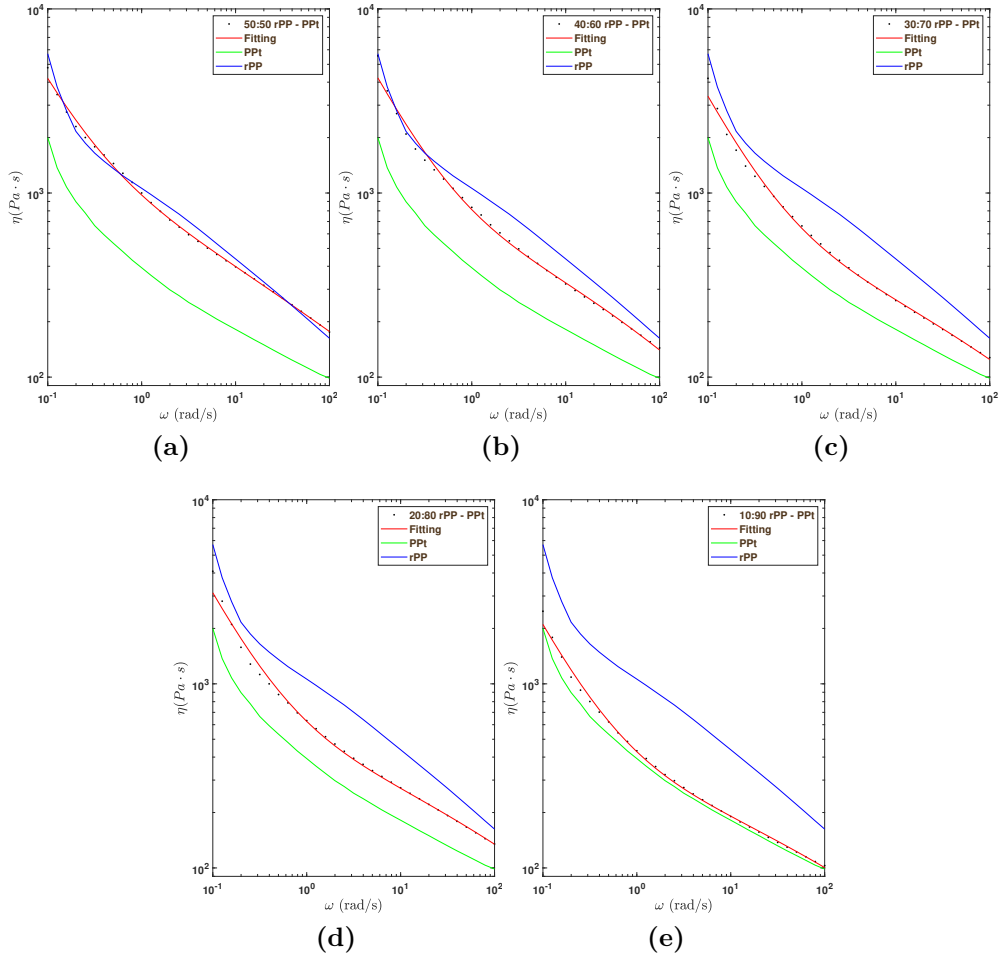


Figure 5.4: Comparison between the rheological curves at 230°C, between base materials and mixtures produced with mini-extruder. (a) 50 %wt rPP. (b) 40 %wt rPP. (c) 30 %wt rPP. (d) 20 %wt rPP. (e) 10 %wt rPP.

Sample	Symbol	Value	Unit
50:50 rPP - PPt	$\sigma_{T=230\text{ }^{\circ}\text{C}}$	326,1	$\text{Pa} \cdot \text{s}$
40:60 rPP - PPt	$\sigma_{T=230\text{ }^{\circ}\text{C}}$	368,2	$\text{Pa} \cdot \text{s}$
30:70 rPP - PPt	$\sigma_{T=230\text{ }^{\circ}\text{C}}$	292,9	$\text{Pa} \cdot \text{s}$
20:80 rPP - PPt	$\sigma_{T=230\text{ }^{\circ}\text{C}}$	269,4	$\text{Pa} \cdot \text{s}$
10:90 rPP - PPt	$\sigma_{T=230\text{ }^{\circ}\text{C}}$	181,7	$\text{Pa} \cdot \text{s}$

Table 5.5: Yield Stress values for all blends at 230°C.

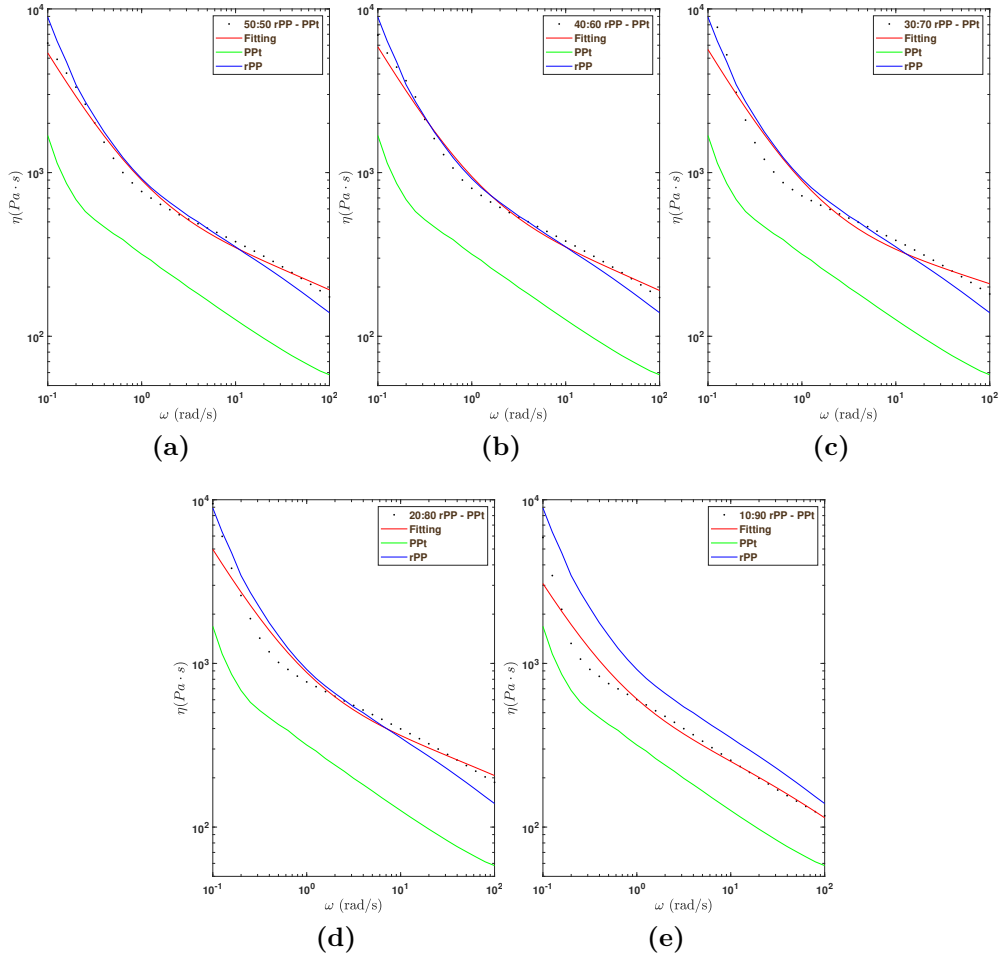


Figure 5.5: Comparison between the rheological curves at 260°C, between base materials and mixtures produced with mini-extruder. (a) 50 %wt rPP. (b) 40 %wt rPP. (c) 30 %wt rPP. (d) 20 %wt rPP. (e) 10 %wt rPP.

Sample	Symbol	Value	Unit
50:50 rPP - PPt	$\sigma_{T=260\text{ }^{\circ}\text{C}}$	488,7	$\text{Pa} \cdot \text{s}$
40:60 rPP - PPt	$\sigma_{T=260\text{ }^{\circ}\text{C}}$	536,9	$\text{Pa} \cdot \text{s}$
30:70 rPP - PPt	$\sigma_{T=260\text{ }^{\circ}\text{C}}$	520,3	$\text{Pa} \cdot \text{s}$
20:80 rPP - PPt	$\sigma_{T=260\text{ }^{\circ}\text{C}}$	445,6	$\text{Pa} \cdot \text{s}$
10:90 rPP - PPt	$\sigma_{T=260\text{ }^{\circ}\text{C}}$	266,8	$\text{Pa} \cdot \text{s}$

Table 5.6: Yield Stress values for all blends at 260°C.

5.1.2 Thermal Gravimetric Analysis - TGA Results

In the same way as the rheology test, knowing the behavior of the base materials is required. Thermogravimetric analysis (TGA) is a method in which is possible to define the amount of inorganic phase in the plastic materials. Moreover, TGA also can be used to evaluate the thermal stability of material through the loss mass.

Figure 5.6 shows both signals of TGA, blue curves are related to PPt and orange curves to rPP. The left figure represents the loss of mass measured while the right curve is the derivative of mass.

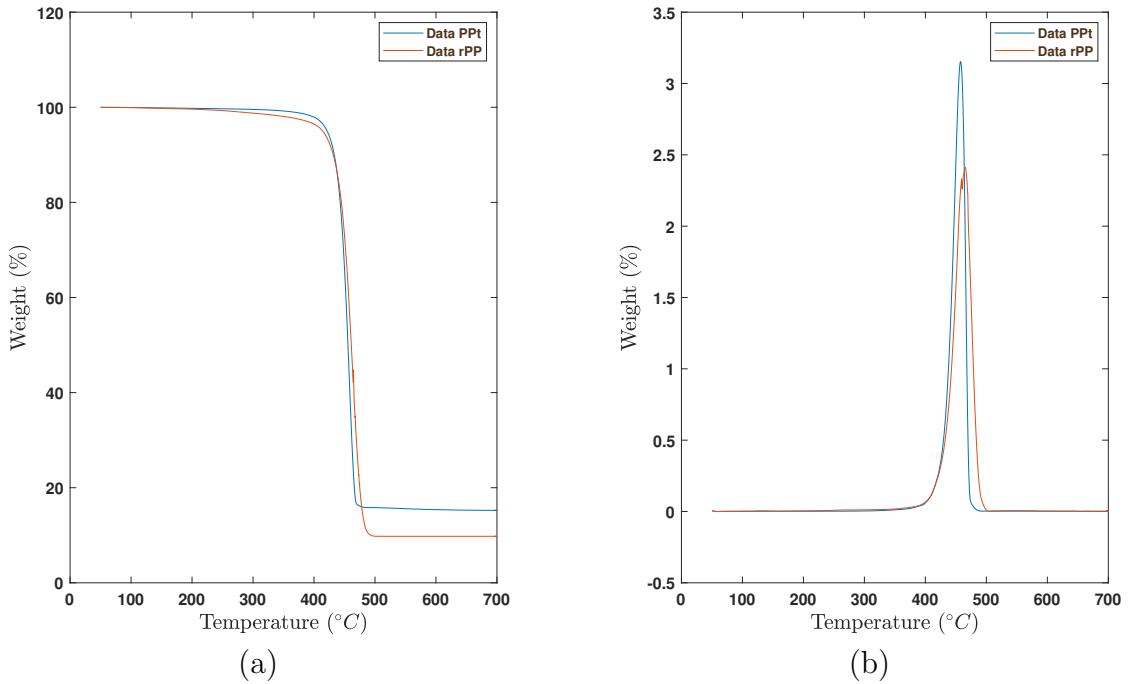


Figure 5.6: TGA results for base materials, PPt and rPP. (a) Loss of mass measured (TG). (b) Derivative of mass (DTG).

In the case of PPt, it is known that it is composed of two materials, PP and talcum. So, it is possible to determine the ratio between the inorganic phase and plastic phase. As a result, the residue is just 16%wt. This value is related to the quantity of talcum. Moreover, the loss of weight process begins first in the case of rPP than PPt.

On the other hand, the residue in the rPP was just 10%wt, which means that the recycled materials have also an inorganic phase or elements that degrade at high temperatures, such as carbon black or PET.

The second signal (figure (b)) is related to the first derivative or rate of weight changes, which gives information about the temperature of degradation at a

maximum rate of weight change. These temperature for both materials are 463,5°C and 465,2°C.

Figure 5.7 shows both signals from each blend. The first outcome shows the weight loss starting after 300 °C. This value is important because it gives a guide to the heat capacity of the blend or the maximum temperature before begins the loss of weight (thermal stability).

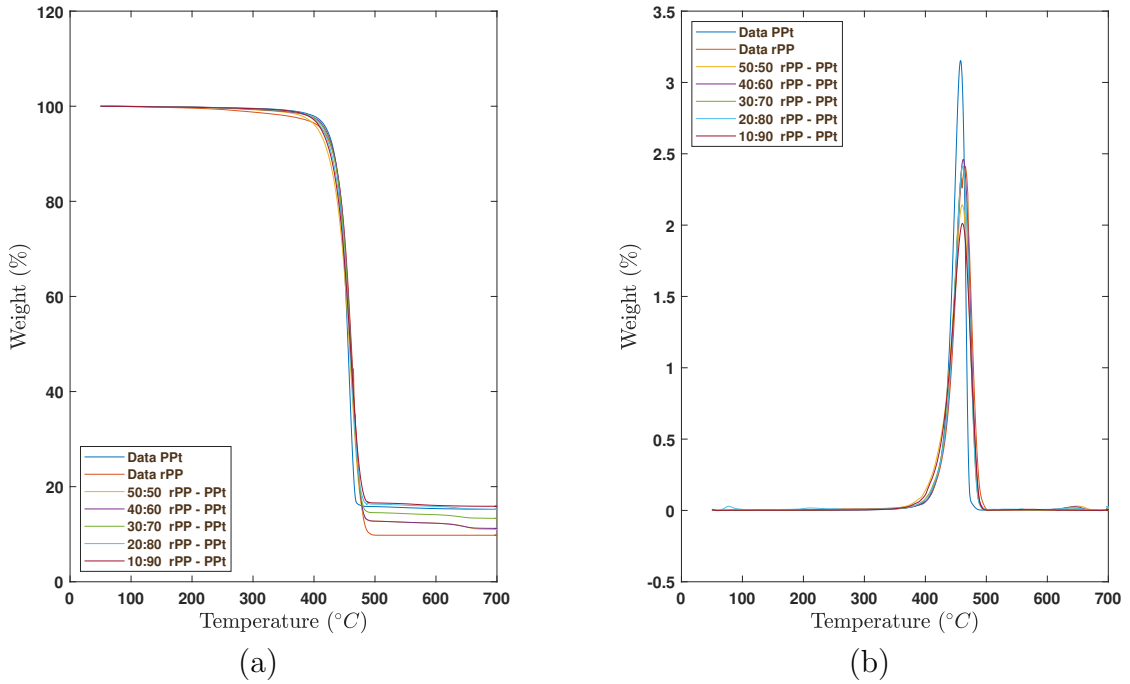


Figure 5.7: TGA results for base materials and all blends. (a) Loss of mass measured (TG). (b) Derivative of mass (DTG).

Sample	Temperature (98 % wt)	Residue	Peak
50:50 rPP - PPt	379,9	11,5	460,4
40:60 rPP - PPt	391,8	11,5	462,1
30:70 rPP - PPt	393,1	13,5	461,3
20:80 rPP - PPt	391,3	15,4	461,3
10:90 rPP - PPt	388,0	15,90	460,8

Table 5.7: TGA results values for each blend.

Table 5.7 resume the principal values of TGA test. As mentioned above, the mass loss begins after 300 °C, approximately, while residue values for each case

are 11 to 16 percent. In addition, the peak of the derivative signal shows that the maximum rate is obtained is just 460°C for each blend.

Figures 5.8 and 5.9 show the results of TGA test for each blend. The former is related to loss of mass signal (TG) while the latter is the derivative of mass (DTG). In both cases, the figures show a comparison between the base materials and each blend.

From the figure 5.8 is possible to notice a reverse relationship between the residue and the percentage of rPP. Decreasing the amount of rPP brings a raise on the residue.

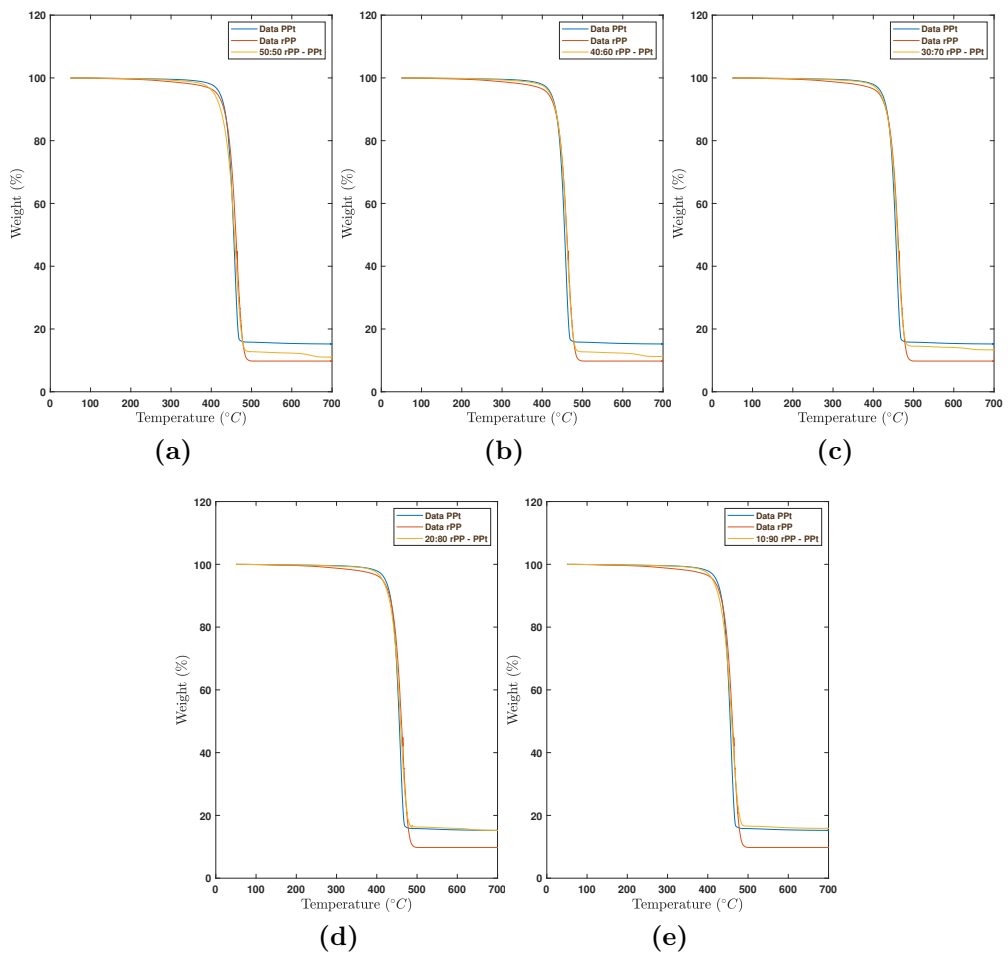


Figure 5.8: Thermogravimetric analysis results of each mixtures. (a) 50 %wt rPP. (b) 40 %wt rPP. (c) 30 %wt rPP. (d) 20 %wt rPP. (e) 10 %wt rPP.

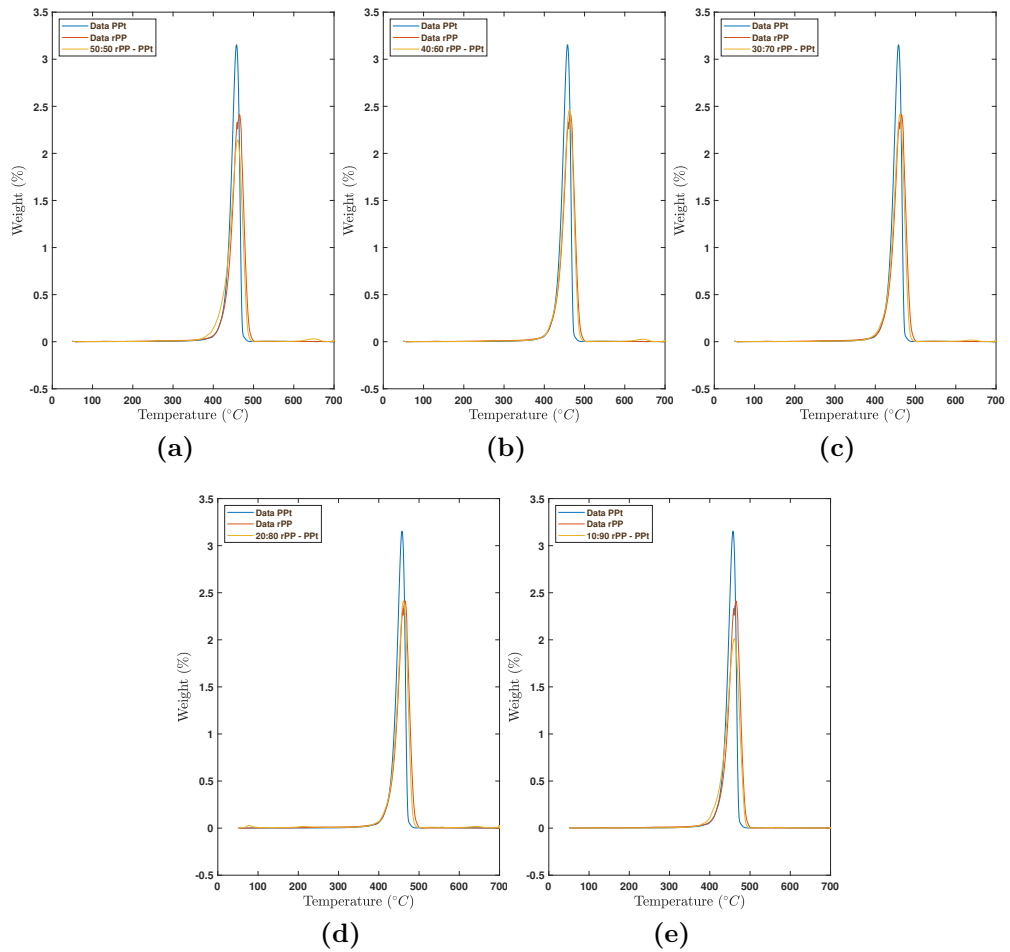


Figure 5.9: Derivative thermogravimetric analysis results of each mixtures. (a) 50 %wt rPP. (b) 40 %wt rPP. (c) 30 %wt rPP. (d) 20 %wt rPP. (e) 10 %wt rPP.

5.1.3 Differential Scanning Calorimetry - DSC Results

The result of the DSC test is presented into two curves, the Heating Cycle and Cooling Cycle. The information collected on both curves is related to the materials state, such as change phase, melting temperature, percentage of crystalline, etc. It is a common procedure, since the first heating scan is useful to erase the thermal history of the materials while the subsequent heating after the crystallization in controlled conditions allows determining the "true" crystallinity content of polymeric materials.

Figure 5.10 shows both curves cycle for PPI and rPP. The left figure displays the heating cycle while the right figure the cooling cycle. As a result of the heating cycle (third cycle), it is possible to identify for all curves the peak or peaks that are

related to the endothermic process or melting temperature. Moreover, it is possible to identify the percentage of crystallinity which is an important value because it is related to the printing process (shrinkage).

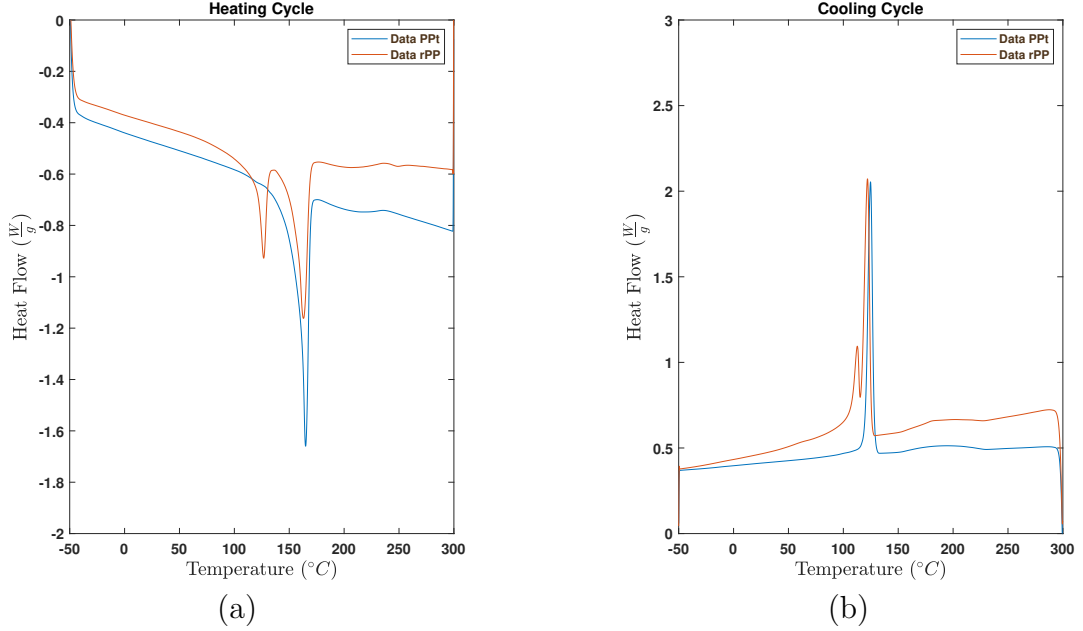


Figure 5.10: a) Heating Cycle b) Cooling Cycle

In the case of rPP, both thermal cycles give more than one peak. To identify those peaks is necessary to know the characteristic temperature. The first peak is related to PE, but the third one could be different types of materials, such as Poly(methyl methacrylate) - syndiotactic, Nylon 10-10, Poly(vinyl fluoride), Poly(vinylidene chloride), etc. The second peak is related to PP.

Table 5.8 shows the values for each peak and table 5.9 the degree of crystallinity for both materials, which are considered as a starting point and criteria for the chosen blend.

Material	$T_{melting}$ (°C)	$T_{crystallization}$ (°C)	ΔH_m (J/g)
PPT	164,9	159,2	66,5
	127,4	121,0	15,0
rPP	163,0	155,3	42,7
	207,0	179,7	4,0

Table 5.8: DSC results for PPT and rPP

Material	Degree Crystallinity (%)
PpT	39
rPP	17
	29

Table 5.9: Degree of crystallinity for PpT and rPP

It is relevant to highlight that reducing the percentage on this parameter guarantees the possibility to print the material for two reasons. The former is related to contractions of materials, which means a variety of dimensional sizes. At a high degree of crystallinity, all polymer chains are orientated and increase shrinkage. The latter is related to the the physical and mechanical properties. An increasing on this parameter results in rise on density, hardness, and strength.

On the other hand, figure 5.11 shows the DSC results for all blends- Figure (a) corresponds to the heating cycle while (b) is the cooling cycle. For all blends, it is possible to observe that there are three principal peaks, which are related to the material mentioned above. However, the last peak is not taken into account because it is relatively small.

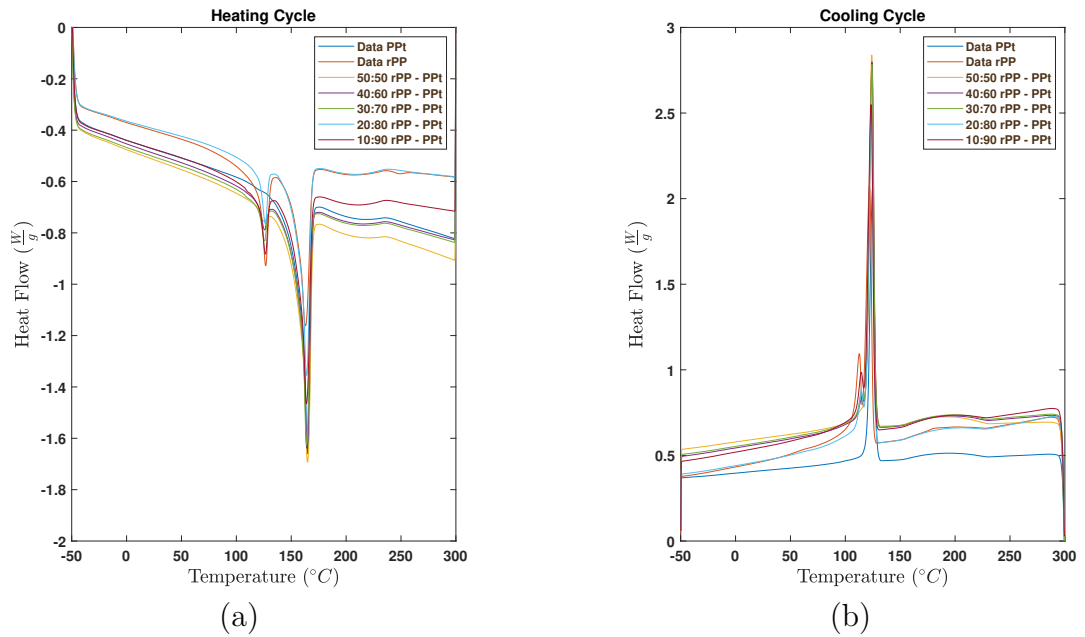


Figure 5.11: a) Heating Cycle. b) Cooling Cycle

Tables 5.10 and 5.11 resume the relevant values for this test, such as the melting

temperature and delta of enthalpy. According to both tables, there is a significant effect as a result of the addition of rPP. This effect is a reduction of the enthalpy for the PP peak and the rise for the PE peak, which means a variation on degree crystallinity.

Material	$T_{melting}$ °C	$T_{crystallization}$ °C	ΔH_m (J/g)
50:50 rPP - PPt	126,3	120,8	9,7
	165,2	157,4	52,7
40:60 rPP - PPt	126,18	120,9	8,3
	165,08	157,7	50,5
30:70 rPP - PPt	126,31	120,4	4,3
	166,18	158,3	56,1
20:80 rPP - PPt	125,21	119,9	3,4
	165,31	158,5	57,8
10:90 rPP - PPt	125,55	119,0	1,5
	166,88	158,5	61,8

Table 5.10: Principle peak values of DSC test for all blends.

Run	Degree of Crystallinity of PE (%)	Degree of Crystallinity of PP (%)
50:50 rPP - PPt	11	36
40:60 rPP - PPt	9	35
30:70 rPP - PPt	5	39
20:80 rPP - PPt	4	40
10:90 rPP - PPt	2	43

Table 5.11: Degree of crystallinity for all blends.

As mentioned above, introducing a recycled material allows reducing the degree of crystallinity of PPt. For small quantities of rPP, the degree of crystallization is similar to the PPt, but to increase the amount of recycled material it is possible to reduce as far as 4%. The first two blend (50%wt - 40%wt R-PP) show the greatest reduction of it, while the third and four blend (30%wt - 40%wt R-PP) show a similar value. The last blend exhibit a rise on this parameters which is a undesirable effect.

As a result, it is expected that the percentage of shrinkage is reduced as the quantity of R-PP increases.

At this point, it was possible to identify the proportion of proportions that maximized the Yield Stress and minimized the degree of crystallinity. In the first case, at 230 °C, the first two blends exhibited the maximum values for Yield Stress (326,13 - 368,23 Pa), while at 260 °C are second and third one (536,86 - 520,33 Pa). On the other hand, the degree of crystallization has an inverse relationship with the amount of rPP. The blend with a higher rPP percentage displayed the minimum value of crystallinity. As a result, it is a possible choice between the second and third proportions to continue with the experimental process.

5.2 Second stage

According to the results for the first stage, there is two possible proportion that satisfies all requirements, which are the proportion 40%wt rPP and 30%wt rPP. Both blends exposed significant Yield Stress values, but also have a considerable amount of recycled material.

In the interest of reducing the waste material and time, it was used only one proportion. The blend selected was the second one (30%wt rPP), because it satisfies all requirements of Yield Stress and degree crystallinity. Indeed, the proportion between both materials (PPt and rPP) in this blend is the middle of all possible combinations.

However, after finding the optimization parameter process, both proportions are used to produce a new blends for the next stage.

5.2.1 Rheology Test Results

As mentioned in chapter 4, the objective sought to maximize the value of Yield Stress through the Taguchi method. This parameter is related to the non-Newtonian behavior. The parameters and levels evaluated in this method are chosen based on post-processing, such as filament and printer. For that reason, the stage was divided into two sections, rheological and optimization results.

As mentioned in chapter 4, the samples to be tested in this stage correspond to an orthogonal array L16 (table 4.7). The difference between all samples, called runs, is a combination between factors and levels (table 4.7). Hence the first step to make to know the complex viscosity curve for each run.

The figures below show the complex viscosity curve of all possible combinations. The results are divided into two figures. The left figure shows the result of the standard extruder screw while the right shows the case of the transport extruder screw. It was decided to split the results in this way due to the number of experiments.

At 230 °C (figure 5.12), in both profile 1 and 2, the complex viscosity curve of all samples presents a marker non-Newtonian behavior at low frequency and an

analogous trend. For the standard extruder screw, the complex viscosity curve of Run 7 presents an interesting behavior due to a reduction of the viscosity at high frequency and the marked non-Newtonian behavior at low frequency. Moreover, Run 5, Run 6 and Run 8 exhibit a marked non-Newtonian behavior.

On the other hand, for transport extruder screw, all runs exposed the same behavior as mentioned above. Indeed, run 10 and run 14 show not only a marker of non-Newtonian behavior but also an increase in viscosity, which is undesirable effect. However, the rise of viscosity will be neglected due to the small value.

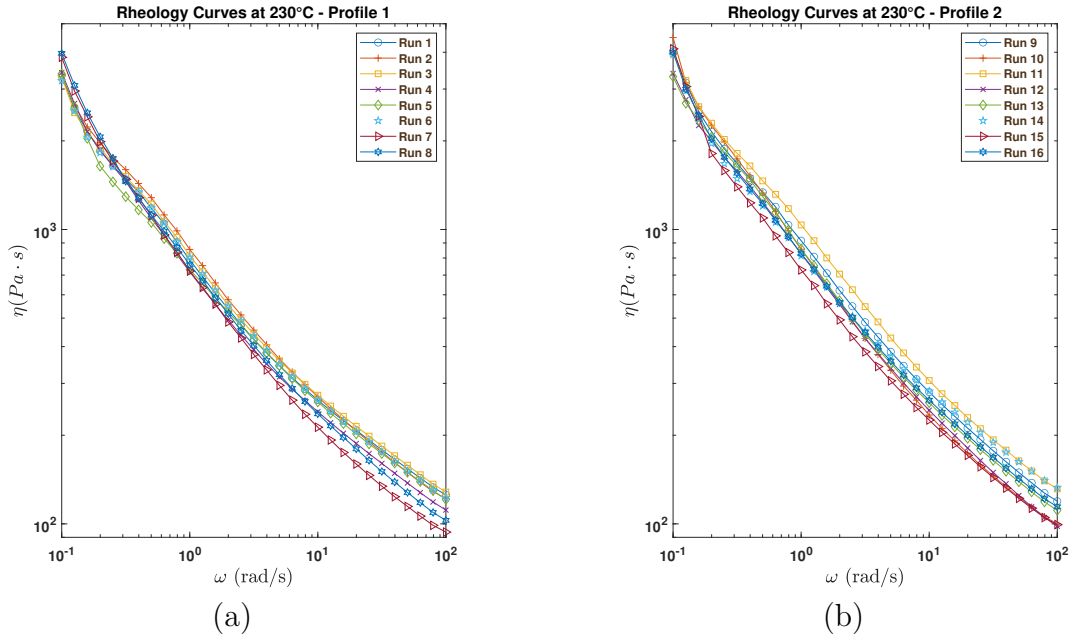


Figure 5.12: Comparison of rheological curves for each run produced with profile 1. (a) Rheological curves at 230 °C. (b) Rheological curves at 260 °C.

At 260 °C (figure 5.13), there are two different situation according to the extruder screw (profiles). In the former, standard extruder screw (profile 1), all example shows analogous complex curves except run 7 in which the viscosity at low frequency is minor. Run 8, Run 5 and Run 2 show a marked non-Newtonian behavior.

The latter, transport extruder screw (profile 2), the samples show dis-homogeneous complex viscosity curves at high frequencies. However, the main effect of the printing process is the non-Newtonian behavior in which all samples exhibit similar trends. The most significant non-Newtonian behavior is exposed in run 10, run 11, run 12, run 14, and run 15. Indeed, it is possible to see that the slope value is larger in this configuration. On the other hand, at high frequency, the samples could be divided into viscosity values. The critical case is shown in runs 13 and 14, while runs 10, 11, and 15 exposed a lesser value.

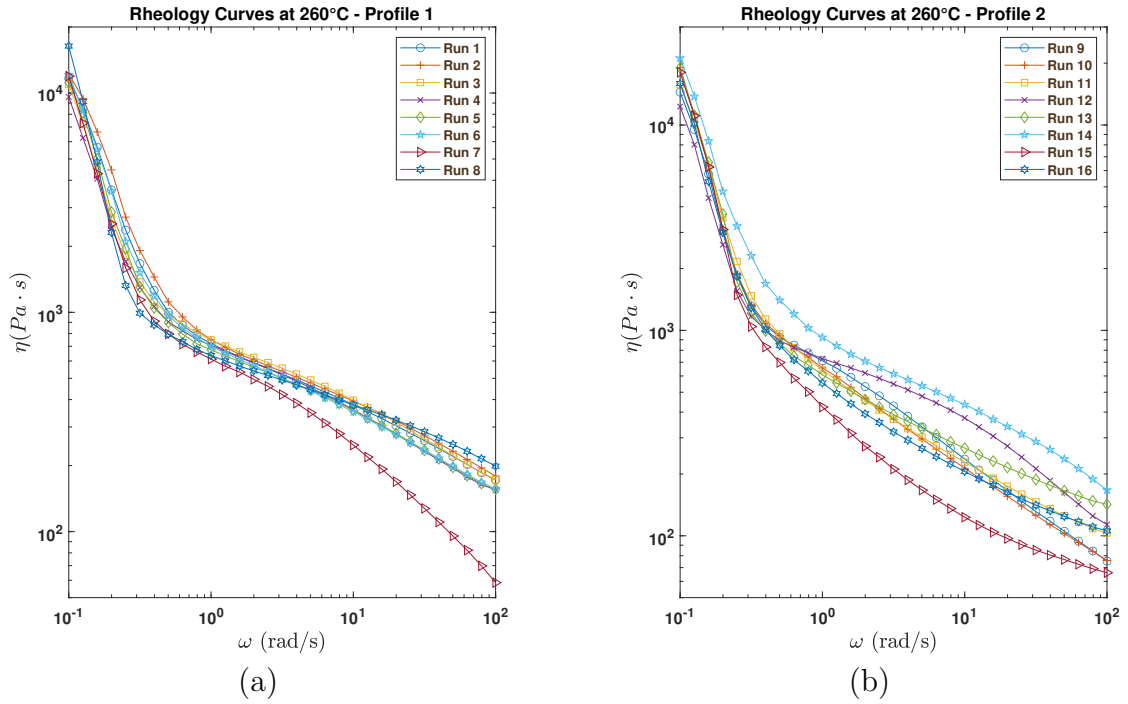


Figure 5.13: Comparison of rheological curves for each run produced with profile 2. (a) Rheological curves at 230 °C. (b) Rheological curves at 260 °C.

Table 5.12 shows the values of yield stress. The range of values for this parameter at 230 °C is between 212 to 320 Pa, while at 260 °C is 438 - 844 Pa. The first thing to highlight is the difference between the values of yield stress with the previous stage. This difference could be explained as to how the result of the variation of process conditions. However, using recycled materials produces huge dispersion in their response due to the different types of materials inside on it, the number of cycles for re-use, as an example.

On the other hand, there are different configurations in which the Yield Stress is maximized. At 230 °C, the higher Yield Stress values are in runs 7, 8, 10, and 15. At the same time, at 260 °C, the runs with a higher value are run 9, 10, 14, and 16. For both cases, run 10 exposed the better possible behavior.

Finally, a marker non-Newtonian behavior is obtained in the configuration of the second profile (transport extruder screw). However, seeing the complex behavior of curve at 260 °C for this configuration is expected a difference between model (fitting) and experimental data, which could be seen as a variation of their Yield Stress Values.

Sample	Symbol	Value	Unit	Sample	Symbol	Value	Unit
Run 1	$\sigma_{T=230 \text{ } ^\circ C}$	236,73	Pa	Run 9	$\sigma_{T=230 \text{ } ^\circ C}$	260,88	Pa
	$\sigma_{T=260 \text{ } ^\circ C}$	710,12	Pa		$\sigma_{T=260 \text{ } ^\circ C}$	567,79	Pa
Run 2	$\sigma_{T=230 \text{ } ^\circ C}$	218,66	Pa	Run 10	$\sigma_{T=230 \text{ } ^\circ C}$	320,48	Pa
	$\sigma_{T=260 \text{ } ^\circ C}$	792,16	Pa		$\sigma_{T=260 \text{ } ^\circ C}$	621,70	Pa
Run 3	$\sigma_{T=230 \text{ } ^\circ C}$	222,86	Pa	Run 11	$\sigma_{T=230 \text{ } ^\circ C}$	233,80	Pa
	$\sigma_{T=260 \text{ } ^\circ C}$	629,70	Pa		$\sigma_{T=260 \text{ } ^\circ C}$	629,46	Pa
Run 4	$\sigma_{T=230 \text{ } ^\circ C}$	258,06	Pa	Run 12	$\sigma_{T=230 \text{ } ^\circ C}$	220,61	Pa
	$\sigma_{T=260 \text{ } ^\circ C}$	528,57	Pa		$\sigma_{T=260 \text{ } ^\circ C}$	438,91	Pa
Run 5	$\sigma_{T=230 \text{ } ^\circ C}$	216,04	Pa	Run 13	$\sigma_{T=230 \text{ } ^\circ C}$	228,40	Pa
	$\sigma_{T=260 \text{ } ^\circ C}$	627,98	Pa		$\sigma_{T=260 \text{ } ^\circ C}$	599,85	Pa
Run 6	$\sigma_{T=230 \text{ } ^\circ C}$	212,99	Pa	Run 14	$\sigma_{T=230 \text{ } ^\circ C}$	267,32	Pa
	$\sigma_{T=260 \text{ } ^\circ C}$	688,15	Pa		$\sigma_{T=260 \text{ } ^\circ C}$	844,90	Pa
Run 7	$\sigma_{T=230 \text{ } ^\circ C}$	294,01	Pa	Run 15	$\sigma_{T=230 \text{ } ^\circ C}$	286,67	Pa
	$\sigma_{T=260 \text{ } ^\circ C}$	469,63	Pa		$\sigma_{T=260 \text{ } ^\circ C}$	506,45	Pa
Run 8	$\sigma_{T=230 \text{ } ^\circ C}$	292,10	Pa	Run 16	$\sigma_{T=230 \text{ } ^\circ C}$	269,28	Pa
	$\sigma_{T=260 \text{ } ^\circ C}$	561,09	Pa		$\sigma_{T=260 \text{ } ^\circ C}$	563,09	Pa

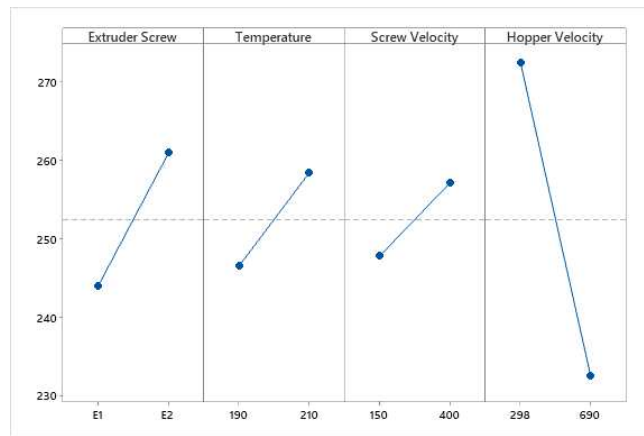
Table 5.12: Yield Stress values for all possible configuration and temperatures.

5.2.2 Taguchi Test Results

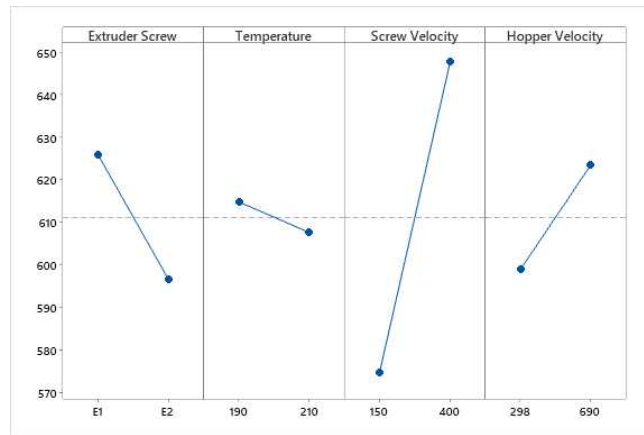
As seen in table 4.7 (chapter 4), the array used in this research was L16 which has sixteen different combinations (runs) of parameters and levels. As mentioned before, the value considered for each level corresponds to the extreme case, which means the limit value for each one (table 4.6).

To understand the relevance and the impact for each factor and level, it decided to use an optimization process based on Taguchi Method, where it was looked to maximize the response. The object was not only understanding the importance and the effects of process parameters but also finding the maximum Yield Stress value.

The results of this process show throughout two figures which display the characteristic average for each factor and level. The line slope value in these figures determines the relevance of each factor and level. If the slope value is zero, the factor and level have influenced the results in the same way. On the opposite side, if the slope is greater than zero, the factors and levels of influence will be significant. As a result, it is possible to arrange by relevance the factors and determine which level governs the results.



(a)



(b)

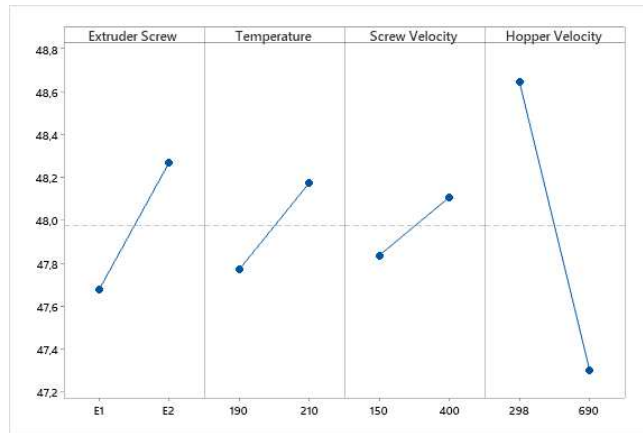
Figure 5.14: Main effects for Extrusion parameters. (a) Average of Yield Stress at 230 °C. (b) Average Yield Stress at 260 °C.

Figure 5.14 shows the average of response for all parameters and levels in both cases. It was possible to conclude, at 230 °C, the highest Yield Stress value was obtained with the second level for Extruder Screw, Temperature, and Screw velocity, while the first level to the Hopper Velocity. On the other hand, at 260 °C, the maximum value was obtained as a combination of levels and factors. In this case, it was not possible to choose a unique solution. Furthermore, the temperature could be neglected due to the small difference between levels response.

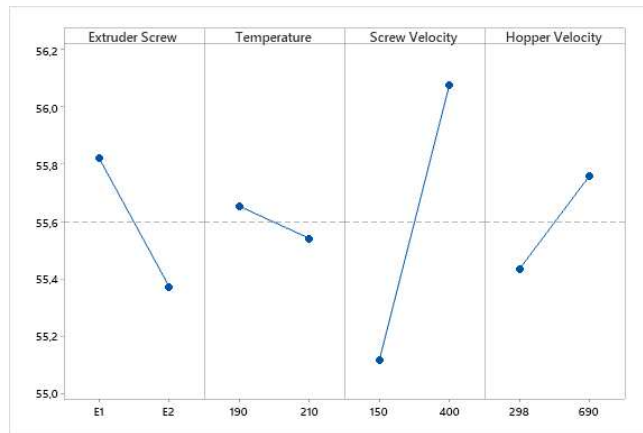
On the other hand, figure 5.15 shows the effect and relationship for each parameter. Also, it was possible to determine the factors that could be considered as principal. As mentioned above, at 230 °C, the factor that shows relevant change is Hopper Velocity. However, the Extruder Screw also exhibits a significant variation

between levels. As a consequence of mentioned above, both factors were regarded as principal.

At 260 °C, Hopper velocity did not display the most relevant change, while Screw Velocity did. It was possible to notice a common effect between both temperatures, which is the variation on Extruder Screw. The difference between both is the value of the slope, as it is positive in figure a and negative in figure b. Finally, the temperature was neglected due to the small variation in its response.



(a)



(b)

Figure 5.15: Main effects for SN ratios of Extrusion parameters. (a) SN of Yield Stress at 260 °C. (b) SN of Yield Stress at 260 °C.

In conclusion, it was not a unique configuration in which the Yield Stress Value was maximum. Furthermore, the response will depend on the temperature at which the rheological test was conducted. For the reasons mentioned above, parameters can be arranged in order of importance as follows Screw Velocity, Hopper Velocity,

Extruder Screw, and Temperatures. At low temperature, (230 °C), the main parameter will be Hopper Velocity, while at high temperatures, (260 °C), is Screw velocity. It did not consider the rheological temperature test, the main parameter will be Extruder Screw.

5.2.3 Final selection

According to the results and conclusion mentioned above (rheology and Taguchi results), it was decided to repeat the experimental process for runs 10, 11, 14, and 15. They display a combination of factors and levels chosen in chapter 4. Even more, the Yield Stress for each one displays the most significant value. The scope was simulated as a continuous process (line production) and corroborated the previous results.

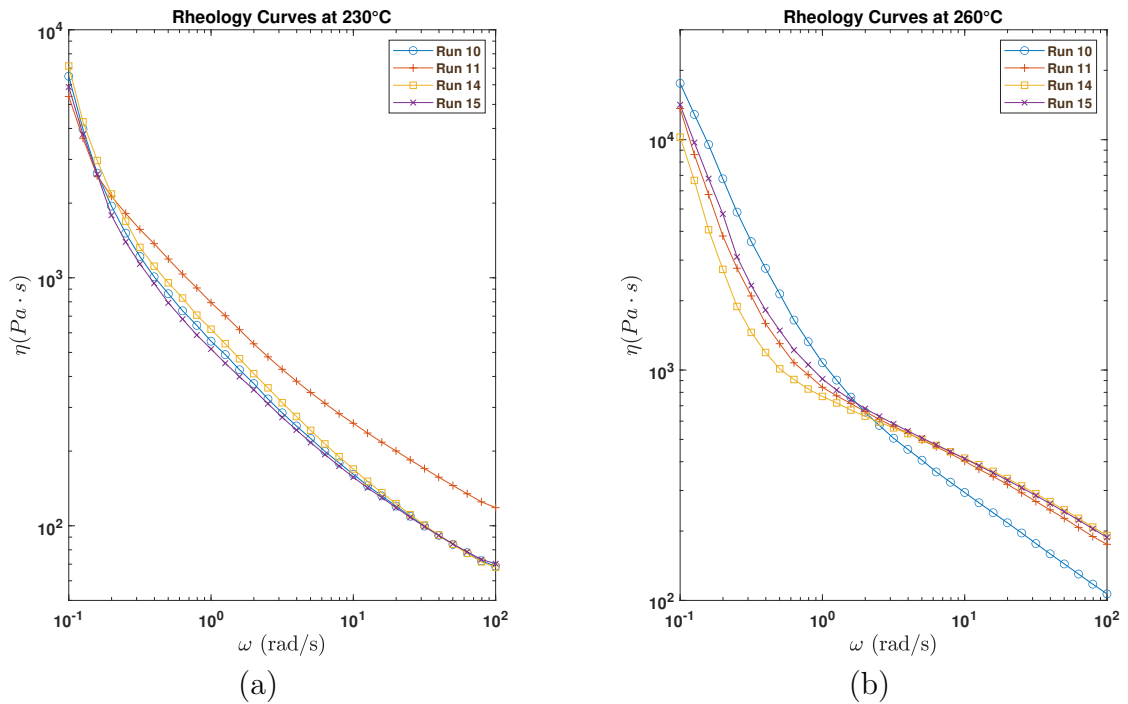


Figure 5.16: Viscosity curve for all runs selected a) Viscosity curve at 230. b) Viscosity curve at 260.

Figure 5.16 shows the complex viscosity curve for runs selected above. As seen in previous figures, the curves show a marked non-Newtonian behavior. However, at 230 °C, run 11 exhibits a variation in viscosity at high frequency. According to the slope at low frequency, Run 14 exposed the most marked non-Newtonian behavior. However, the difference between all runs is minute.

On the other hand, at 260 °C, run 10 shows not only a marker of non-Newtonian behavior but also is reduced viscosity at high frequency, while your trend exhibit a variation between all of them. Run 11 and Run 15 display an analogous complex behavior, while run 14 is distinct due to a viscosity reduction.

Table 5.13 resume the values for Yield Stress for all runs. At 230 °C, the values for Yield Stress show a small variation to previous values (table 5.12). Their range, in this case, is between 350 - 423 Pa. However, the variation in the complex behavior is unimportant. So, it could be neglected.

In the same way, at 260 °C, the yield strength values increase. The increase is relatively small for most runs, but not for run 10. In this run, the increase was significant, but it is probably a consequence of the use of recycled material. The Yield Stress range, at this temperature, was between 466 - 1136 Pa.

Sample	Symbol	Value	Unit
Run 10	$\sigma_{T=230\text{ }^{\circ}C}$	381,47	Pa
	$\sigma_{T=260\text{ }^{\circ}C}$	1135,35	Pa
Run 11	$\sigma_{T=230\text{ }^{\circ}C}$	369,66	Pa
	$\sigma_{T=260\text{ }^{\circ}C}$	663,73	Pa
Run 14	$\sigma_{T=230\text{ }^{\circ}C}$	422,86	Pa
	$\sigma_{T=260\text{ }^{\circ}C}$	466,37	Pa
Run 15	$\sigma_{T=230\text{ }^{\circ}C}$	354,15	Pa
	$\sigma_{T=260\text{ }^{\circ}C}$	767,21	Pa

Table 5.13: Yield Stress values for all runs selection.

According to the results above, it was possible to choose Run 10 as the better possibility. This run not only describes the highest yield stress value, but also includes Taughci's results. The configuration for this run corresponds to level one for extrusion machine parameters, while it is the second level for Hopper velocity.

Figure 5.17 shows the complex viscosity curves comparison between PPt, rPP, and Run 10. It is possible to notice the difference in viscosity behavior for all materials. For both temperatures, 230 °C and 260 °C, Run 10 displays not only significant non-Newtonian behavior but also it has a shift to the right. This shift could be considered a desirable effect because extends the range in which is present non-Newtonian behavior.

Another relevant effect was the viscosity at high frequency. For both cases, it did not increase significantly. On the contrary, at 230 °C, the viscosity decrease.

As mentioned in previous chapters, the theoretical model fits correctly at 230 °C while at 260 °C display a small difference. This difference will be neglected due to is the limit of the model.

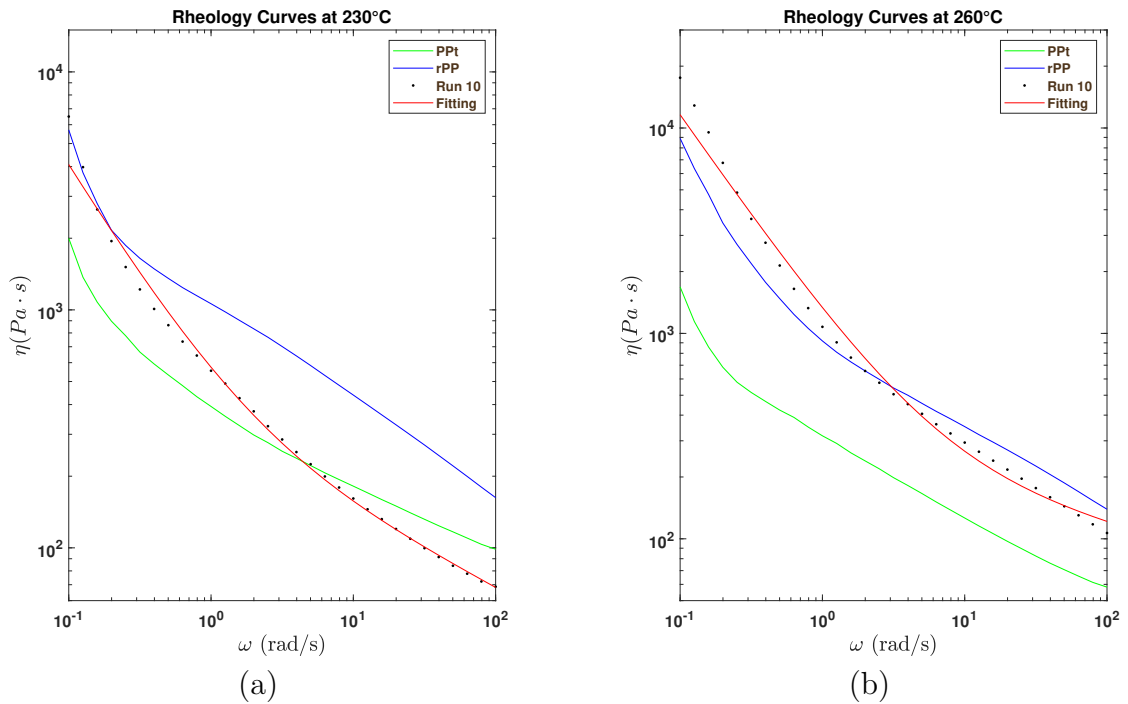


Figure 5.17: Comparison between First stage and Second stage results a) Complex viscosity curve at 230 °C. b) Complex viscosity curve at 260 °C.

5.3 Third stage

As mentioned in chapter 4, this stage was making a filament with two proportions 30%wt rPP, and 40%wt rPP. Both blends are produced, taking to account the optimization process.

According to Bernagozzi's research and Bertolino's research, Temperature, Screw Velocity, and Fan Speed are the parameters that make significant modifications in the filament. Following their results, it was decided to begin the experimental process with the parameter combination in which they have obtained a constant diameter and continuous filament for rPP.

It was founded that Fan parameters (percentage speed and angles) modify the diameter and shape of filament. The reason for it is the way how airflow arrives on the filament. Bertolino and Bernagozzi used equipment that controlled the airflow without modifying the heat transfer.

As seen before, the temperature and screw velocity has significant relevance for the extrusion process. At high temperatures, the fluidity of material increases because the energy amount increases, and it is possible to change the state of the material. On the other hand, a variation of screw velocity reduces the residence

time, which gives modify the time for transformation phases.

Afterward, various tests were conducted to find a combination that satisfies all requirements. These processes were made with only one proportion. Then, it proceeded to make the second filament with the other proportion.

Table 5.14 shows the tests that are conducted to obtain the diameter target (1,5 - 1,8 mm) and continuous filament. In the first three tests were modified the screw velocity, while temperature and fan speed also was changed in the other ones.

Attempt	Temperature (°C)	Screw Velocity (RPM)	Fan Speed (%)
1	200 - 200 - 195 - 195	2,3	10
2	200 - 200 - 195 - 195	2,7	10
3	200 - 200 - 195 - 195	2,7	10
4	200 - 200 - 195 - 195	3,7	30
5	220 - 215 - 215 - 210	3,7	30
6	220 - 215 - 215 - 210	4,5	30

Table 5.14: Parameters used to produce filament for both blends (30%wt and 40%wt rPP).

At low screw velocity (tests 1-3) the diameter of the filament did not satisfy the target. Even more, at the same temperature condition, it was evidenced that increasing this parameter reduces the diameter.

At constant screw velocity (test 3 and test 4), the filament displayed a diameter range that could be used in the printing process. However, test 3 showed an issue when the filament was collected. The filament at this temperature broke, so it was decided to increase the percentage of fan speed (test 4). For this case, the diameter ranges were acceptable (1,7 - 2,0 mm), and the reel collection was possible.

Furthermore, reducing the diameter ranges was necessary because there was a possibility that the printer could not extrude the filament. So, it was decided to increase the temperature (test 5). For this test, the diameter range is reduced (1,5 - 1,9 mm), and it was possible to produce a continuous filament. On the other hand, in test 6, temperature values newly increase, as an attempt to carry on the reduction of diameter range. However, there was a limitation because increasing screw velocity carries on to another issue, such as collected problems, continuous filament, etc.

The goal of this experimental process was to obtain a continuous filament in a diameter range between 1,5 - 1,9 mm. According to the previous review and research, the problem with recycled material is the impossibility to produce a continuous filament and enough quantity. For this research, was possible to produce

a filament in the diameter range but also in huge quantities.

For both filaments, it was identified, with a visual inspection, that there are zones on the filament in which the roughness increase. Those zones could be related to the recycled materials and inorganic phases.

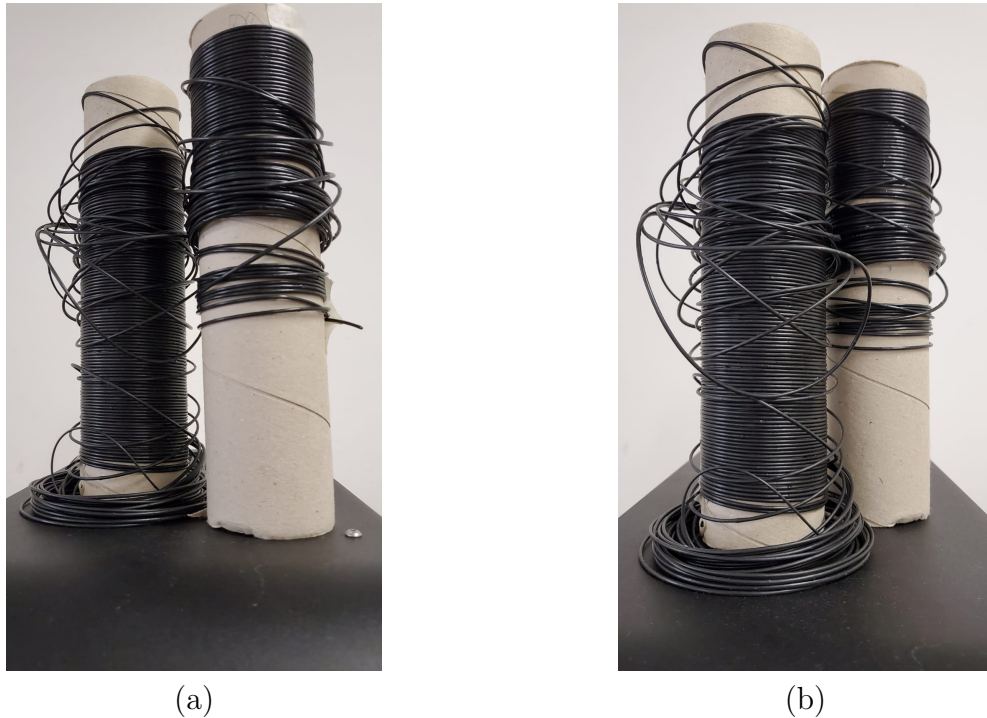


Figure 5.18: Filaments produced for both proportion with the best configuration. (a) 30%wt rPP. (b) 40 %wt rPP.

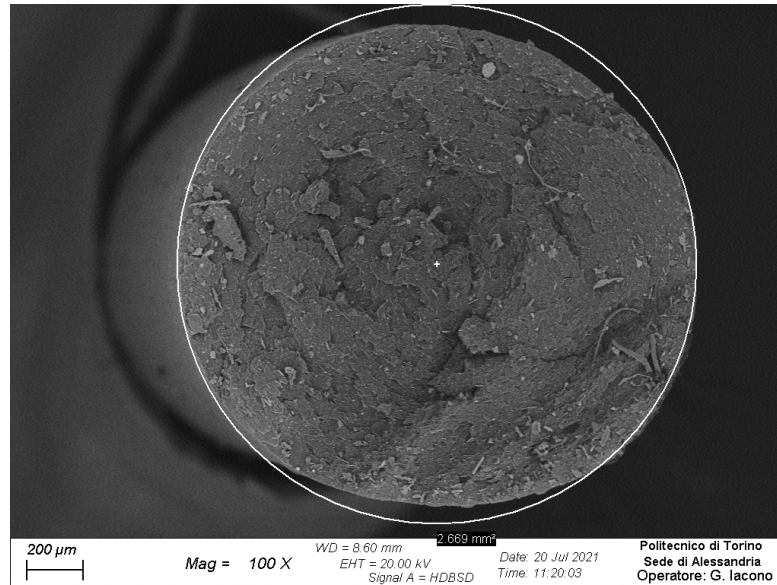
5.3.1 SEM results - Filament

As mentioned earlier, it was necessary to know the characteristic dimensions of the filament. Through the Scanning Electron microscopy test (SEM), it is got information regarding the surface topography and composition. The experimental procedure carried on with a brittle fracture through immersion of the filament in liquid nitrogen. This process allows avoiding any type of deformation, which could modify the size of the filament.

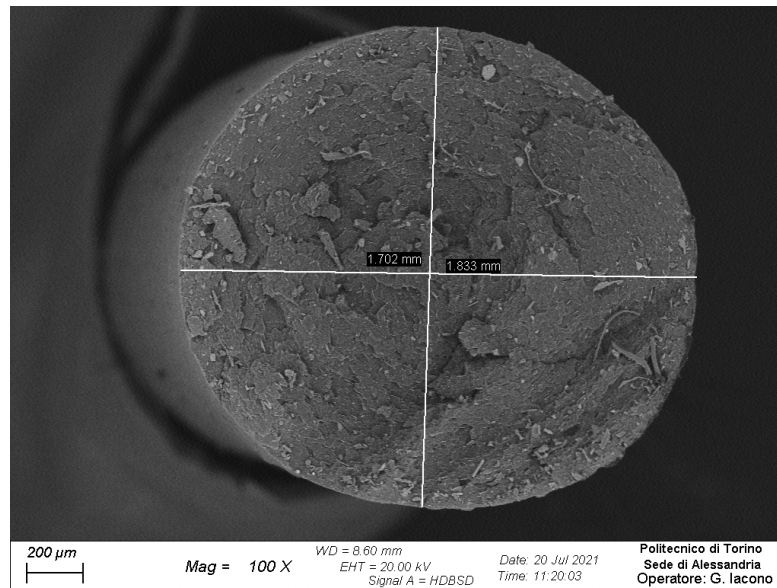
Figures below show different views of filament for both blends, 30 %wt and 40 %wt of rPP. Figure 5.19 shows the top view of filament at 30%wt rPP while figure 5.20 the side view.

The difference between the two radii (1,702 mm and 1,833 mm) is minuscule, with a 7% of relative error. However, as seen in figure 5.19 (a), the filament is

not perfectly concentric. Another important point to highlight regarding these images is the absence of areas without material. However, those variation does not represent a relevant issue for the printing process.



(a)

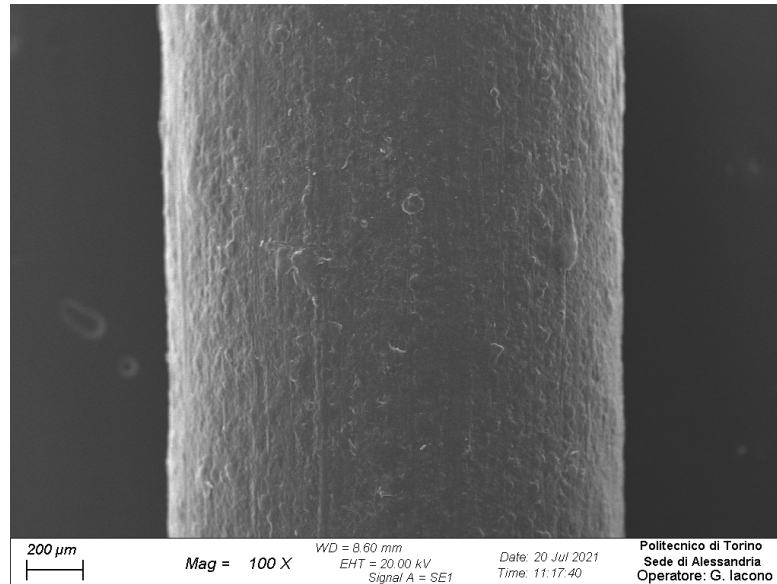


(b)

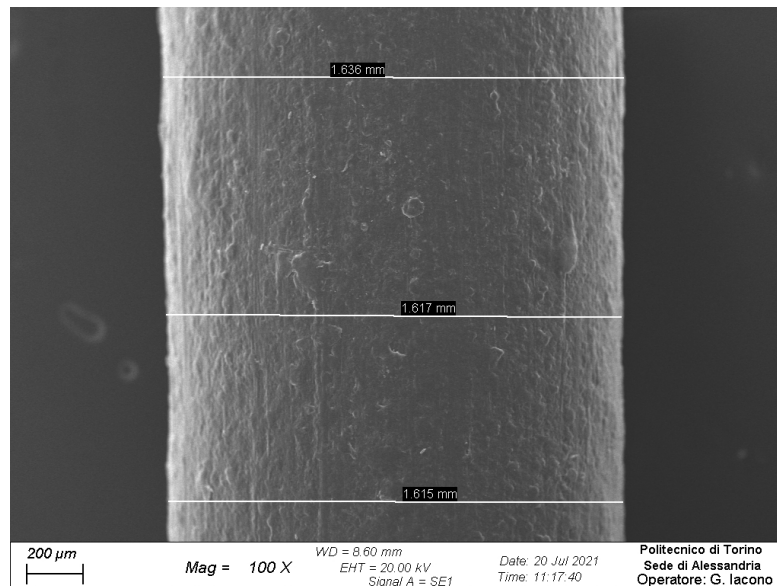
Figure 5.19: Top view of filament at 30 %wt rPP.

On the other hand, figure 5.20 (a) exposes the roughness of filament. As

mentioned before, the surface of the filament is not smooth. The difference between the maximum and minimum values is less than 0,02 mm, which represents a smallest variation (figure 5.20 (b)). However, as seen before, this variation could increase until 10 %.



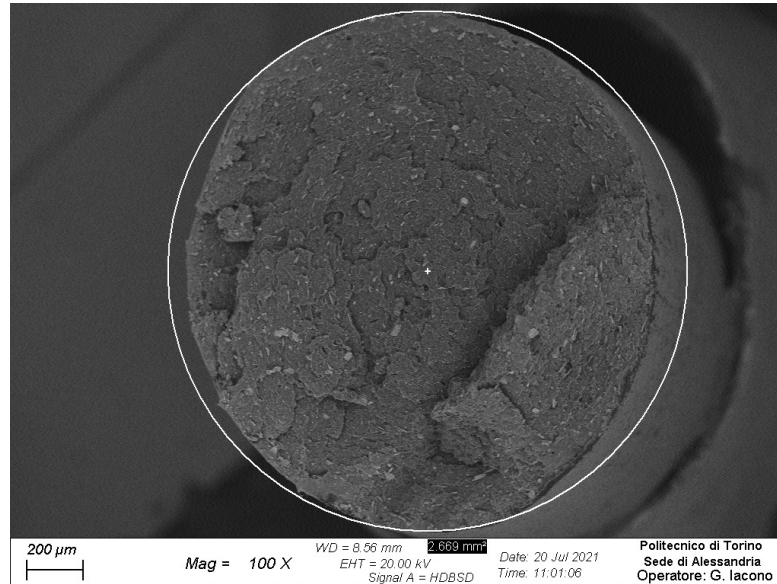
(a)



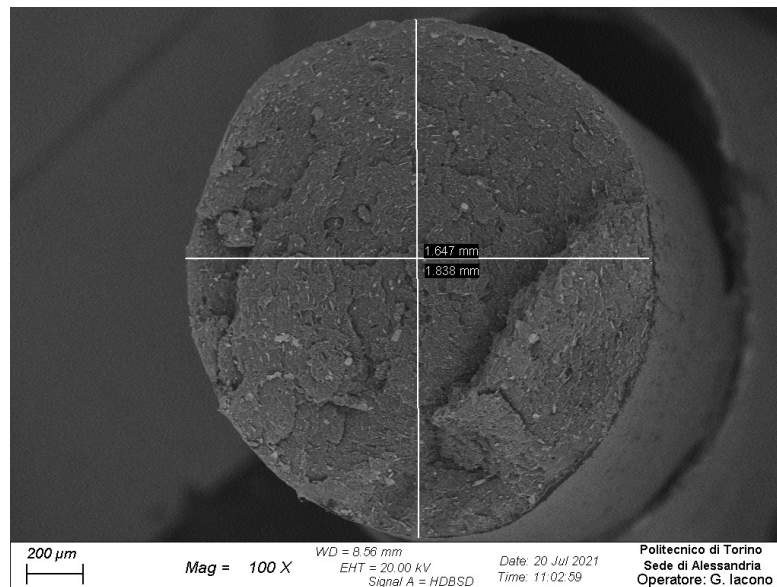
(b)

Figure 5.20: Side view of filament at 30 %wt rPP.

In the case of 40 %wt rPP, figure 5.21 (b), the different between both radius (1,647 mm and 1,838 mm) is a little bigger. However, the relative error is just 10% which is acceptable as tolerances. As same as the previous case, the filament exhibit a continuous matrix without empty zones.

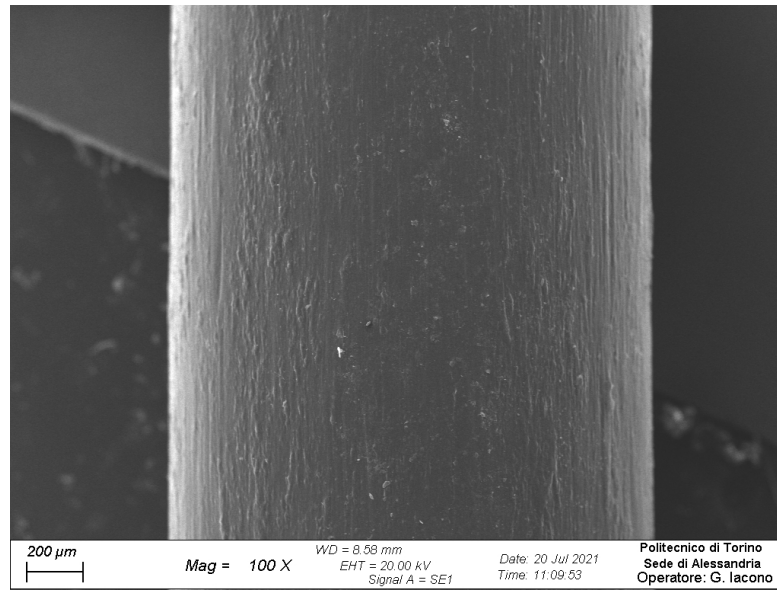


(a)

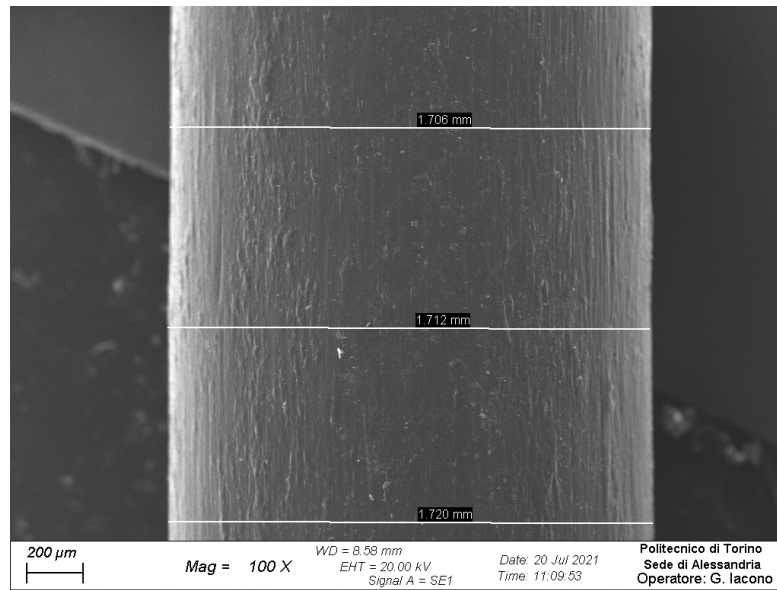


(b)

Figure 5.21: Side view of filament at 40 %wt rPP.



(a)



(b)

Figure 5.22: Side view of filament at 40 %wt rPP.

On the other hand, figure 5.22 (a) shows the surface roughness. For these cases, the filament shows a smooth roughness if it is compared with the cases of 30%wt rPP. This situation could be an advantage because improve the visual aspect. Moreover, it is possible to reduce the variance between the thickness. As seen in

figure 5.22 (b), which measure the thickness at different distances are similar.

Figure 5.23 shows a image of filament at 40%wt rPP at 5000x. For this figure, it was carried out at computational analysis throughout secondary electrons emission. It was chosen different points of surface (1, 2, 3, 4, and 5) to identify ta fractional chemical composition. The difference between each point was related to the presence or not of charges.

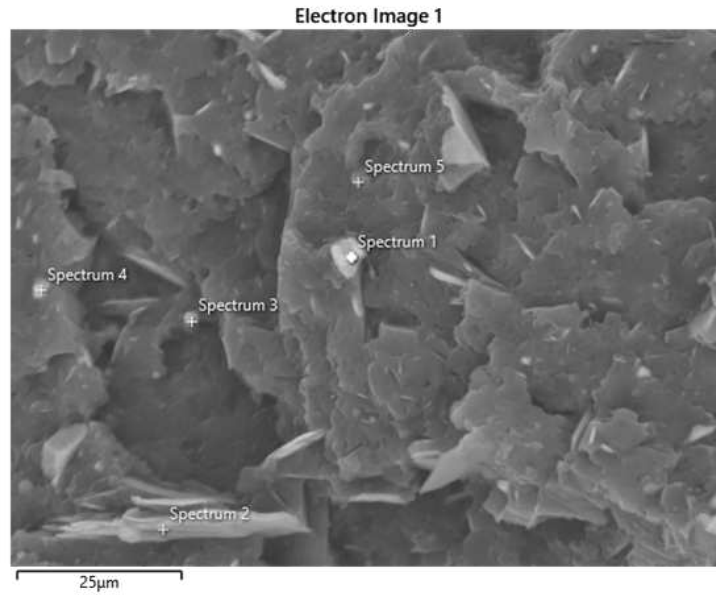


Figure 5.23: AA.

Table 5.15 resume the values for all point. For points 3, 4, and 5, it was found at carbon weight around 98%.

Spectrum	Element	Weight (%wt)
1	C	40
	O	32
	Ca	20
2	C	55
	O	28
	Si	8
	Mg	5

Table 5.15: Weight fractions (%wt) of the elements at points 1 and 2.

For both cases, the filament satisfies all requirements to be used in 3D printing.

5.3.2 Rheology results

In order to highlight the effect of the process on the blend, it was decided to know the rheological behavior of both filaments. It was carried out three samples, called for now runs. These runs allow identifying the range of value for Yield Stress. Additionally, it was able to know the viscosity curve for each case.

Figure 5.24 shows the complex viscosity behavior for three different samples of the filament with 30%wt rPP. For this figure, it was possible to observe that complex viscosity curves for all samples are similar to rPP. All samples exhibit a non-Newtonian behavior, and, in some cases, it is bigger than rPP. At both temperatures, 230 °C and 260 °C, the viscosity increases at high frequency, although this did not represent an issue because at low frequency came about the same effect. As mentioned in the previous result, there is a sample in which the range of non-Newtonian behavior increase.

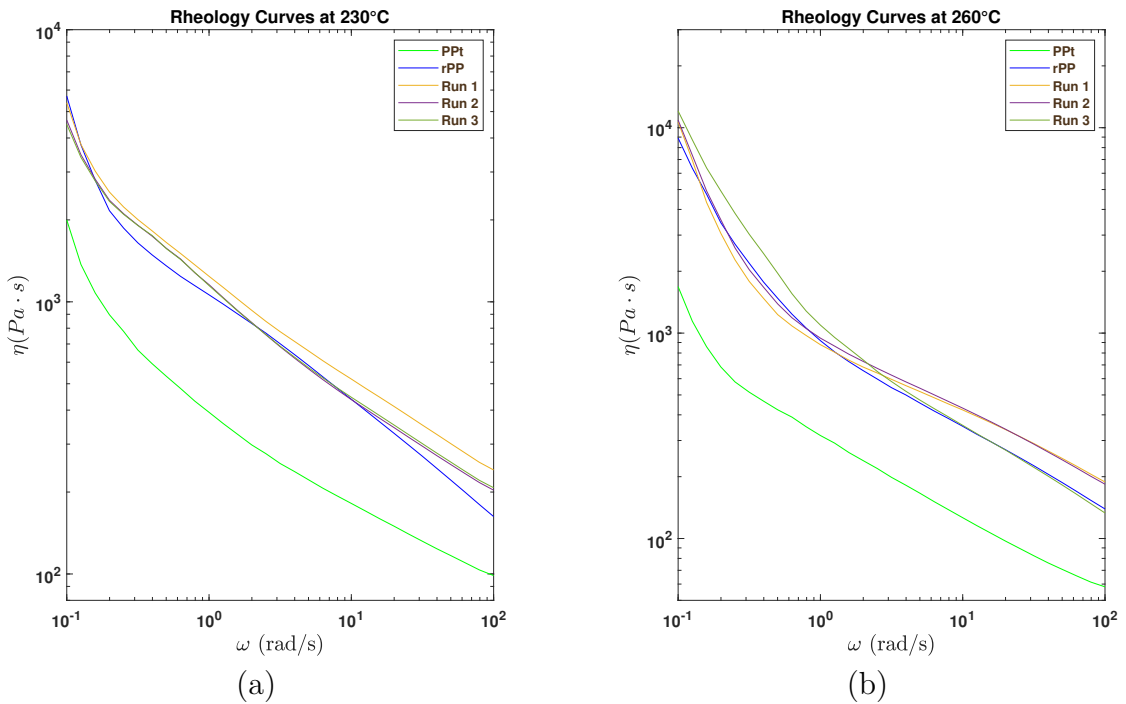


Figure 5.24: Comparison between First stage and third stage results (30%wt rPP). (a) Complex viscosity curve at 230 °C. (b) Complex viscosity curve at 260 °C.

Table 5.16 resume the Yield Stress values for all samples. The range of Yield stress is just 297 - 331 Pa at 230 °C, and 575 - 916 Pa at 260 °C. At low temperature, the samples exhibit an analogous trend. However, at high temperatures, the variation between their values is relevant. The average for both temperature is $312,3 \pm 17,2$ Pa and $712,5 \pm 179,5$ Pa respectively.

Sample	Symbol	Value	Unit
Run 1	$\sigma_{T=230\text{ }^{\circ}\text{C}}$	331,23	Pa
	$\sigma_{T=260\text{ }^{\circ}\text{C}}$	575,27	Pa
Run 2	$\sigma_{T=230\text{ }^{\circ}\text{C}}$	307,86	Pa
	$\sigma_{T=260\text{ }^{\circ}\text{C}}$	646,67	Pa
Run 3	$\sigma_{T=230\text{ }^{\circ}\text{C}}$	297,74	Pa
	$\sigma_{T=260\text{ }^{\circ}\text{C}}$	915,73	Pa

Table 5.16: Yield Stress values for filament at 30 %wt rPP.

Figure 5.25 shows a comparison between the complex viscosity of PPt, rPP, and the best filament sample results. Figure (a) show the case at 230 °C, in which run 1 exhibited the higher Yield Stress, while (b) shows the run 3.

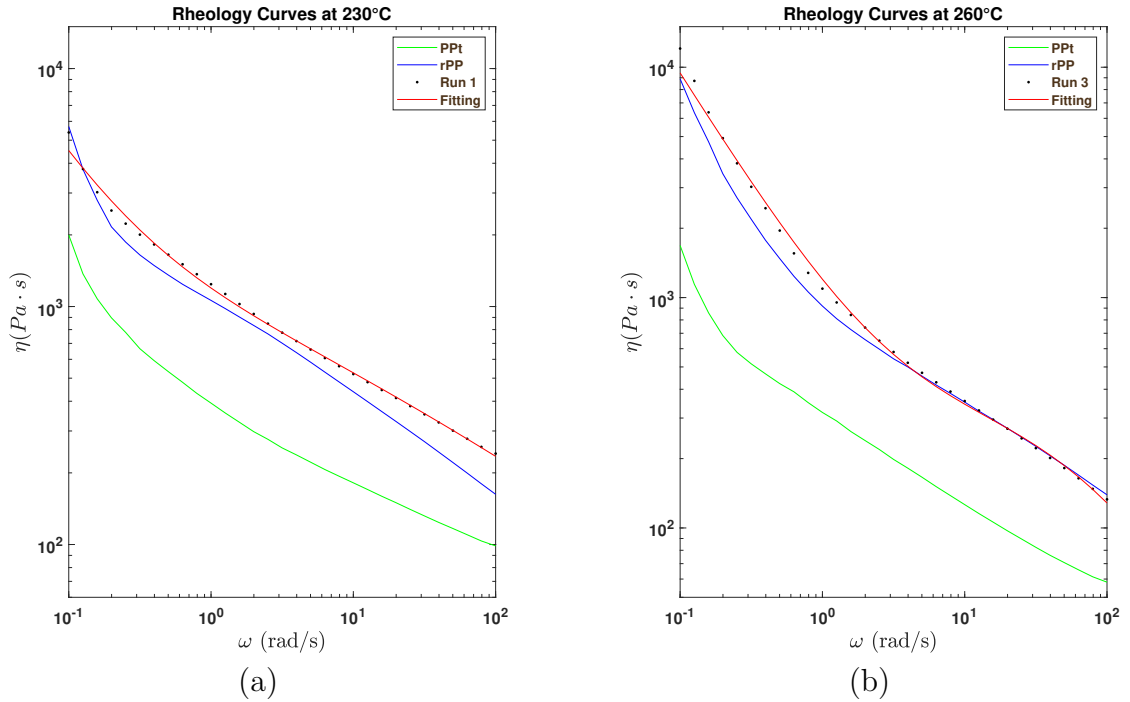


Figure 5.25: Comparison between First stage and third stage results (30%wt R-PP). (a) Complex viscosity curve at 230 °C. (b) Complex viscosity curve at 260 °C.

In the same way, figure 5.26 shows the complex viscosity behavior for filament samples with 40%wt rPP. Compared with PPt and rPP, the filament samples exhibit the most marked non-Newtonian behavior. Moreover, the viscosity curves

for all sample shows a significant difference between references curves.

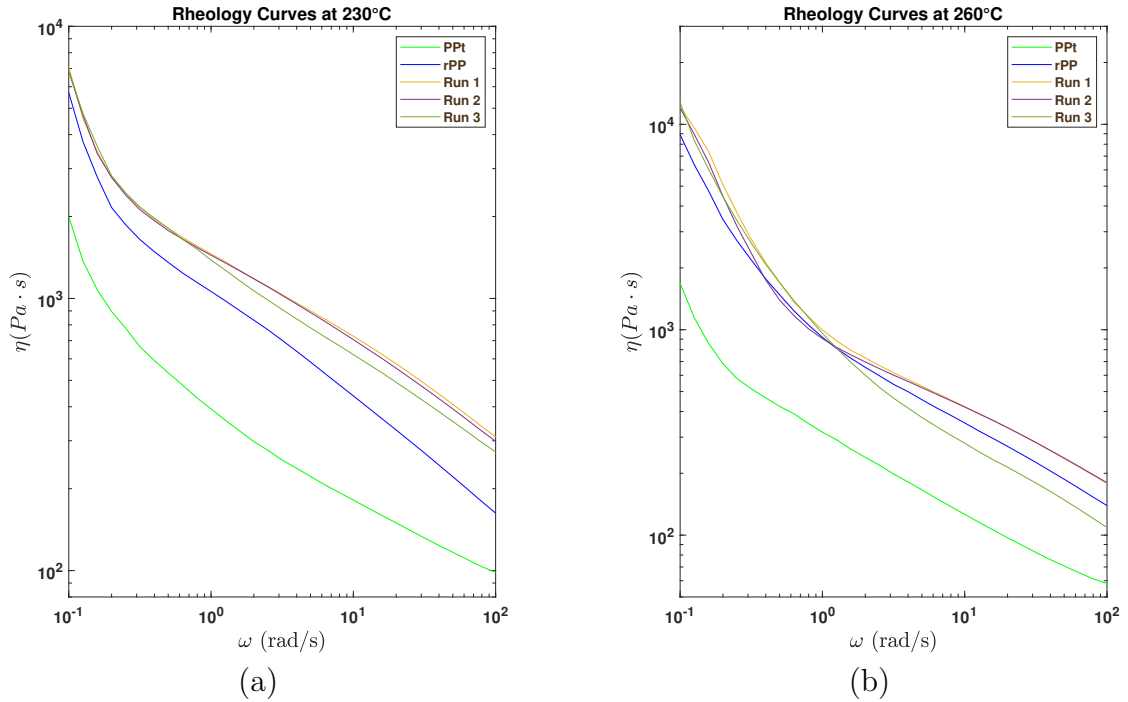


Figure 5.26: Comparison between First stage and third stage results (40%wt rPP). (a) Complex viscosity curve at 230 °C. (b) Complex viscosity curve at 260 °C.

At 230 °C, all runs show a significant increase in the viscosity values at high frequencies. This effect could generate issues on the 3D printing because, at higher viscosity values, the energy needed to extrude the material increases. However, the relationship (difference) between viscosity at high and low frequencies did not change significantly (decreases). At low frequency, the viscosity curve shows a steep slope which states a marked non-Newtonian behavior, and it is bigger than rPP. This phenomena is desirable because reduce the shrinkage for printing process.

On the other hand, at 260 °C, the difference between the filament and based materials curves (PPt and rPP) increases, which determine a non-Newtonian behavior on the filament is more marked at high temperatures. Moreover, the viscosity at high frequency did not show a significant rise as seen in the previous temperature.

Finally, table 5.18 shows the Yield Stress values for both temperatures. The first thing to highlight is that the filament process did not decrease the non-Newtonian behavior, quite the opposite, it is possible to increase this behavior again. At 230 °C, a narrow range of Yield Stress values is found with an average of $423,7 \pm 16,1$ Pa, while at 260 °C, a wide range is displayed with an average of $815,2 \pm$

62,5 Pa.

Sample	Symbol	Value	Unit
Run 1	$\sigma_{T=230\text{ }^\circ\text{C}}$	418,26	Pa
	$\sigma_{T=260\text{ }^\circ\text{C}}$	855,47	Pa
Run 2	$\sigma_{T=230\text{ }^\circ\text{C}}$	410,94	Pa
	$\sigma_{T=260\text{ }^\circ\text{C}}$	743,10	Pa
Run 3	$\sigma_{T=230\text{ }^\circ\text{C}}$	441,86	Pa
	$\sigma_{T=260\text{ }^\circ\text{C}}$	847,31	Pa

Table 5.17: Yield Stress values for filament at 40 %wt R-PP.

In order to examine the viscosity curve better, it was decided to compare the best results obtained for the filament process. Figure 5.27 shows the samples in which the effects of the optimization process are maximized and requirements are satisfied.

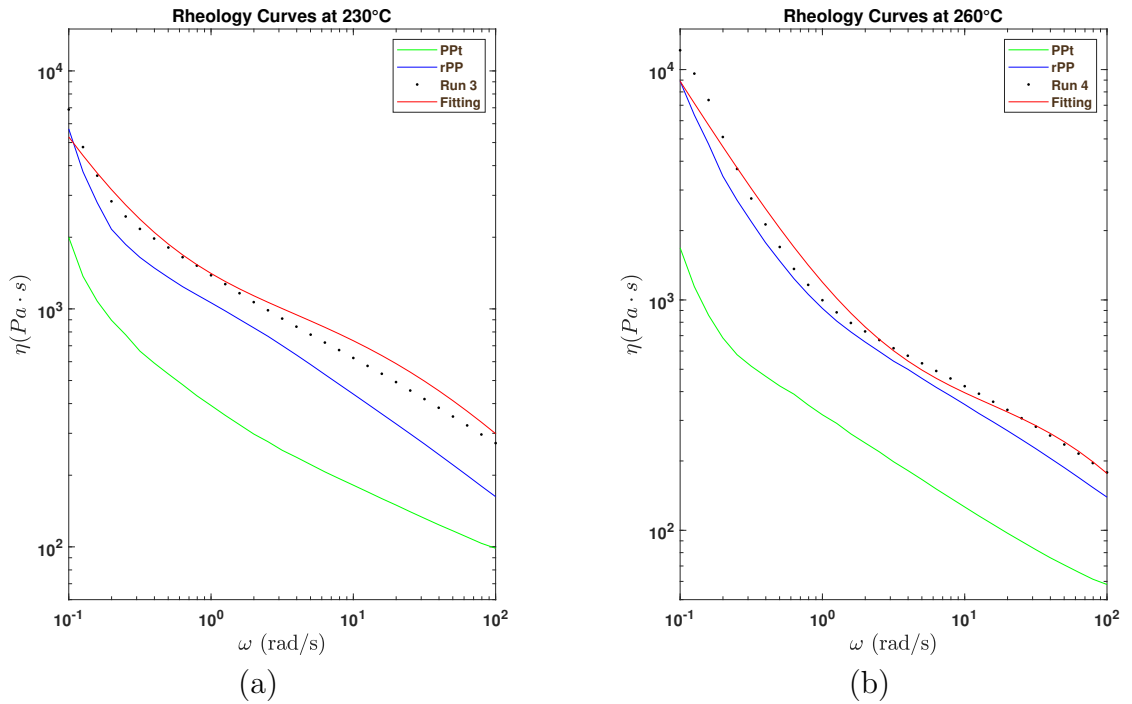


Figure 5.27: Comparison between First stage and third stage results. (a) Complex viscosity curve at 230 °C. (b) Complex viscosity curve at 260 °C.

5.4 Fourth stage

Finally, the last stage was printing both filaments at 30%wt and 40%wt rPP. According to chapter 4, it was conducted several experiments to find the parameters in which the printed will expose a smooth roughness, and without distorting dimensions. However, the experimental process began defining and understanding the effect of the parameters process.

The first step was defining the parameters process throughout the Simplify3d Software. According to previous research and the guide-line of software, there are six different tabs (Extruder, Layer, Infill, Cooling, Temperatures, and other) in which the printing process will be modified.

The second step was to define the effect of temperature and filament diameter. As mentioned in the third stage, both filament (30%wt and 40%wt rPP) showed a significant roughness. In some sections, this variation increases the diameter outside the allowed value diameter (1,5 - 1,8 mm). The experimental results showed that at low temperature (230 °C), the diameter variation hindered the extrusion and generated zones that did not fill. For the blend with 40%wt rPP, it was impossible to make a continuous process.

On the other hand, increasing enough the temperature (>260 °C) reduces the effect mentioned before and increases the fluidity. It was possible to make a continuous extrusion and homogeneous extrusion cord. However, it is impossible to avoid the effect due to the roughness unless improves the surface.

Furthermore, the contribution of bed temperature in the printing process was related to the adhesion and dimension stability. Increasing this parameter achieved a better adhesion between layers because the heat flux is reduced. However, the adhesion between the first layer or raft also increases, which means an issue to take the piece. For both filaments, high bed temperatures increase enough adhesion to generate the issue mentioned before.

Moreover, the adhesion also is related to the cooling process, in which increases or decreases its values produces a variation on it. Increasing the fan speed reduces the adhesion between layers, raft, and bed. However, the effect could be considered as a problem when adhesion between layers is not enough.

Afterward, the last experimental process was to determine the effects of extruder speed and fill. It was found that high-speed results in poor adhesion and empty zones. In addition, the outer perimeter loses its size and shape. One possible reason for the issues mentioned is the filament diameter range and roughness.

Finally, to improve the setting mentioned above several tests were carried out. Table 4.10 in chapter 4 shows the three studies cases in which temperature (extruder and bed) and raft were varied. It was obtained an enhancement on the adhesion between layer-layer increasing the temperatures while reducing the problems to take off the piece at low temperatures.

However, the combination of both temperatures depends on the percentage of rPP. At 40%wt rPP, the best combination of both temperatures was case 2 (280 °C and 50 °C), while at 30%wt rPP, the best combination parameters were case 1 (280 °C and 50 °C). For most parameters and settings mentioned it was decided to take the values of previous results (Berganozzi’s research and Bertolino’s research) to concentrate on the extrusion and shrinkage problems.

5.4.1 Rheology Results

As seen in the previous results, it was important to know the rheological behavior throughout the viscosity curves. Figure 5.28 shows the viscosity curves for printer and based materials at 260 °C.

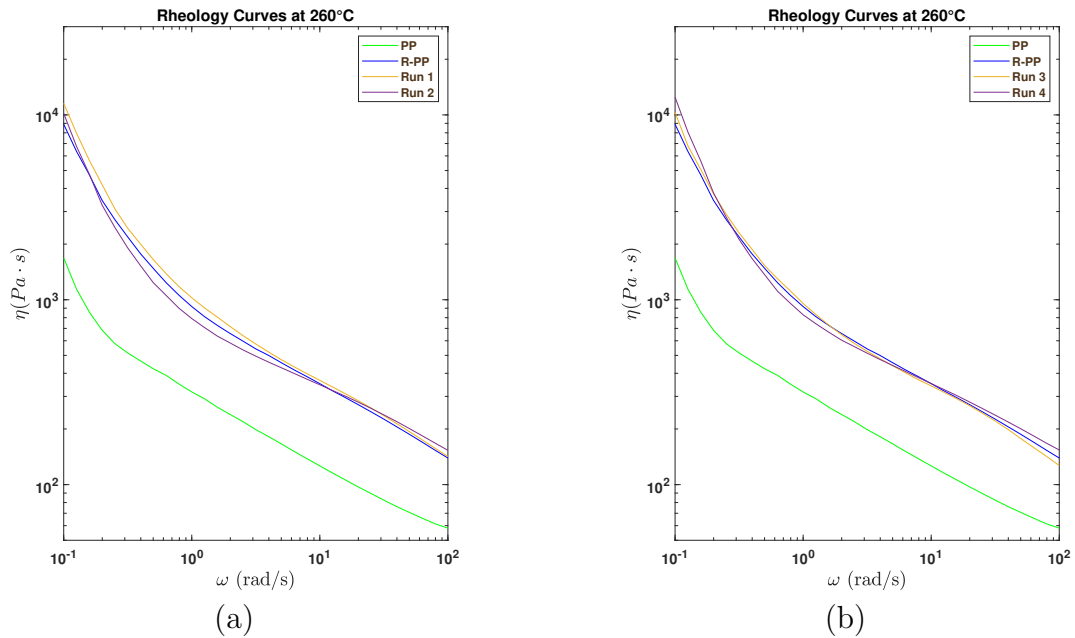


Figure 5.28: Comparison of rheological curves between First Stage and Four Stage . (a) Rheological curves at 260 °C for 30%wt rPP. (b) Rheological curves at 260 °C for 40%wt.

Figure (a) shows two samples in the case of 30%wt rPP while (b) shows the case of 40%wt rPP. In both cases, the viscosity curves exhibit an analogous behavior with rPP. Moreover, there is a narrow difference in viscosity at a low frequency between all samples and R-PP which means a more mark non-Newtonian behavior. The advantage of the blend was the possibility to print the material and at the same time retain the viscosity behavior of rPP.

Table 5.18 resumes the Yield Stress values for all samples. The better case was

for 30%wt rPP with 781,81 Pa. The range of Yield Stress is between 695 to 782 Pa which is a similar range found in the previous results. The possible deviation between values could be related to the recycled material, thermal cycles, and extrusion process. As seen in the first stage, recycled material is a mix between PP, PE, and other elements. Those elements could be another polymeric material or another type of material which is impossible to guarantee a homogeneous dispersion on the matrix.

Sample	Symbol	Value	Unit	R-PP
Run 1	$\sigma_{T=260\text{ }^{\circ}\text{C}}$	781,81	Pa	30%wt
Run 2	$\sigma_{T=260\text{ }^{\circ}\text{C}}$	604,53	Pa	30%wt
Run 3	$\sigma_{T=260\text{ }^{\circ}\text{C}}$	708,46	Pa	40%wt
Run 4	$\sigma_{T=260\text{ }^{\circ}\text{C}}$	695,21	Pa	40%wt

Table 5.18: Yield Stress values for filament at 30 %wt rPP and 40 %wt rPP.

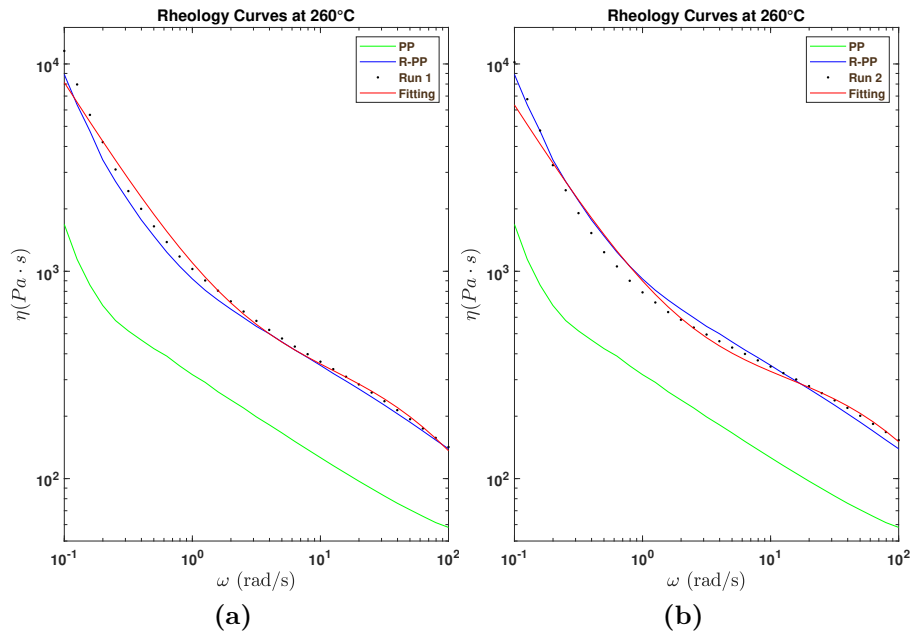


Figure 5.29: Rheological curves for 30%wt R-PP. (a) Run 1 . (b) Run 2.

Figures 5.29 and 5.30 show the complex viscosity curves for all samples. For both figures, it is possible to highlight the difference between fitting and experimental data, which is small. This difference does not represent an issue because Yield Stress values are underestimated.

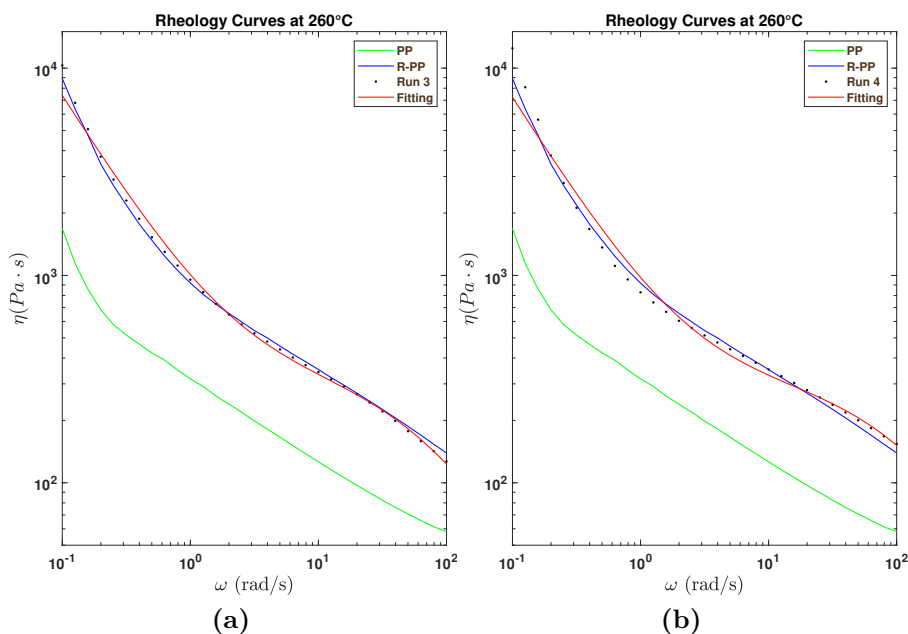


Figure 5.30: Rheological curves for 40%wt rPP. (a) Run 1. (b) Run 2.

On the other hand, figures (a) and (b) at 40%wt rPP, and (b) for 30%wt rPP exhibit and similar complex viscosity curve. It could corroborate with Yield Stress values (table above). On the other hand, the most pronounced change in slope is in run 1 at 30%wt rPP. Figure (a) shows the slope change which is related to a most marked non-Newtonian behavior.

5.4.2 Optical Microscopy Results - Printed

It was carried out a qualitative test to determine some aspects of the printed product, such as adhesion, roughness, dimension, and filling between layers. It was taken three pictures throughout optical microscopy.

The first one, figure (a), is a top view of printing, and it was related to the filling. The second one, figure (b), is the fill pattern chosen for the printing. It was decided to make a fill pattern at ± 45 degrees. The last one, figure (c), is a front view of the printer where it is possible to observe the adhesion and gap between layers.

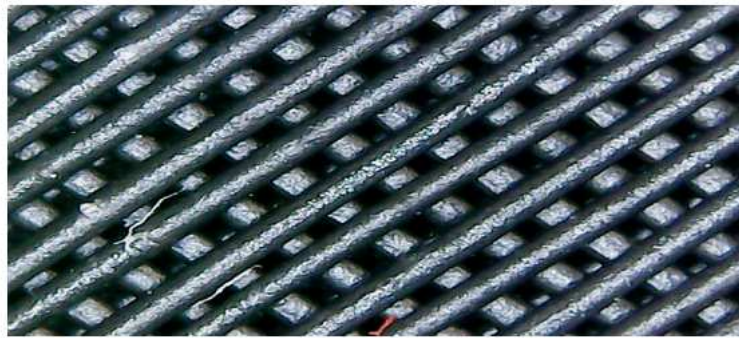
Figure 5.31 shows one sample of printing for the blend at 30%wt rPP. From the first figure (a), it was possible to conclude that there is no significant zone without material. Moreover, there is a high roughness, such as peaks between cords.

Furthermore, from figure (b) was possible to observe the variance of filament diameter as a distance between cords. However, the fill pattern is acceptable to

generate a framework. Finally, figure (c) was highlight the good adhesion between layers.



(a)



(b)



(c)

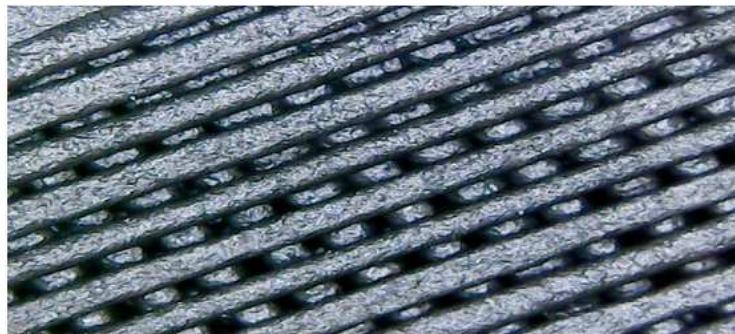
Figure 5.31: Optical Microscopy result for blend at 30%wt rPP at 260 °C. (a) Top view of printing. (b) Fill pattern. (c) Front view of printing.

On the other hand, figure 5.32 shows the results for the blend at 40%wt rPP. The first difference between both blends was the roughness. Form the blend, the

rough at surfaces is not smooth enough, and it is possible to observe zones in which there is an overlap of cord.



(a)



(b)



(c)

Figure 5.32: Optical Microscopy result for blend at 40%wt rPP at 260 °C. (a) Top view of printing. (b) Fill pattern. (c) Front view of printing.

From figure (b), the gap between the cord on the fill patter is more homogeneous. However, as seen above, the printing shows an in-homogeneous space between fill

patterns. However, the gap present in printing was reduced.

Lastly, figure (c) shows the front view of printing. Like a previous sample, it is noted a good adhesion between layers and the thickness of each layer is possible to considered as homogeneous.

5.4.3 SEM Results - Printed

Figures 5.33 and 5.34 show an images for filament and printed for the both blends. The former is related to the blend at 30%wt rPP, while the latter is for 40%wt rPP.

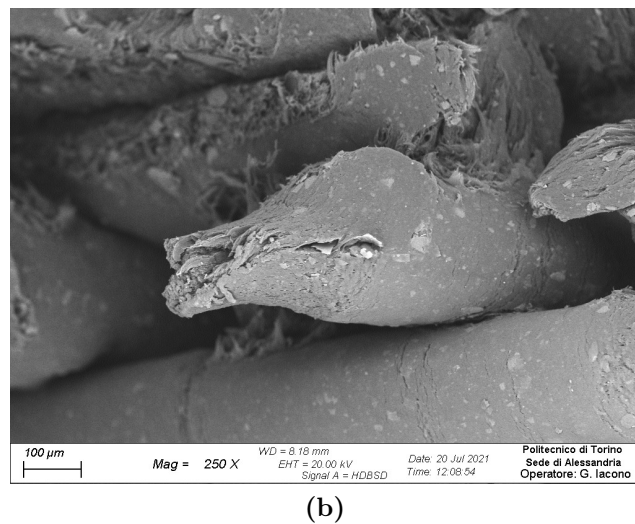
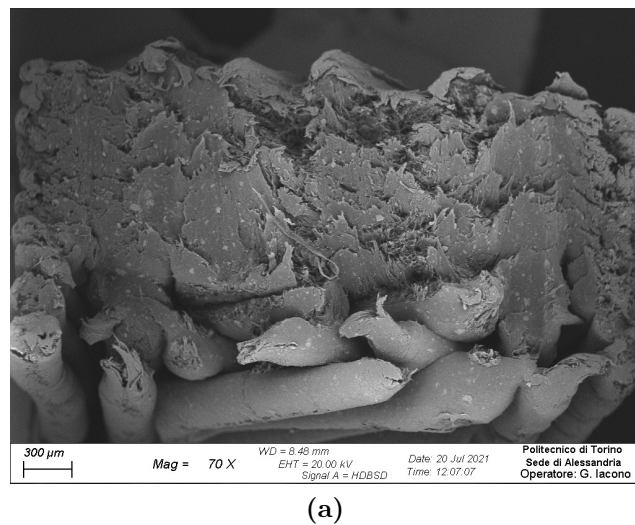


Figure 5.33: SEM results for blend at 30 %wt rPP.

Firstly, it was possible to observe plastic deformation in all samples. At 30%wt

rPP, the plastic strain is seen as a reduction in the cross-sectional area. Figure (a) gives not only information about it, but also gives information about the adhesion of layer-layer. As seen at bottom in this figure, the infill angles ($\pm 45^\circ$) generate a 100% filling.

Furthermore figure (b) shows the specific plastic deformation of a single filament. The cross-sectional evolution before the break allows us to affirm that material exhibits a considerable elongation before breaking. However, as seen in the tensile test the elongation varies between samples.

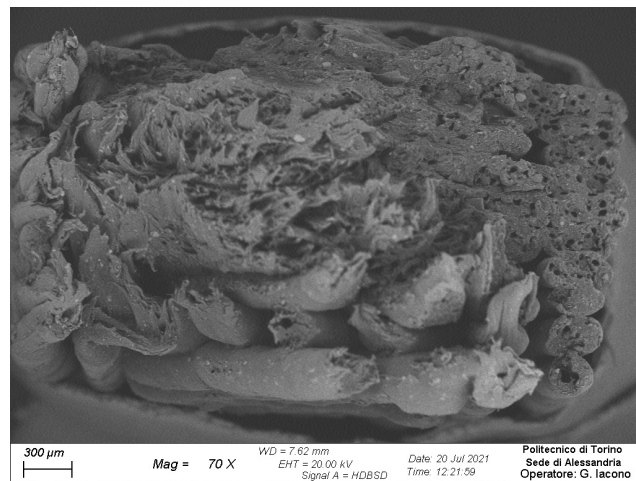
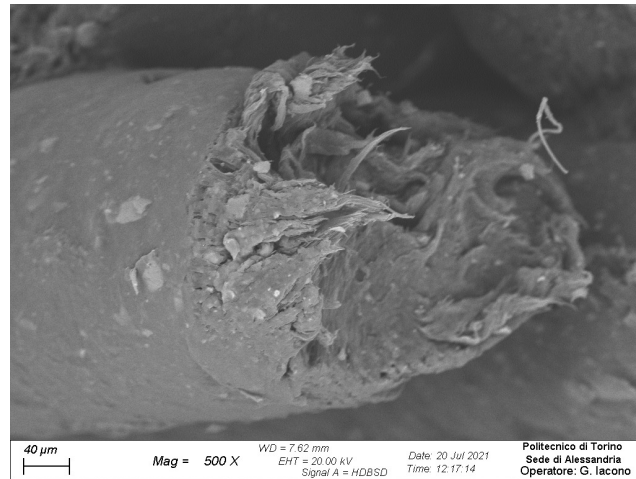


Figure 5.34: SEM results for blend at 40 %wt rPP.

Finally, at 40%wt rPP, it is possible to see two different types of deformation. Figure (b) shows the sample after the tensile test. In this figure, there are two

zones, plastic (left-down) and brittle (right-up) zone. The difference between both is the way how the material is strained.

Moreover, figure (a) shows a single filament break. The reduction of the cross-sectional area is more smallest compared with the previous one (30%wt rPP). Even though, the elongation break for all runs shows a different percentage (mechanical results). So, it is not possible to conclude that a variation in the percentage of rPP puts out a brittle behavior.

5.4.4 Mechanical Test Results

For different samples of both blends, it was carried out Mechanical Tensile Tests. Figure 5.35 shows the stress (σ) vs strain (ϵ) curves for all runs. The first figure (figure (a)) shows the result of 30%wt rPP while the second one (figure (b)) shows the 40%wt rPP.

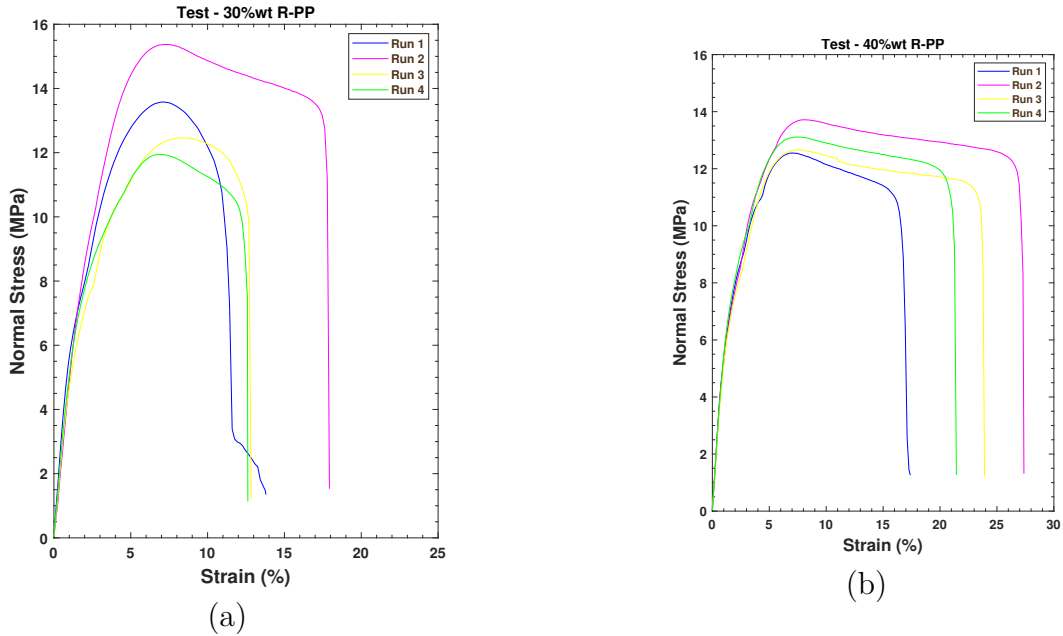


Figure 5.35: Mechanical Test, σ vs ϵ curve. (a) Mechanical Test for 30%wt rPP. (b) Mechanical Test for 40%wt rPP.

At 30%wt rPP, the necking strain zone is narrow for runs 2, 3, and 4. Moreover, run 1 shows a huge necking zone which is analogous at curves for the second blend. In general, the behavior of this blend presents a significant elastic region.

On the other hand, at 40%wt R-PP, it was evidenced that the Tensile Strength value is minor than the first blend. Furthermore, the necking strain showed a significant increase, which implies an increase in an elongation break. As mentioned

before, the samples exhibit a mixed behavior between brittle fracture and elastic-plastic deformation (figure 5.34). For that reason, the elastic zone is minor, and the necking zone is the biggest. The difference between the elongation fracture for all runs could be explained as the percentage of the matrix in which the behavior is more or less brittle.

Tables 5.19 and 5.20 resume the relevant values for mechanical test. The former shows the results for 30%wt R-PP and the latter the results for 40%wt R-PP. The modules between all runs are more or less analogous with a range between 500 to 654 MPa. The average are

On the other hand, both blends expose an important difference between the plastic behavior (elongation). The elongation range before fracture for 30%wt was around 13%, while 40%wt was 24%. However, the first blend shows a large elastic region which allows to hold on more energy before permanent deformation (plastic).

Sample	Modulus (MPa)	Tensile Strength (MPa)	Elongation (%)	Fracture Stress (MPa)
1	654,4	12,9	11,1	3,4
2	416,7	15,4	17,6	12,7
3	492,5	13,6	12,7	9,8
4	555,7	11,9	12,4	9,0
Average	654	13,4	13,4	8,7
DS	100	1,4	2,9	3,9

Table 5.19: Mechanical results for 30%wt rPP at 260 °C.

Sample	Modulus (MPa)	Tensile Strength (MPa)	Elongation (%)	Fracture Stress (MPa)
1	632,82	12,5	16,6	9,9
2	588,42	13,7	27,1	10,2
3	585,24	12,7	23,9	8,5
4	608,38	13,1	21,3	9,2
Average	604	13,0	22,2	9,4
SD	22	0,5	4,5	0,7

Table 5.20: Mechanical results for 40%wt rPP at 260 °C.

Chapter 6

Conclusion

This chapter will conclude the research by summarizing the findings and discussing the value and contribution thereof. It will also review the limitation of the result and propose opportunities for future investigations.

This research aimed to investigate the possible use of plastic waste on Fused Deposition Modeling (FDM). Although Additive Manufacturing is an attractive solution to innovate the way to produce and make commodities, there are different limitations and issues on using recycled materials. The main restraint is that they exhibit amiss behavior that avoids their use.

The results indicate that, at different proportions (30%wt and 40%wt rPP), it is achievable to use recycled material in FDM. Further findings, throughout statistical methods, show that the main parameters and their values, which modify the rheological behavior on the blend and change the features, are temperature and screw profile.

As mentioned before, other challenges of using recycled materials are linked with the mechanical and physical properties, even more with the deviation of their typical values. The results show a decrease in these variations, but it was impossible to avoid completely.

The research highlighted the possibility of using recycled plastic on 3D printing, but also it shows the conditions in which obtained the best behavior and properties. Given the plastic waste around the world, the result turns out to be an opportunity to reduce plastic waste and produce custom commodities through 3D Printing.

On the other hand, it is relevant to carry out more samples in the different steps. These samples will not only help to obtain robust data but also give more information about rheological behavior. Based on the Thaguchi's method will be possible evaluated more parameters that could be modify the blend behavior.

Finally, it is recommended to proceed with the printing process, varying the geometry and using supports. This process will be able to evidence the effect of the printing process. Moreover, it is recommended to increase the quantity of rPP

and reduce PP. Future studies can address the effect of roughness and how to avoid them. Further, it can be studied other materials to generate the blend.

Bibliography

- [1] Tuan D. Ngo; Alireza Kashani; Gabriele Imbalzano; Kate T.Q. Nguyen; David Hui. «Additive manufacturing (3D printing): A review of materials, methods, applications and challenges». In: 143 (June 2018), pp. 172–196 (cit. on pp. 3, 6, 9, 10, 12).
- [2] Carneiro O.S; Silva A.F; Gomes R. «Research on 3D printing layered algorithm based on FDM technology». In: 1798 (Feb. 2021), p. 12027 (cit. on p. 3).
- [3] Lalegani Dezaki Mohammadreza; Mohd Ariffin Mohd Khairol Anuar; Hatami Saghi. «An overview of fused deposition modelling (FDM): research, development and process optimisation». In: 27 (Mar. 2021), pp. 562–582 (cit. on pp. 3, 4, 11).
- [4] Christian Weller; Robin Kleer; Frank T. Piller. «Economic implications of 3D printing: Market structure models in light of additive manufacturing revisited». In: 164 (June 2015), pp. 43–56 (cit. on pp. 4, 5).
- [5] Lu-Yu Zhou; Jianzhong Fu; Yong He. «A Review of D Printing Technologies for Soft Polymer Materials». In: 30 (Sept. 2020), p. 2000187 (cit. on pp. 4, 5).
- [6] Jia Hongwei; Xu Wei. «Fused deposition modeling with polypropylene». In: 83 (2015), pp. 768–776 (cit. on p. 6).
- [7] Calignano Flaviana; Fino Paolo; Manfredi Diego; Ambrosio Elisa Paola; Biamino Sara; Lombardi Mariangela; Atzeni Eleonora; Salmi Alessandro; Minetola Paolo; Iuliano Luca. «Overview on Additive Manufacturing Technologies». In: 105 (Apr. 2017), pp. 593–612 (cit. on p. 6).
- [8] Soyeon Park; Kun (Kelvin) Fu. «Polymer-based filament feedstock for additive manufacturing». In: 213 (Sept. 2021), p. 108876 (cit. on pp. 7, 14).
- [9] Mario Enrique Hernandez Korner; María Pilar Lambán; JoséAntonio Albajez; Jorge Santolaria; Lisbeth del Carmen Ng Corrales; Jesús Royo. «Systematic Literature Review: Integration of Additive Manufacturing and Industry 4.0». In: 10 (Aug. 2020), pp. 1–24 (cit. on p. 8).

- [10] Mohsen Attaran. «The rise of 3-D printing: The advantages of additive manufacturing over traditional manufacturing». In: 60 (Sept. 2017), pp. 677–688 (cit. on p. 8).
- [11] Bouge R. «3-D printing: The dawn of a new era in manufacturing?» In: *Assembly Automation* 33.4 (2013), pp. 307–311 (cit. on pp. 8, 9).
- [12] Fish E. «Rapid prototyping how it is done at GM: Additive manufacturing technology is helping the automaker reduce product development times and costs.» In: *Automotive Design and Production* 123.5 (2011), pp. 46–48 (cit. on p. 8).
- [13] Murphy S. V.; Atala A. «3-D bioprinting of tissues and organs». In: *Biotechnology* 32.8 (2014), pp. 773–785 (cit. on p. 8).
- [14] Berman B. «3-D printing: The new industrial revolution.» In: *Business Horizons* 55.2 (2012), pp. 155–162 (cit. on p. 8).
- [15] Oxford. *Overview Anova*. URL: <https://www.forbes.com/sites/centurylink/2014/06/03/how-3d-printing-is-reinventing-retail/> (cit. on p. 9).
- [16] Wohlers Associates. *Analysis Trends Forecast. Feel the pulse of the 3D printing industry*. URL: <https://wohlersassociates.com/2020report.htm> (cit. on p. 9).
- [17] Diana Popescu; Aurelian Zapciu; Catalin Amza; Florin Baci; Rodica Marinescu. «FDM process parameters influence over the mechanical properties of polymer specimens: A review». In: 169 (Aug. 2018), pp. 157–166 (cit. on pp. 9, 10).
- [18] A.H Akhoundi B.; Behraves. «Effect of filling pattern on the tensile and flexural mechanical properties of FDM 3D printed products». In: 59 (Jan. 2019), pp. 883–897 (cit. on pp. 10, 11).
- [19] O.S. Carneiro; A.F. Silva; R. Gomes. «Fused deposition modeling with polypropylene». In: 83 (June 2015), pp. 768–776 (cit. on p. 12).
- [20] Tofail Syed A.M; Koumoulos Elias P; Bandyopadhyay Amit ; Bose Susmita; O’Donoghue Lisa; Charitidis. «Additive manufacturing: scientific and technological challenges, market uptake and opportunities». In: 21 (Jan. 2018), pp. 22–37 (cit. on p. 12).
- [21] Tuan Nguyen Huu. *Creative Mechanisms Blog*. URL: <https://www.creativemechanisms.com/blog/all-about-polypropylene-pp-plastic> (cit. on pp. 12, 13).
- [22] British Plastics Federation. *Polypropylene (PP)*. URL: <https://www.bpf.co.uk/plastipedia/polymers/pp.aspx> (cit. on pp. 12, 13).

- [23] Valco Group. *Manufacturing process of PP*. URL: <https://guichon-valves.com/faqs/pp-polypropylene-manufacturing-process-of-pp-polypropylene/> (cit. on p. 13).
- [24] Gholamhossein Sodeifiana; Saghar Ghaseminejad; AliAkbar Yousefid. «Preparation of polypropylene/short glass fiber composite as Fused Deposition Modeling (FDM) filament». In: 12 (Mar. 2019), pp. 205–222 (cit. on pp. 14, 15).
- [25] M. Bertolino; D. Battegazzore; R. Arrigo; A. Frache. «Designing 3D printable polypropylene: Material and process optimisation through rheology». In: 40 (Apr. 2021), p. 101944 (cit. on p. 14).
- [26] Valentina Mazzanti; Lorenzo Malagutti; Francesco Mollica. «FDM 3D Printing of Polymers Containing Natural Fillers: A Review of their Mechanical Properties». In: 11 (June 2019), p. 1094 (cit. on p. 14).
- [27] C. Aumnatea; P. Potiyarajab; C. Saengowc; A. J. Giacomincde. «Reinforcing polypropylene with graphene-poly(lactic acid) microcapsules for fused-filament fabrication». In: 198 (Jan. 2021), p. 109329 (cit. on p. 15).
- [28] Donald G. Baird Jier Y. Han; Tianran Chen; Qingmin Mu. «Thermotropic liquid crystalline polymer reinforced polypropylene composites enhanced with carbon nanotubes for use in fused filament fabrication». In: 42 (May 2021), pp. 4115–4127 (cit. on p. 15).
- [29] Herianto ; Atsani S. I. ; Mastrisiswadi H. «Recycled Polypropylene Filament for 3D Printer: Extrusion Process Parameter Optimization». In: 722 (Jan. 2021), p. 12022 (cit. on p. 15).
- [30] Nicole E. Zander; Margaret Gillan; Zachary Burcjhared; Frank Gardea. «Recycled polypropylene blends as novel 3D printing materials». In: 25 (June 2019), pp. 122–130 (cit. on p. 15).
- [31] Jeffrey W. Stansbury; Mike J. Idacavage. «3D printing with polymers: Challenges among expanding options and opportunities». In: 32 (Mar. 2016), pp. 54–64 (cit. on p. 15).
- [32] P. Krawczak. «Additive manufacturing of plastic and polymer composite parts: Promises and challenges of 3D-printing». In: 9 (Nov. 2015), p. 959 (cit. on p. 15).
- [33] Paul D Berger; Robert E Maurer; Giovana B Celli. *Experimental Design*. Gewerbestrasse 11, 6330 Cham, Switzerland: Springer, 2017 (cit. on pp. 17, 20).
- [34] R. L. Plackett; J. P. Burman. «The Design of Optimum Multifactorial Experiments». In: *Oxford Journals* 33.15 (1946), pp. 305–325 (cit. on pp. 17, 20).

- [35] Forbes. *How 3-D printing is reinventing retail*. URL: <https://www.oxfordreference.com/view/10.1093/oi/authority.20110803095415398> (cit. on p. 18).
- [36] John A. Cornell. *Experiments with Mixtures: Designs, Models, and the Analysis of Mixture Data*. New York: John Wiley Sons, Inc., 2002 (cit. on p. 19).
- [37] Inc The MathWorks. *Matlab*. URL: https://www.mathworks.com/products/matlab.html?s_tid=hp_products_matlab (cit. on p. 20).
- [38] M.T. Gallagher; R.A.J. Wain; S. Dari; J.P. Whitty; D.J. Smith2. «Non-identifiability of parameters for a class of shear-thinning rheological models, with implications for haematological fluid dynamics». In: *physics.flu-dyn* 3.4 (2018), pp. 68–70 (cit. on pp. 21, 22, 38).
- [39] Matlab. *fmincon*. URL: <https://www.mathworks.com/help/optim/ug/fmincon.html#busog7r-fun> (cit. on p. 21).
- [40] Lu Cui; Lan Yi; Yating Wang; Yunchong Zhang; Péter Polyák; Xiaofeng Sui; Béla Pukánszky. «Rheology of PLA/Regenerated Cellulose Nanocomposites Prepared by the Pickering Emulsion Process: Network Formation and Modelings». In: *Materials & Design* 206.8 (2021), p. 109774 (cit. on pp. 23, 38, 39).
- [41] Bernagozzi Giulia. «Sviluppo di formulazioni a base polipropilene contenenti cariche inorganiche per stampa 3D: studio del comportamento reologico e delle proprietà meccaniche». MA thesis. Turin - Italy: Politecnico di Torino, 2021 (cit. on pp. 25, 26, 36, 43).
- [42] Bertolino Michele. «Sviluppo di formulazioni a base polipropilene con funzionalità di ritardo alla fiamma per stampa 3D». MA thesis. Turin - Italy: Politecnico di Torino, 2019 (cit. on pp. 25, 26, 36).
- [43] Repsol Technology Center. *Isplen Polypropylene. Chemicals. Technical data Sheet*. URL: <https://www.repsol.com/en/energy-and-innovation/technology-lab/index.cshtml> (cit. on p. 26).
- [44] Felice De Santis; Roberto Pantani. «Melt compounding of Poly(Lactic Acid) and talc: assessment of material behavior during processing and resulting crystallization». In: 22 (Oct. 2015), pp. 1–9 (cit. on p. 26).
- [45] IMI FABI SpAr. *Talc*. URL: <https://www.imifabi.com/327-HTP1s-a-novel-talc-additive-for-smart-polymer-pro.html> (cit. on pp. 26, 27).
- [46] Breplast SpA. *Datasheet of BRETENE*. URL: <https://www.materialdatacenter.com/ms/en/Bretene/Breplast+S%252Ep%252EA/BRETENE+PP/b3c21562/6906> (cit. on pp. 27, 28).

- [47] Spalla. «Sviluppo di formulazioni polimeriche per il settore autobasate su plastiche riciclate dalla filiera urbana dei rifiuti». MA thesis. Turin - Italy: Politecnico di Torino, 2018 (cit. on p. 28).
- [48] Xplore Instruments BV. *Xplore MC 15*. URL: http://www.jrtogether.com/upload/files/MC15_micro%20compounder%2015cc_Small.pdf (cit. on p. 28).
- [49] Collin Lab & Piplot solutions. *Press Collin P200T*. URL: <https://www.collin-solutions.com/en/product/presses-e-e-air-and-e-plus/> (cit. on p. 29).
- [50] Thermo Fisher Scientific. *Process 11 Thermo Fisher Scientific*. URL: <https://www.thermofisher.com/order/catalog/product/567-7600> (cit. on pp. 31–33).
- [51] 3devo B.V. *3devo Filiment makers*. URL: <https://3devo.com/filament-makers/> (cit. on pp. 33, 34).
- [52] 3D Printers. The most accurate 3D Printers in the world. *Roboze One*. URL: <https://www.roboze.com/en/3d-printers/> (cit. on p. 35).
- [53] P. Gill; T. Moghadman; B. Ranjbar. «Differential scanning calorimetry techniques: applications in biology and nanoscience». In: 21 (Apr. 2010), pp. 167–193 (cit. on p. 39).
- [54] Ghijssels A; Waals F.M.T.A.M. «Differential scanning calorimetry: A powerful tool for the characterization of thermoplastics». In: 1 (Feb. 1980), pp. 149–160 (cit. on p. 40).
- [55] Instron. *5960 Series Dual Column Table Frames System*. URL: <https://www.instron.com/en-us/search-results?ss360Query=5966> (cit. on p. 41).
- [56] Techmate is a Laboratory Equipment. *Digital USB Manual Microscope ODC 895*. URL: <https://techmate.co.uk/product/digital-usb-manual-microscope-odc-895/> (cit. on p. 42).